Biosensors and Bioelectronics 184 (2021) 113245

Contents lists available at ScienceDirect

Biosensors and Bioelectronics

journal homepage: http://www.elsevier.com/locate/bios

Graphene nanoribbon: An emerging and efficient flat molecular platform for advanced biosensing

Asha P. Johnson [a], Chinnu Sabu [b], N. Kumara Swamy [c], Annstephy Anto [d], H. V. Gangadharappa [a,**], K. Pramod [b,*]

[a] JSS College of Pharmacy, JSS Academy of Higher Education and Research, Sri Shivarathreeshwara Nagara, Mysuru, 570015, Karnataka, India
[b] College of Pharmaceutical Sciences, Government Medical College, Kozhikode, 673008, Kerala, India
[c] Department of Chemistry, J S S Science and Technology University, Mysuru, 570006, Karnataka, India
[d] Calea Ltd., 2785 Skymark Ave Unit 2, Mississauga, Ontario, Canada

ARTICLE INFO

Keywords:
Biosensor
Biomarker
Graphene nanoribbons
Nanomaterial
Nanobiosensor

ABSTRACT

Graphene nanoribbons (GNRs) are lengthened one-dimensional monolayer strips of graphene and have a hexagonal honeycomb lattice structure. The captivating properties like electrical conductivity, emerging band gap, optical property, thermal conductivity, high mechanical strength, and ultrahigh surface area make them a better candidate for biomedical applications. The properties can be significantly reformed and controlled by altering the edge functionalities and geometry. The exhibition of a wide potential window coupled with an ultra-high surface area to host sensing element makes GNR an excellent biosensing platform. Consequently, biosensing is one of the most explored applications of GNR. This review presents an overview of the characteristics, methods of synthesis, and biosensing applications of GNR. Overall, GNR is considered a promising platform for efficient signal transduction compared to conventional biosensing platforms. Further, it offers high electrical conductivity, large surface area, high adsorption, synergistic effects with combined materials, fast response, sensitivity, and selectivity.

1. Introduction

The exploration of carbon-based nanomaterials began in the 1980s with the invention of fullerenes. After introducing graphene in 2004, the research on carbon-based nanomaterial got much attention (Geim and Novoselov, 2007; Yang et al., 2018). Graphene is a two-dimensional sheet of one-atom-thick, hexagonally organized sp^2 hybridized carbon atoms and can be easily modified to its single, a few, or multilayer derivatives (Bianco et al., 2013; Meyer et al., 2007). Graphene attracted significant technological and scientific attention due to its unique physicochemical characteristics. It has shown boundless potential in fields such as energy storage (Bhushan et al., 2020; Thiruppathi et al., 2020), engineering (Si et al., 2020; Wang et al., 2020), electronics (He et al., 2020; Liu et al., 2020), sensing (Haridas et al., 2020; Kudr et al., 2020), and biomedical applications (Arsenin et al., 2018; Lacatus, 2020; Menazea and Ahmed, 2020; Pathmanapan et al., 2020; Shahabi and Raissi, 2020; Su et al., 2020)

Extensive research on graphene delivered its various derivatives, such as nanoribbons, carbon nanotubes, nanohorns, nanoplatelets, graphene quantum dots (GQDs), etc. (Elmarakbi et al., 2020; Liao et al., 2018; Seekaew et al., 2018). Among these, graphene nanoribbon (GNR) recently attained more attraction due to the uniqueness in nature. GNRs are one-dimensional lengthened graphene strips with a high aspect ratio (length to width ratio) (Bu et al., 2009). The oxygenated derivatives of GNRs (GONRs) are very useful in biomedical applications due to their amphiphilic nature and good biocompatibility. Compared to other graphene-family nanomaterials, the most attractive feature of GNR is its ultrahigh surface area and open-ended structure. Different reduction reactions can convert GONRs to reduced GONRs (rGONRs) (Chowdhury et al., 2015; Rajaji et al., 2018). The fascinating and favorable characteristics like high electron transport, high mechanical strength, optical properties, and thermal characteristics opened their possibilities in the biomedical field (Johnson et al., 2020). The biomedical applications of GNRs are depicted in Fig. 1. Among all other biomedical applications, biosensing is one of the most explored areas of application.

The development and implementation of highly sensitive biosensors need new approaches for effectual point-of-care detection with great

* Corresponding author.
** Corresponding author.
E-mail addresses: hvgangadharappa@jssuni.edu.in (H.V. Gangadharappa), pramodkphd@yahoo.com (K. Pramod).

https://doi.org/10.1016/j.bios.2021.113245
Received 9 December 2020; Received in revised form 27 January 2021; Accepted 9 April 2021
Available online 15 April 2021

Abbreviations

2,4-DCP	2, 4 dichlorophenol
2-AP	2- aminophenol
4-AP	4-aminophenol
4-NP	4-Nonyl phenol
A	Adenine
AsA	Ascorbic acid
AA	Amino acids
Ab	Antibody
AChE	Acetylcholinesterase
AFP	Alpha-fetoprotein
AGNRs	Armchair Graphene nanoribbons
AuNPs	Gold nanoparticles
BPA	Bisphenol-A
BSA	Bovine serum albumin
BTX-2	Brevetoxin-B
C	Cytosine
CD	Cyclodextrin
ChOx	Cholesterol oxidase
CNS	Central nervous system
CoPc	Cobalt phthalocyanine
COVID-19	Corona virus disease- 2019
CS	Chitosan
CV	Cyclic voltammetry
CVD	Chemical vapor deposition
CySH	Cysteine
DA	Dopamine
DM	Diabetes mellitus
DNA	Deoxy nucleic acid
DPV	Differential pulse voltammetry
ECL	Electrochemiluminescence
EIS	electrochemical impedance spectroscopy
EPPG	Edge plane pyrolytic graphite
FAD	Flavine adenine nucleotide
FET	Field effect transistors
FRET	Fluorescence resonance energy transfer
G	guanine
Gal-3	Galectin-3
GCE	Glassy carbon electrode
GERS	Graphene enhanced raman scattering
GNR	Graphene nanoribbon
GO	Graphene oxide
GONR	Graphene oxide nanoribbons
GOx	Glucose oxidase
GQDs	Graphene quantum dots
GS	graphene sheet
GSH	Glutathione
HChA	Hydrodynamic chronoamperometry
HS-CD	Thiol-β-cyclodextrin
HSPCE	Heated Screen-printed carbon electrode
IL	Ionic liquid
IL-6	Interleukin-6
ISFET	Ion-sensitive field-effect transistor
L-Arg	L-arginine
LSV	Linear sweep voltammetry
MB	Methylene blue
MCPE	Magnetic carbon paste electrode
MMP-9	Matrix metallopeptidase-9
MOF	Metal organic framework
MOF	metal-organic framework
MoS_2	Molybdenum disulfide
MrGO	Multilayer reduced graphene oxide
MWCNT	Multi-walled carbon nanotube
NADH	Nicotinamide adenine dinucleotide
Nf	Nafion
NPs	Nanoparticles
NSAID	Nonsteroidal anti-inflammatory drug
NT	Norepinephrine tartrate
NV-ZGNRs	nitrogen-doped vacancy ZGNRs
PANI	Polyaniline
PCSK9	Proprotein convertase subtilisin/kexin type 9
PDA	Polydopamine
PDDA	Polydiallyldimethylammonium chloride
PdPt	Palladium platinum
PGNR	Porous Graphene nanoribbon
PPO	Polyphenol oxidase
PS	Polystyrene
PSA	Prostate-specific antigen
QDs	Quantum dots
Rf	Radiofrequency
rGO	Reduced graphene oxide
rGONRs	Reduced Graphene oxide nanoribbons
rGOS	Reduced graphene oxide sheets
SERS	Surface enhanced raman scattering
SPCE	Screen-printed carbon electrode
ssDNA	single-stranded deoxy nucleic acid
STM	Scanning tunneling microscopy
SWCNT	Single-walled carbon nanotube
SWV	Square wave voltammetry
T	Thiamine
TNOS	Terminator nopaline synthase
UA	Uric acid
ZGNRs	Zig-zag graphene nanoribbons

accuracy and low cost is an all-time need in health care (Park et al., 2020). The biosensors should exhibit a large detection range, small detection limit, and high level of sensitivity, selectivity, and specificity to the analyte molecule. Colorimetric, potentiometric, fluorescent, electrochemical, and Raman spectroscopy-based biosensors are there. Among all these, electrochemical sensing is more facile, less expensive, and highly sensitive(Azeredo et al., 2020). This allows the detection of a broad range of analytes with rapid response-recovery times and a very low detection limit. Graphene-based electrode materials have shown superior performance in electrocatalysis (Pumera, 2011; Terse-Thakoor et al., 2019)

GNRs exhibit an open reactive edge and might even possess step edges that improve the adsorption and electrocatalytic activity of analyte molecules (Li et al., 2015). GNRs have high thermal conductivity, superior mechanical properties, an ultrahigh surface area for chemical modification, and electronic transport properties. Besides, they exhibit specific properties like straight edges, high aspect ratio, tunable electronic properties, high electron transfer rate, and defect sites. Therefore, GNR is considered a promising platform for efficient signal transduction. GNR-based hybrid nanomaterials and GNR-based nanocomposites enhance signal transduction by promoting electron transfer and catalytic activity towards the analyte (Feng et al., 2018; Jothi et al., 2020). Therefore, GNR-based biosensors are significant not only in health care diagnostics but also in environmental and industrial monitoring.

This review is mainly based on the biosensing applications of GNR and summarizes the GNR types, properties, various synthetic approaches, fabrication of sensing platforms, and its application in biosensing. It also provides a critical comparison of various GNR based sensors by pointing out the significant characteristics and outcomes. In addition, this review attempts to provide novel conceptual insights that

can stimulate the generation of new research questions related to the use of GNRs in biosensors and bioelectronics.

2. Types of GNRs

The quasi-one-dimensional ribbon-like structures with two diverse possible edge geometries have resulted from the finite termination of graphene. Generally, GNRs are categorized into two types depending on the basic shape of graphite edges; armchair GNRs (AGNRs) and Zig-zag GNRs (ZGNRs) (Fig. 2a & b)(Marmolejo-Tejada and Velasco-Medina, 2016; Nakada et al., 1996).Chiral GNRs are a combination of AGNR and ZGNR. Interestingly, the biosensing application of GNRs can be influenced by the type of GNR used.

2.1. Armchair GNRs

AGNRs are either metallic or semiconducting direct gap semiconductors, where the bandgap is proportional to the inverse of the width (Hod and Scuseria, 2006). AGNR does not have any localized states, and the bonds are constituted by the atoms from two distinct sublattices. Moreover, AGNR with smaller energy bandgaps augments the sensing signal carrier densities (Lyu et al., 2018). Depending upon the value of the number of atoms (m), AGNRs can be classified into three categories, m = 3p, 3p + 1, and 3p + 2 (where, p is a positive integer) with varying electronic properties where the number of atoms along their width is m. Among these, metallic behavior is m = 3p+2, and the other two show semiconducting behavior (Dutta and Pati, 2010). The edge state and transmission of AGNR facilitates their use as spectrograph sensor device (Chowdhury et al., 2012).

2.2. Zig-zag GNRs

ZGNRs are metallic middle gap semiconductors and form a localized edge state at the Fermi level, which means that the electrical movement can be spin-polarized and atoms come from the same sublattice(Hernandez et al., 2012). The edge state is defined as the localized electronic state at the edges, which dwindle exponentially towards the ribbon center (Shen-Lin Chang, Bi-Ru Wu, Po-Hua Yang, 2016). ZGNRs impart appropriate interfaces to frame junctions at the atomic level, which helps them to directly connect to the circuit in biosensors(Rashid et al., 2020).

Cove GNRs are a subclass of ZGNR with intermittent carbon atom vacancies on both edges (Fig. 2a) (Lee et al., 2018b). In addition, GNR can be an open edge or closed edge based on the presence of dangling bonds in the long axial direction. GNRs having dangling bonds mainly in the long axial direction can be open edge GNRs. In contrast, GNRs without the presence of dangling bonds in the long axial direction can be closed edge GNRs (He et al., 2019). Modifications on the edges of cove type GNR can smoothly reduce the energy band gaps making them potential material for optoelectronic application (de Sousa Araújo Cassiano et al., 2020).

2.3. Chiral GNRs

Chiral GNR exhibits alternating zig-zag and armchair segments along their edges. As the chiral angle decreases, the length of zig-zag segments increases. The low bandgap in chiral GNR is explained by the high degree of aromaticity and electron delocalization (Corso et al., 2018). Chiral GNRs can fine-tune the sensing signal and offer a promising

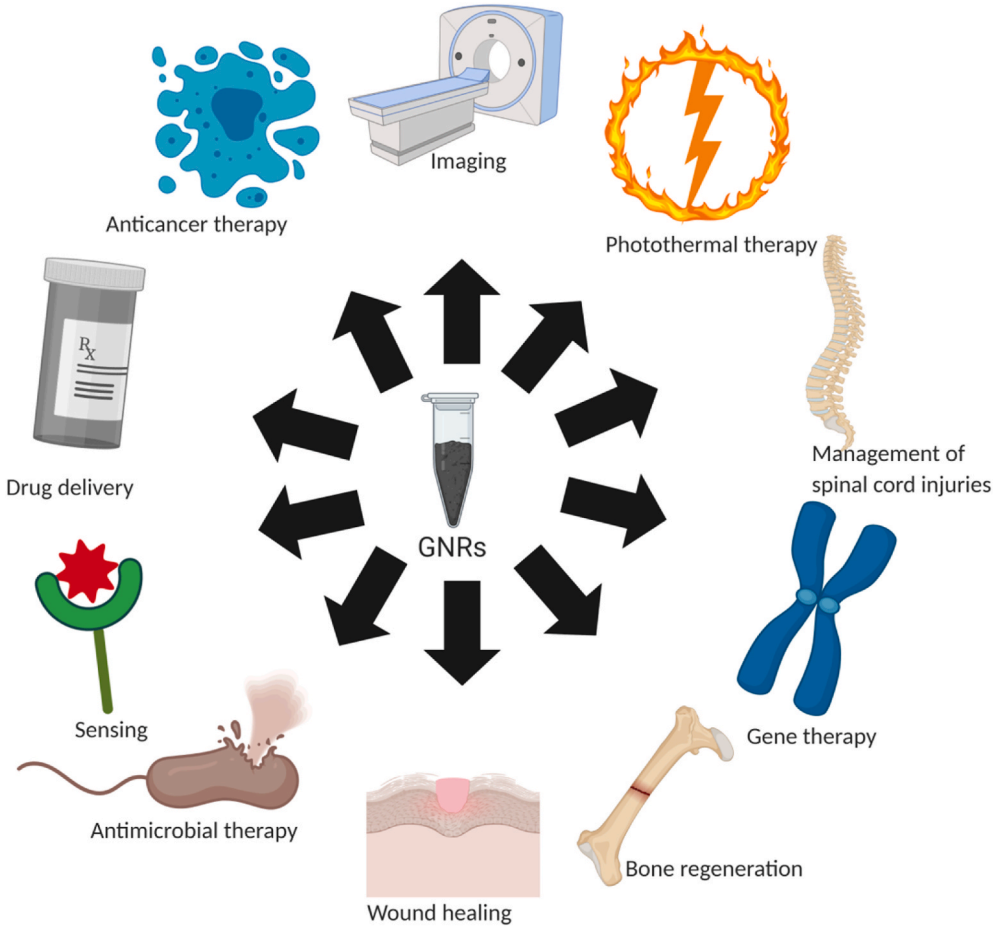

Fig. 1. Biomedical applications of GNRs.

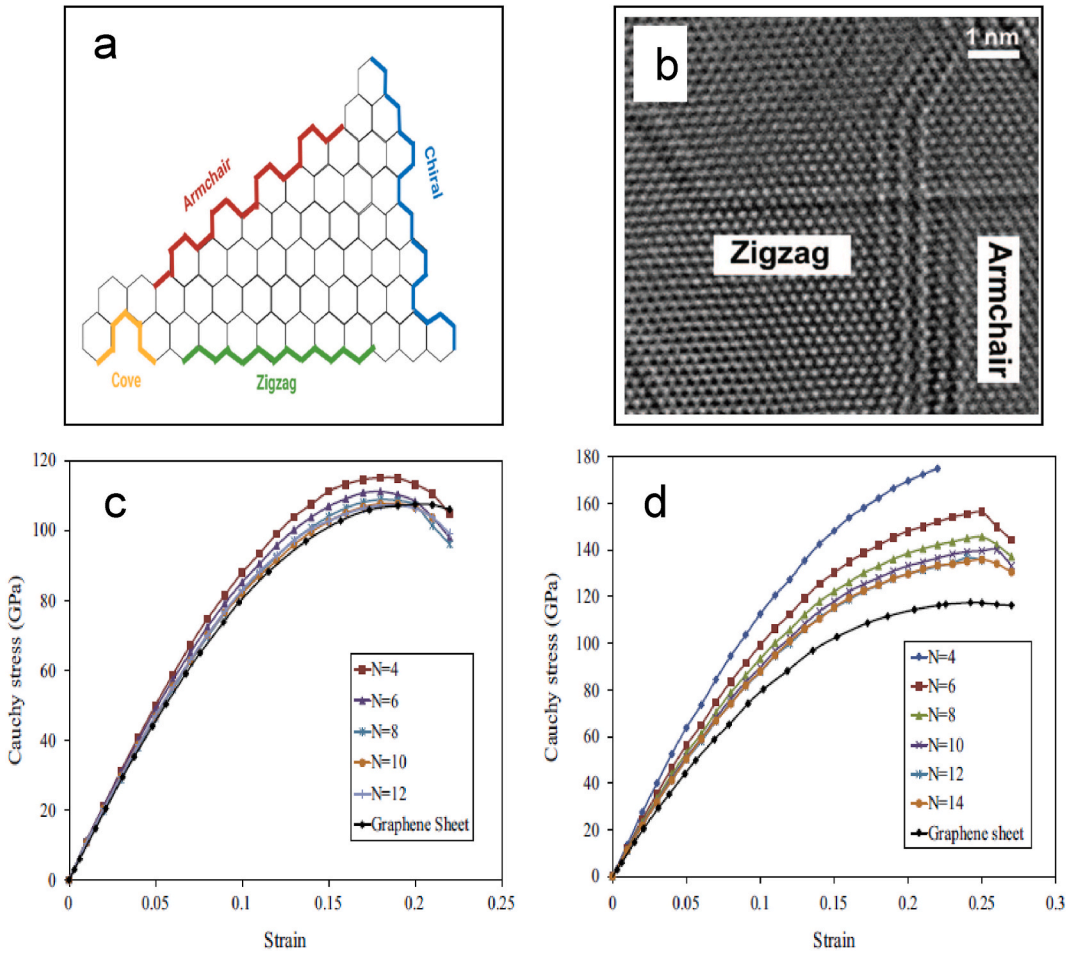

Fig. 2. **a**) Different edge states of GNRs **b**) HRTEM image of GNR. "Reprinted with permission from (Campos-Delgado et al., 2008) Copyright (2008) American Chemical Society. **c**) Stress-strain curve of AGNRs with different width **d**) Stress-strain curve of ZGNRs with different width. "Reprinted with permission from (Tabarraei et al., 2015) Copyright (2014) Elsevier.

approach towards the field of biosensing(Lyu et al., 2018).

3. Properties of GNRs

3.1. Physico-chemical properties

GNRs are extended strips of single-layered graphene with definite width or graphitic quasi-one-dimensional nanostructure and have sp^2-hybridized carbon (Prezzi et al., 2008). GNRs possess a crystalline structure and have an ultra-high surface area (Mousavi et al., 2019; Zhu et al., 2009). The non-functionalized GNRs show high solubility in chlorosulfonic acid, but are insoluble in most other solvents. GNRs are water-insoluble and significantly reduce their ability to interact with water molecules by trying to form a closely packed self-assembled layer of stacked nanoribbons(Mehdi Pour et al., 2017).

GNR surfaces often seem to be chemically inert, and these surfaces normally interact with other molecules via physical adsorption (interactions) similar to graphene. The properties of GNRs rely on edge type and the nature of edge substituents. Intrinsically, nanoribbons possess dangling bonds at the edges to provide active sites for chemical modification. Modifications can be done in several ways: by s-type, p-type, and d-type elements functionalization or by functional groups (Kan et al., 2008; Lee et al., 2010; M. Wu et al., 2010a). Various functional groups such as carbonyl (-CO), carboxyl (-COOH), amines ($-NH_2$), and hydrogenated (-CH) could be positioned at the chemically more reactive edges of GNRs (Terrones et al., 2010). Based on the nature of carbon termination, the chemical reactivity of the edge could be changed (Terrones et al., 2010).

GONR is perfect for the biosensing of molecules having high oxidation potential, while rGONR show an excellent response to aromatic molecules in which π- π interactions are dominant. rGONR can restore the sp^2 structure that reduces during the oxygenation, which results in high electrical conductivity of rGONRs. The presence of high sp^2 content increases the interaction of rGONR with aromatic molecules. Hence rGONRs are a better candidate for the sensing of aromatic molecules in which π- π interactions were dominant. Also, the presence of remaining oxygen functionalities and high sp^2 content of rGONR results in a better electrochemical performance towards analytes (Martín et al., 2014, 2015b). The high oxygen functionalities on the GONR surface provide an opportunity for the analytes to interact through hydrogen bonding interactions and trigger an electrochemical response at the electrode. The high surface area, wide bandgap, and presence of high oxygen functionalities make GONRs an ideal platform for the detection of molecules having high oxidation potentials (Martín et al., 2014).

3.2. Electronic properties

Bandgap engineering of graphene is a crucial move towards electronic and sensing applications. The fact implies that GNR can act as a semiconductor switch (Abbas et al., 2014). Electron confinement, edge structure, strain, width, elastic strain, and doping are the key factors affecting the emergence of the bandgap (Corso et al., 2018).

The modification of electronic properties can be done by electric fields, magnetic quantization, and lateral confinement. The energy

dispersions are collapsed with zero energy spacing for a strong electric field. Various characteristic features like large electron mobility and improved sensitivity to electronic perturbations resulting from the binding of molecules make them attractive for fabricating biosensor devices (Mao and Chen, 2017). Replacement of one or more carbons by adding impurities into the framework is another successful means of controlling the electronic properties of GNR. Impurities intrinsically associated with boron (B) and nitrogen (N) play the role of n-type and p-type doping in carbon-based materials. Moreover, the doping mechanism is exquisitely sensitive to the position and density of dopants along with the type and width of the nanoribbon (Gorjizadeh and Kawazoe, 2010; Lherbier et al., 2008; Yu et al., 2008). When B(N) substitution happens in the center of the AGNRs, a semiconductor to metal transition takes place (Cervantes-Sodi et al., 2008). Meanwhile, the substitution at the edge position does not change the electronic properties of the ribbon. In the case of Z-GNRs, the B and N substitution at the ribbon edges induce semiconductor to metal transition have shown rendering them semiconducting, half-metallic, or metallic by regulating the distance of the N or B impurity atoms to the edge (Cervantes-Sodi et al., 2008; Zheng et al., 2010). The replacement of one edge carbon with B atoms and the other edge carbon with N atoms make the ribbons half-metallic. Half-metallicity can also be attained by substituting the carbons in the middle of zig-zag nanoribbon by B-N chains (Dutta et al., 2009). Theoretically, the bandgap can be minimized up to 0.27 eV by the steric repulsion between the aromatic protons and the inserted alkyl chains through the structural distortion. These systematic and uniform deviations from planarity can influence the electronic and optical properties of GNRs (Hu et al., 2018).

Interestingly, the electronic properties of both AGNR and ZGNR are different. For ZGNR, the energy subbands are parabolic dispersions with the exception of two partial flat subbands at the Fermi level. Moreover, the energy spacing is almost consistent and will shrivel as the ribbon width increases. The two partial subbands are intensely attached to the ribbon edges, and the charge density decomposes in proportion to the distance from the edges. In contrast, AGNR has many parabolic subbands, and energy spacing is non-uniform. Besides, the energy gap varies inversely to ribbon width (Chung et al., 2016).

A nonlinear current-voltage relationship was observed for ZGNRs because overlapping of π and π* bands around the Fermi level. Within a certain limit, the current increases linearly with applied bias voltage. As the width of ZGNR increases, the overlapping of the bands increases. Thus, the linear relationship of the current-voltage response gets narrower. On the other hand, the bandgap decreases with an increase in ribbon width for AGNRs, resulting in semiconductor properties (Hou and Yee, 2007).

3.3. Mechanical properties

Graphene is suitable for the fabrication of robust biomedical devices due to its high strength. The Young's modulus is directly proportional to the nanoribbon width for both armchair and zig-zag directions (Orlov and Ovid'ko, 2015). The fracture stress and strain are inversely proportional to nanoribbon width. However, this effect is less sensitive for armchair direction. The maximum fracture stress for tension in the zig-zag and armchair directions is around 130 and 98 GPa, respectively. Meanwhile, the maximum fracture strain for nanoribbons deformed in the zig-zag and armchair directions is around 0.2 and 0.12, respectively (Fig. 2c & d) (Orlov and Ovid'ko, 2015). The zig-zag edge energy is lower than the armchair edge energy, which indicates that the fracture surface is mostly the zig-zag type (Xu et al., 2012). Poisson's ratio of nanoribbon can be calculated by uniaxial loading. Poisson's ratio of AGNR is size-dependent(Tabarraei et al., 2015). The inherent tensile and field strengths of GNR serve as a gold standard for high-stress mechanical tuning of an electrochemical sensing system (Mazilova et al., 2019).

3.4. Optical properties

A wide range of photons can be absorbed by GNRs from terahertz, infrared, and visible regions. A lot of absorption peaks are observed for the low energy optical spectra of GNR (Balarastaghi et al., 2016). Although AGNRs and ZGNRs have entirely different optical selection rules, the edge structures and finite width play a major role in the selection rule (Hsu and Reichl, 2007). The photoluminescence character of GNR arises from the reduction of the π electron network (Goenka et al., 2014).

The effects of an electrical field, lateral confinement, and magnetic quantization can alter the optical spectra of GNRs. With an increase in the electric field, the eminent peaks are lowered, and subpeaks emerge. The intensities of the two peaks can be compared when they coexist. Extra optical transitions take place in the presence of an electric field resulting from the mixing of adjacent standing waves in the distorted wave function (Chung et al., 2016). GNR's ability to absorb the wide range of photons from terahertz to infrared and visible makes them a strong choice for biosensing as photodetectors (Balarastaghi et al., 2016). The tunable and broadband absorption and strong polarization-dependent effects are the basis for the construction of GNR-based biosensors (Li et al., 2019).

3.5. Thermal properties

The thermal properties are important from the perspective of the device performance of the electronic industry. Identifying material with large thermal conductivity, which can be integrated with Si complementary metal-oxide-semiconductor (CMOS) technology, is a probable way of resolving the thermal dilemma (Semenov et al., 2006). Carbon and diamond nanotubes were considered for such applications (Biercuk et al., 2002; Jin and Mavoori, 1998). Because of the large thermal contact resistance they are not suited for integration with CMOS. Whereas, the diamond and CNTs, GNRs can be coupled directly to heat sinks and hence mitigate the concern of thermal contact resistance (Ghosh et al., 2008). It indicates that GNRs can be an ideal element in the CMOS systems and circuits for thermal control. Investigations reveal that GNRs exhibit long phonons represent free paths and strong thermal conductivities. It is susceptible to the GNRs edge shapes, length, width, and strain, and it varies depending on the length, width, and strain (Guo et al., 2009). These do not unite to a fixed value with the increase of GNRs length up to 60 nm. Also, it is susceptible to the width of GNRs (i.e., no. of atoms N). The thermal conductivity of ZGNRs upsurges first and then decreases with the increase in N, while, for AGNRs, it increases with N (Guo et al., 2009). Combined with their specific electronic properties, the thermal properties of the GNRs render them ideal candidates for potential CMOS nanodevices.

The thermal conductivity of GNR increases with the length along with the entire temperature range. The heat transport anisotropy of GNR at room temperature indicates that the thermal conductivity of ZGNR is higher in comparison with AGNR. However, the anisotropy disappears when the width is higher than 100 nm indicating that the thermal conductivity can be regulated by adjusting edge orientation (Johnson et al., 2020). Also, the compressive uniaxial strain can decrease the thermal conductivity of GNR (Guo et al., 2009). Moreover, as the distance decreases or the temperature rises, the thermal conductivity decreases considerably due to declining relaxation times (Ye et al., 2015). Interestingly, the thermal conductivity can decrease by inserting pores into them to increase their thermo-electrical efficiency in devices (Sharafat Hossain et al., 2015).

The presence of bandgap yields a great thermosensitivity to GNRs and is useful in the fabrication of temperature sensors. The thermally activated electrons and hole pairs of GNRs produce temperature responses. The nanoscale effects like bandgap, local traps, and oxygen doping increase the thermosensitivity of GNR-based sensors. The GNR-based temperature sensor can operate directly without any reduction

process due to the good conductivity of GNR with relatively low-defect density. Hence GNRs are well suited for fabricating disposable temperature sensors (Gong et al., 2020).

4. Synthesis of GNRs

The top-down and bottom-up approaches are the two methods for the synthesis of GNRs (Fig. 3). The top-down approaches consist of patterning a graphene sheet (GS) until a required shape and size is reached (Marmolejo-Tejada and Velasco-Medina, 2016). The bottom-up approaches consist of assembling the building blocks into a composite structure (Curri et al., 2010). Both methods have advantages and disadvantages. The notable advantage of top-down approaches is the ability to produce GNR with micrometer length. However, their demerits include poorly defined chiralities, complicated procedures, and lack of reproducibility. On the other hand, bottom-up methods produce GNRs with discrete geometrical and structural properties with a low polydispersity (Pefkianakis et al., 2015). The bottom-up approaches result in GNRs with exceptional optical, electrical, and magnetic properties (Niu et al., 2019).

4.1. Top-down synthesis

4.1.1. Lithographic patterning

The lithographic method eludes the complications of gathering nanoscale components and allows the realization of complete integrated circuits in biosensing. GNRs with a minimum width of 10 nm are fabricated by E-beam lithography (Fig. 4a)(Celis et al., 2016). The method has the advantage of forming a large number of arrays of aligned single layer GNR. However, there is no precise control over the edge smoothness and ribbon width since the etching process causes damage. Also, the large-scale production of GNR by lithographic patterning is challenging because of its high vacuum and tedious nature (Han et al., 2007). Meanwhile, the helium ion beam lithography offer a high resolution than E-beam lithography (Xu et al., 2016). Ultranarrow-aligned GNR arrays down to 5 nm with superior chemical sensing property can be achieved with this method (Abbas et al., 2014).

Dip pen nanolithography can draw nanowires and nanorods directly with precise control (Demers et al., 2002). Here, the unprotected areas of the graphene sheets (GS) are removed on exposure to oxygen plasma after thermal drying under a vacuum. The dry etching process results in graphene removal, and subsequent sonication with an organic solvent and distilled water results in the removal of nanorods. Dip pen nanolithography creates patterns directly on the substrate using a tip. The GNRs produced by dip-pen nanolithography have a width down to 25 nm (Xu et al., 2016). Scanning tunneling microscopy (STM) lithography helps to learn the unique properties of GNR with atomic level precision (Tapasztó et al., 2008).

In order to overcome the challenges inherent with the conventional approaches, many advanced lithographic techniques are available for the large scale fabrication of GNRs. Block-copolymer lithography, graphene edge lithography based on selective atomic layer deposition, meniscus-mask lithography, and nanowire lithography are among them. In block co-polymer lithography, block co-polymers are used as templates to synthesize GNR arrays (Liu et al., 2012; Son et al., 2013). Graphene edge lithography and meniscus-mask lithography are used to protect graphene etches during dry etching (Abramova et al., 2013; Xie et al., 2012). Nanowire lithography can be either inorganic nanowire lithography, where inorganic nanowires are used as a physical etching mask during lithographic fabrication of GNR, or which prints organic nanowire with digitally controlled precision of alignment (Holmes et al., 2000; Min et al., 2013).

4.1.2. Sonochemical method

Long and narrow layer GNRs with a smooth edge can be synthesized by sonochemical cutting of chemically derived GS (Fig. 4b)(Wu et al., 2010b). This method is a mechanochemical approach that involves two steps. The initial step involves the chemical exfoliation of graphite to chemically derived GS (Xu and Suslick, 2011). The second step is the sonochemical cutting of GS into GNR. GSs are produced from artificial graphite by methods like oxidation, dispersion, thermal exfoliation, H_2 reduction, and centrifugation (Wu et al., 2008). GSs line faults formation and distribution play a pivotal role in GNR design and structure. The advantages of the method include high yield and narrow GNR, but with a specific disadvantage of lacking edge orientation (Z.-S. Wu et al., 2010b).

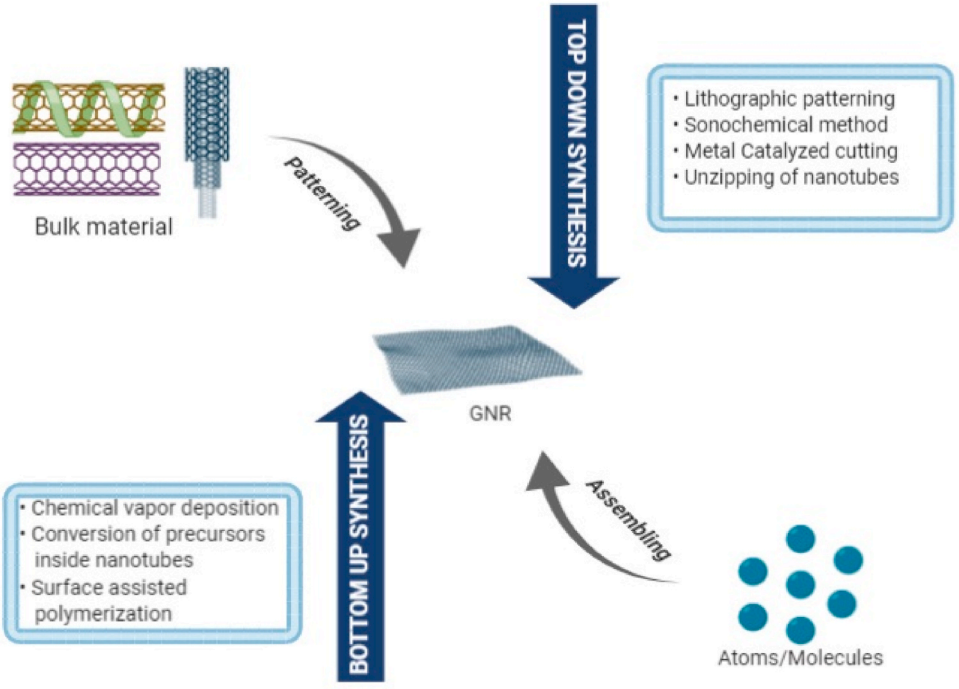

Fig. 3. Different approaches for the synthesis of GNRs.

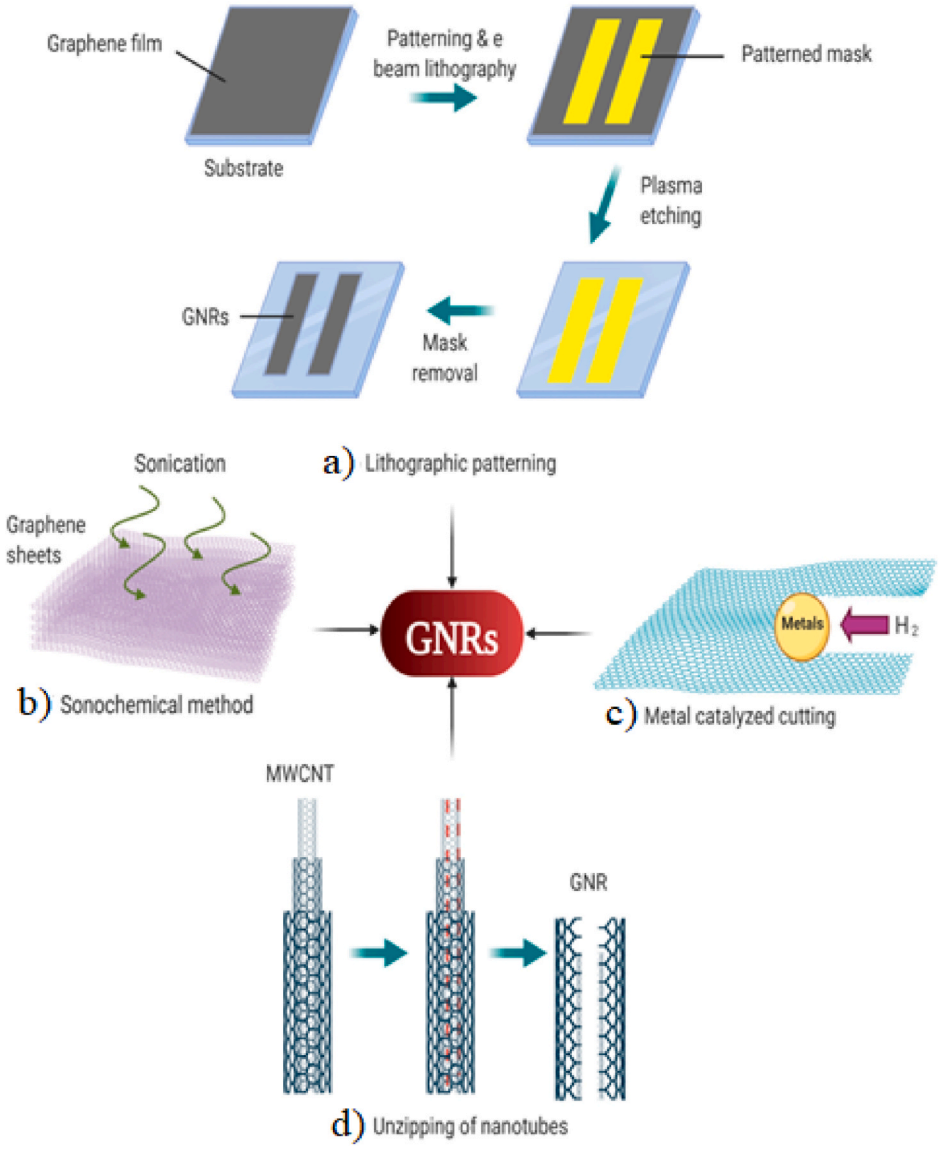

Fig. 4. Schematic representation of various top-down approaches.

4.1.3. Metal catalyzed cutting

The deposition of catalytic metal on graphene flake in the presence of the hydrogen atmosphere results in catalyzed cutting (Fig. 4c). This interaction results in the etching of graphene. Catalytic reaction favors the dissociation of carbon-carbon bonds. GNRs of smooth edges are formed when the cutting paths of the particle run parallel to each other (Campos et al., 2009). The various metals used for catalyst-dependent cutting behavior are iron, nickel, cobalt, platinum, and silver (Elias et al., 2010). The method results in the formation of long straight GNR with smooth edges. The synthesis of highly conductive straight narrow GNRs from ridges and wrinkles of graphene flakes is possible by this method (Park et al., 2016). However, a deep understanding of the cutting direction and catalyst-dependent cutting behavior is still not known (Ma et al., 2014).

4.1.4. Unzipping of carbon nanotubes

Unzipping of carbon nanotube (CNT) is the widely used method for the fabrication of GNR for sensing applications. This method creates many structural defects that are truly favorable for electrocatalytic sensing applications (Rajaji et al., 2018). The chemical reaction can result in the production of GNR with definite size distribution. Graphite precursors can undergo a series of chemical reactions in proper solvents, which results in the synthesis of GNRs. Among them, the use of single-walled carbon nanotube (SWCNT) or multi-walled carbon nanotube (MWCNT) as graphite precursors is most common (Fig. 4d)(Celis et al., 2016). Dispersion of precursors in solution with specific chemical reagents results in the unzipping of the walls. Narrow GNR can be fabricated from an array of SWCNT by polymer-protected Ar plasma etching methods(Jiao et al., 2010). A hydrothermal approach using counter ions results in longitudinal unzipping of MWCNT to GNRs with selective intercalation and exfoliation. This method offers advantages like economical scale-up, one-pot, total unzipping, and large output. However, the intercalation of cations results in a change in electronic properties that can affect sensing properties (Shinde et al., 2014). Meanwhile, longitudinal unzipping of CNT using a mixture of strong acid and oxidant also results in the formation of GNR (Li et al., 2016b). This oxidative unzipping of MWCNT involves three steps; intercalation unzipping, oxidation, and exfoliation (Dimiev et al., 2018).

Plasma etching of nanotube, partly embedded in a polymer film, is another unzipping method of MWCNT to produce GNRs. This method results in the production of GNR with controllable structure and quality (Jiao et al., 2009). Irradiation of MWCNT with excimer results in the

production of GNRs. This method is time-saving and yields pure GNR samples (Kumar et al., 2011).

Another simple and effective method for producing GNR with smooth edges from MWCNT is a microexplosion method. In this method, MWCNTs are filled with potassium vapor and exploded with water, where potassium causes intercalation and exfoliation of graphite. The reaction of potassium with water releases gas and heat and cause exfoliation (Viculis et al., 2005). The high temperature during reaction will cause quick expansion, resulting in the splitting of MWCNT to form GNR. It is a simple and effective technique for the production of GNR with smooth edges. Meanwhile, high production cost and partial unzipping is the disadvantage associated with this method (Fan et al., 2010). Another chemical route for the synthesis of GNR is the longitudinally unzipping of MWCNT. This route involves the exposure of pristine CNTs to hot potassium vapor, followed by protonation. This step is followed by bath sonication in chlorosulfonic acid to affect the highly stacked GNR exfoliation. The resultant low-defect and highly conductive GNRs are well fit for various biosensing applications(Kosynkin et al., 2011).

Moreover, unwrapping of MWCNT by electric current and nanomanipulation creates GNR of definite length. The formation of GNR by this approach involves three steps. Firstly, the electric current induced rupture of the walls of MWCNT occurs. After this, intershell sliding between GNR and inner core results in the production of GNRs with high current carrying capacity. Finally, the partial outer wall rupture of MWCNT leads to the generation of a precursor GNR in the inner core of MWCNT (Kim et al., 2010). The structural defects and edge irregularities are beneficial in electrochemical sensing by facilitating easy and efficient linking of co-transducers and biosensing elements such as enzymes, DNA, RNA, etc.

4.2. Bottom-up synthesis

Various bottom-up approaches for the synthesis of GNRs include chemical vapor deposition (CVD), conversion of precursor inside the nanotube, and surface-assisted polymerization. Necklace-like GNR can be prepared by a bottom-up method based on oxidative cyclodehydrogenation of tailor-made polyphenylene precursors (Schwab et al., 2015).

4.2.1. Chemical vapor deposition

CVD is a process of GNR generation where the substrate is exposed to one or more volatile precursors that decay on the surface of the substrate. In this method, a metal template acts as a catalyst for the decay of hydrocarbon at higher temperatures. The size of the GNR is entirely dependent on the catalytic template(Celis et al., 2016). It is easy to prepare GNR with tunable width and length (Genorio and Znidarsic, 2014).

Metal-organic CVD, plasma-enhanced CVD, low-pressure CVD, laser-assisted CVD, and aerosol-assisted CVD are various modifications of the CVD method (Benelmekki and Erbe, 2019). Facile and large area transfer of GNRs into the insulating substrate and subsequent devices by the CVD method shows their potential application in biosensors. They generate a high current on and off ratio results in high sensitivity than other types of transistors (Chen et al., 2016)

4.2.2. Conversion of precursor inside the nanotube

GNR can be prepared by the encapsulation of small carbon-based molecules inside SWCNT (Talyzin et al., 2011). Interestingly, GNR produced by such a method has exciting properties of both materials. This method offers narrow GNR with well-defined edges. However, the diameter of GNR depends on the precursor. A bottom-up approach was tried recently using boron nitride nanotubes with excellent chemical and thermal stability. The first step involves encapsulation and polymerization of coronene molecules on the exposure of boron nitride nanotubes to vapor of coronene in a vacuum atmosphere (Fujihara et al., 2012). The resultant GNR can be removed by oxidation at temperatures above 500 °C from the inner cavity of boron nitride nanotubes (Barzegar et al., 2016). The electronic properties of GNRs obtained by this method finds potential in photonics and nanoelectronics applications because of their unique properties (Talyzin et al., 2011).

4.2.3. Surface-assisted polymerization

The surface assisted polymerization and cyclodehydrogenation of organic precursors is another approach towards the synthesis of GNRs. The various stages of on-surface synthesis include the design of building blocks, dehalogenation, polymerization, and cyclodehydrogenation (Narita et al., 2019; Talirz et al., 2016). GNRs are prepared from monomeric precursors that react on the catalyst surface. Initially, the polymeric chains are produced by the sublimation of monomers or their derivative on a hot metallic surface. The former step is followed by dehydrogenation of polymers by annealing at higher temperatures resulting in GNRs. Oxidative cyclodehydrogenation is one of the effective methods for the synthesis of GNRs in solution. The surface assisted oxidative cyclodehydrogenation is carried out in two thermal activation steps. The first step involves the coupling of surface adsorbed monomers to linear chain followed by planarization into GNRs by intramolecular cyclodehydrogenation (Hernandez et al., 2012). The atomic structure and dimension can be achieved by this method. However, large scale production is difficult.

4.2.4. Suzuki-Miyaura coupling reactions

Small GNRs can be prepared by synthetic routes through linking tetra- and hexa-phenyl benzenes via Suzuki-Miyaura reaction (Yang et al., 2008). The cyclodehydrogenation of the formed poly-phenylenewith $FeCl_3$ as the oxidant results in the ribbon formation with 6–12 aromatic polycyclic repeating units. This is a real bottom-up strategy for short and thin AGNRs.

4.2.5. Diel's alder polymerization

Diels–Alder (D-A) polymerization route can be used for preparing tailor-made polyphenylenes, which can serve as precursors in the preparation of structurally well-defined GNRs having long lengths, different widths (up to 4600 nm), and tunable electronic bandgaps. Structurally well-defined poly phenylenes begin with D –A polymerization of tailor-made monomers in the case of solution method GNRs synthesis. Such polyphenylenes are transformed straight to GNRs by intramolecular oxidative cyclodehydrogenation(Hou et al., 2018).

4.2.5.1. A_2B_2-type D–A polymerization. Amethodwas developed to synthesize GNRs using A_2B_2 type D-A polymerization (Wu et al., 2003) (Fig. 5a). They reacted 1,4-diethynyl-2,5-di(4′-tert-butylphenyl)benzene (**1**) with 4,4'-(1,4-phenylene)bis(2,3,5-triphenylcyclopenta-2, 4-dien-1-one) (**2**) inorder to get desiredD-A polymerization (A_2B_2 type), giving the tert-butyl-substituted polyphenylene (**3**). On the planarization of this polymer through oxidative treatment with $FeCl_3$ in nitromethane, armchair GNR (**4**) is formed. However, because of the difficulties of precisely monitoring the stoichiometry of these two distinct monomers used in the polymerization, the lengths of such GNRs are limited. This drawback is undesirable for the production of single-GNR-based devices.

4.2.5.2. AB-type D–A polymerization. The difficulty in controlling the stoichiometry can be reduced to get longer GNRs by adopting an AB-type D–A polymerization approach rather than following the A_2B_2-type approach(Hou et al., 2018). This approach was reported by the above group to produce 'cove'-type GNRs (Fig. 5b). The monomers having a cyclopentadienones (**5**),were conjugated diene and an ethynyl group as the dienophile are subjected to D–A polymerization to produce the alkylated polyphenylene precursor (**6**), which on intramolecular oxidative cyclodehydrogenation using $FeCl_3$ as oxidant produce GNRs

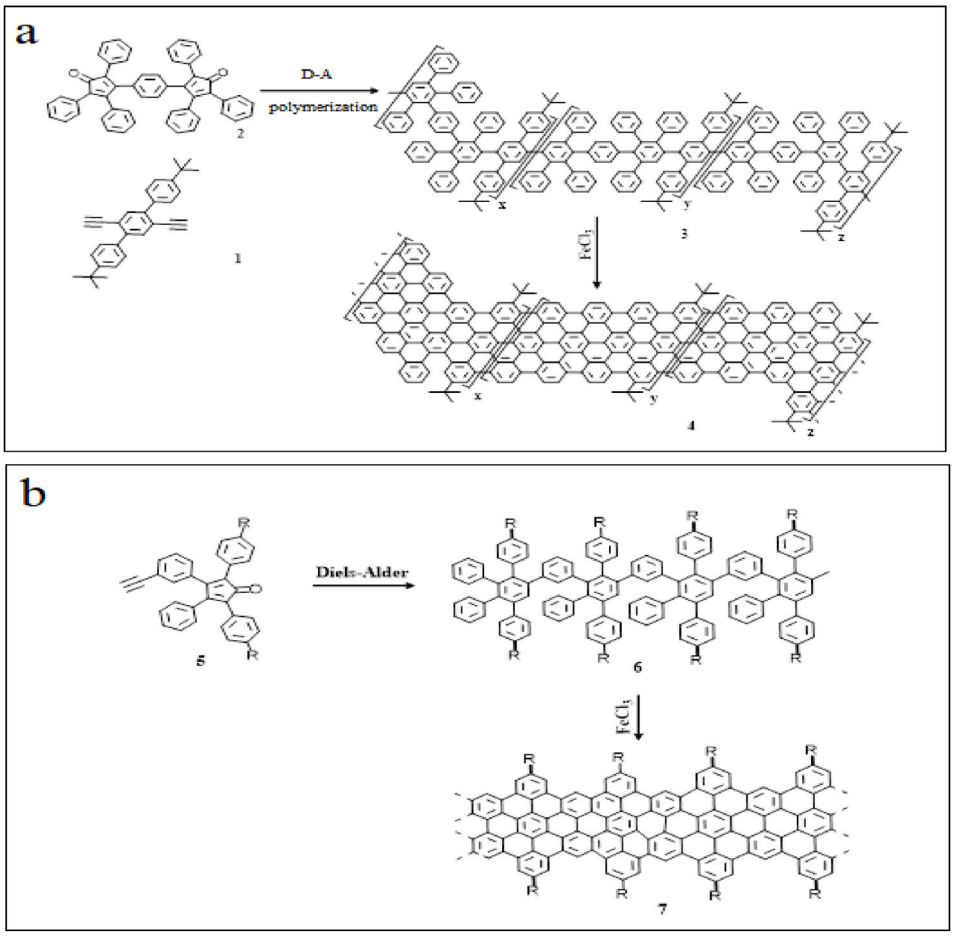

Fig. 5. a) Synthesis of GNRs through A_2B_2-type Diel's Alder polymerization (Hou et al., 2018) **b)**Synthesis of GNRs through AB-type Diel's Alder polymerization (Hou et al., 2018).

(**7**). The alkylated polyphenylenes synthesized by the AB-type D–A polymerization protocol provide extraordinary lengths of up to 600 nm (Narita et al., 2014)generated from their alkylated polyphenylene precursors. The degree of polymerization (GNR length) was markedly higher than that of polyphenylene precursors formed by A_2B_2-type D–A polymerization and other metal-catalyzed coupling reactions like the Suzuki and Yamamoto polymerizations (Hou et al., 2018).

Finally, D–A polymerization generates an appositive strategy toward high-degree polymerized polyphenylenes for bottom-up GNR synthesis. In particular, AB-type D–A polymerization equips GNRs with an extraordinary length of over 600 nm. This length exceeds that of GNRs constructed by other reactions like the aryl–aryl coupling catalyzed by metal, which results up to 100 nm only. Optoelectronic properties can be tuned by expanding the monomer structure and the width of the GNRs. However, effective synthesis of GNR via the AB-type D–A reaction has so far been restricted to monomers dependent on ethynyl-substituted cyclopentadienones. The next task, thus, will be the creation of new AB-type monomers armed with various dienes and dienophiles to synthesize a wider variety of GNRs with inimitable structures, heteroatom doping, and/or additional functional groups, thus maintaining the length of more than 100 nm. Synthesizing low bandgap GNRs with infrared absorption without stretching the ribbons is particularly desirable.

5. Modified GNRs

The construction of a GNR-based biosensor generally needs the surface modification of GNRs. To expand the sensitivity, stability, and electrocatalytic activity, modification of the GNR is needed. Both covalent and non-covalent modifications are possible with GNRs (Genorio and Znidarsic, 2014). Covalent functionalization of the GNRs is achieved with the chemical conjugation of the molecules with the oxygen-containing functionalities of GONRs or by cycloaddition reactions (Reina et al., 2017). Non-covalent modification of GNRs is possible with Van der Waals force and π-π interactions (Liu and Speranza, 2019). GNR-based biosensors work by the non-covalent interactions of bioreceptors on the GNR surface. Nowadays, GNR-modified metal nanoparticles-based electrochemical sensors are more popular because of the enhanced electrocatalytic activity and surface area of the GNR. Metals such as palladium, nickel, gold, silver, cadmium, molybdenum, and ruthenium are useful for modifying GNRs. Besides, graphene-based hybrid nanomaterials enhance the efficiency of detection (Pham et al., 2019). Similarly, hybrid materials of GNR with pristine graphene and other graphene derivatives such as GSs, MWCNTs, SWCNTs, and GQDs are also popular for the enhanced surface area (Lavanya et al., 2017; Yaqi Li et al., 2017; Zakaria and Leszczynska, 2019). Doping with suitable atoms and drilled nanopore on the GNRs offers wide application in sensing and sequencing of nucleobases (Rastgoo and Fathipour, 2019; Wasfi et al., 2019). GNR modification with polymers, molecularly imprinted polymers, and metal-organic frameworks are also used in the fabrication of GNR-based biosensors (Hossain and Park, 2017; Pan et al., 2015; Tang et al., 2017). Various modifications of GNR for biosensing applications are illustrated in Fig. 6a and the different modifications and their effects on sensing are provided in Table 1.

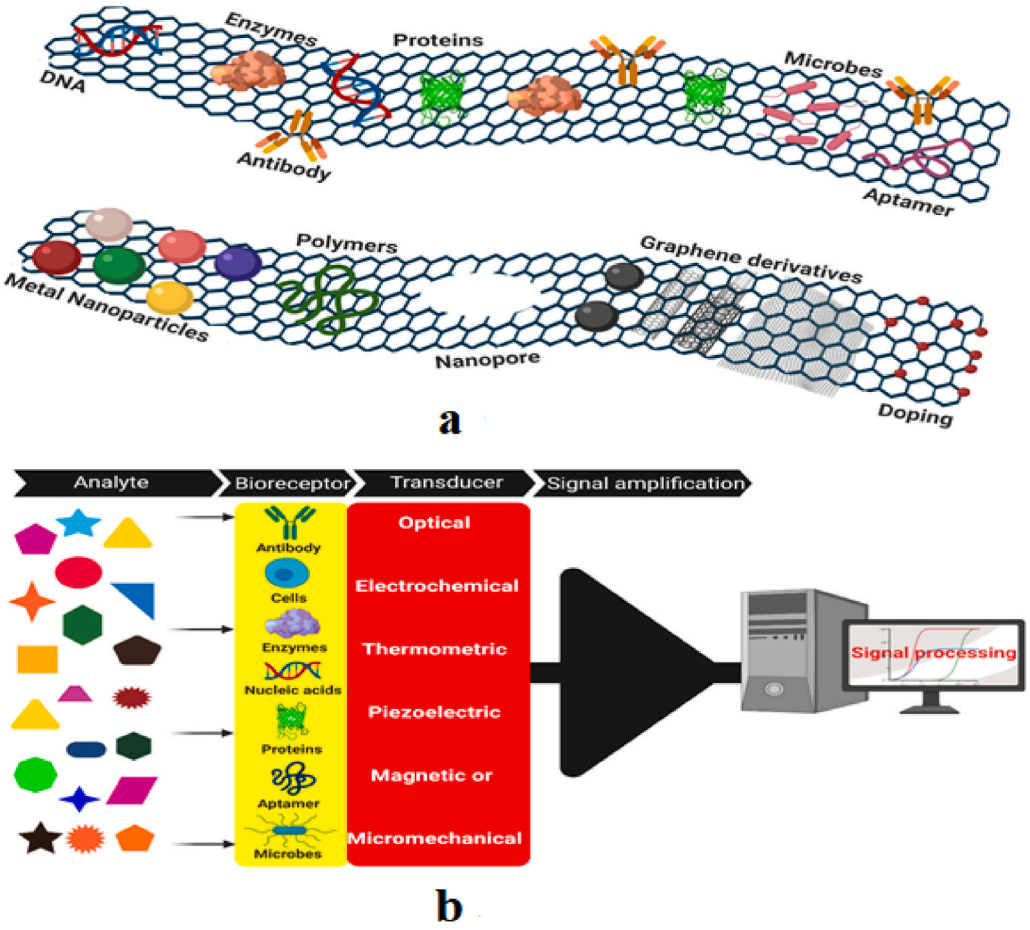

Fig. 6. **a)** Modification of GNRs for sensing applications **b)** Parts of a biosensor.

6. GNRs in biosensing

A biosensor is an analytical device used for the detection of a chemical substance that combines a biological component with a physical transducer. Generally, biosensors consist of two main parts, a receptor (biological recognition element), and a transducer. The receptor interacts with the analyte, and the transducer converts the information regarding the interaction to a measurable signal. The target molecule can be organic, inorganic, or even a cell. The parts of a biosensor are illustrated in Fig. 6b. Graphene-family nanomaterials are used extensively as a transducer of biosensing devices, which are involved in the conversion of interactions between analyte and receptor to an easy-to-use format. GNR and its derivatives offer extensive possibilities in biosensing and electrochemical sensing owing to its unique electrical conductivity, ultrahigh surface area, good adsorption capacity, high mechanical strength, optical properties, and ease of functionalization. Further, as described earlier, the modification of GNR enhances its prospects of biosensing. Based on the transduction elements, GNR biosensors can be classified into electrochemical, optical, and field-effect transistors (FETs).

6.1. GNR-based electrochemical biosensors

An electrochemical sensor is a device that is functioning with an electrochemical transducer that can transform biochemical information such as analyte concentration into an analytically useful signal: current or voltage (Anusha et al., 2019). The main component of an electrochemical biosensor is the working electrode. The electrode used should be an electronic conductor, and hence, the electrodes are of conducting and semiconducting materials. Hence GNRs are better electrodes for electrochemical sensing (Anusha et al., 2019; Cesewski and Johnson, 2020). Electrochemical biosensors with different electrochemical approaches are potentiometric, amperometric, impedimetric, and voltammetric methods. Biocatalytic or biocomplexing like biorecognition elements are used in electrochemical sensing. The most commonly used biorecognition elements are tissues, whole cells, enzymes, antibodies, aptamers, and molecularly imprinted polymers. In biocatalytic type recognition elements, the response is based on the catalytic reaction by macromolecules. But the biosensor response of biocomplexing type is by the interaction of macromolecules with analytes or organized molecular assemblies (Cesewski and Johnson, 2020).

The working of GNR-based devices is based on the principle of changing conductance due to the action of adsorbed chemical or biological species as donors or acceptors. The electrochemical reactions of analyte molecules on the GNR-based electrode are affected due to the excellent electron transport properties and high electrocatalytic activity. Amperometry and voltammetry are the most accepted transducing approaches in the development of GNR-based sensing techniques due to their low cost, simplicity, and significant sensitivity. These belong to the potentiostat techniques in which controlled and applied electrode potential drives the electron transfer reaction, resulting in a measured current. Amperometric biosensors constantly measure the current formed during the oxidative and reductive reactions of electroactive species during the biochemical reactions. Here, the current is linearly dependent upon the analyte concentration. This method exploits the oxidation or reduction property of certain electroactive species in GNR-based electrodes working at a constant applied potential. During the redox reactions, the electrons are transported to the working electrode from the analyte or vice versa (Parkash and Shueb, 2015). Chronoamperometry is an advanced amperometric technique, where the

Table 1
Modification of GNRs and its effects on sensing.

Materials/process used for modification of GNR based sensors	Effect of modification	References
Silver nanoparticles	High catalytic activity and facilitated electron transfer	Kumar and Goyal (2018)
	As a colorimetric sensing probe	Rostami et al. (2020)
Manganese dioxide nanoparticles	Improved electrocatalytic performance and surface area	Vukojević et al. (2018b)
Gold nanoparticles	Improved conductivity, electrocatalytic activity and surface area	(Tang et al., 2017)(Ismail et al., 2014)
Gold nanocages	Enhanced surface area and conductivity	Feng et al. (2018)
Carbon nanotubes	Prevent aggregation tendency of GNRs, facilitates electron transfer, Improved fluorescence quenching ability, superior oxidation currents	(Yi et al., 2016)(Yaqi Li et al., 2017)(Liu et al., 2015)
Ruthenium oxide nanoparticles	Enhanced electron transfer	Vukojević et al. (2018a)
Graphene nanosheets	Enhanced surface area and enhanced electrochemical activity and stability.	(Jothi et al., 2018)(Lavanya and Gomathi, 2015)(
	Reduction of restacking Good conductivity	Lavanya et al., 2017)
Graphene quantum dots	Improved stability and biocompatibility	Zhao et al. (2019)
CdTe quantum dots	Strong fluorescence	Yaqi Li et al. (2017)
	Amplified electrochemiluminescence with graphene nanomaterials	Huan et al. (2015)
Molybdenum disulfide	Strong catalytic property	Zhao et al. (2019)
AuPt-methylene blue	Outstanding electrochemical activity	Tang et al. (2017)
	Signal generation and amplification	
Palladium-platinum alloy nanoparticles	High catalytic performances	Yan Li et al. (2017)
Palladium-nickel alloy nanoparticles	High catalytic performances	Li et al. (2015)
Palladium-silver alloy nanoparticles	Improved electrochemical performances	Shang et al. (2015)
Amino functionalized fullerenes	Introduced as a carrier to increase the loading capacity	Yan Li et al. (2017)
Silver particles	Excellent electrocatalytic activity	Govindasamy et al. (2017a)
Nickel nanoparticles	Good electrocatalytic activity	Lavanya et al. (2017)
Platinum nanoparticles	Conductivity enhancement and reduction of charge transfer resistance	(M. Lee et al., 2018a)
Metal organic frameworks	Large surface area and more active sites	(Tang et al., 2017)(Rezvani Jalal et al., 2020)
B-cyclodextrins	High host-guest recognition and enrichment ability	Yi et al. (2016)
Thiol- B-cyclodextrins	Good enrichment ability	Zhao et al. (2019)
Ionic liquids	Improved conductivity	(Kalcher and
	Film formation ability	Samphao, 2019)(Pan et al., 2015)
Chitosan	Improves the electrochemical properties	Xin et al. (2015)
Molecularly imprinted polymer	Improved selectivity	Pan et al. (2015)
Cobalt phthalocyanine	High electrocatalytic property	Kalcher and Samphao (2019)
Nitrogen-argon radio frequency plasma	Improved electrocatalytic performance	Jothi et al. (2018)
Nitrogen doping	Enhanced chemical activity and adsorption	(Tang et al., 2017)(Yan Li et al., 2017)(
	Enhanced conductivity	Li et al., 2015)
Nitrogen doped vacancy	Enhanced sensitivity	(K. Li et al., 2016a)
Guanines	Improved electrochemical signals	Tang et al. (2012)
L-arginine	Excellent electrocatalytic activity	Yi et al. (2016)
Porosity	High electroactive surface area and electron transfer	Jothi et al. (2020)
Nanopore	Translocated nucleobases helps for sequencing by changing the conductivity	(Wasfi et al., 2019)(Paulechka et al., 2016)

steady current is detected as the function of time after applying a square-wave potential to the working electrode (Xu et al., 2020b). Here, GNRs can provide high electron transfer ability and surface area. In addition, doping of GNR with nitrogen atoms can also supply catalytically active sites for sensitive chronoamperometric biosensing (Shi et al., 2015). Voltammetric techniques are controlled potential techniques based on the current measurement in response to an applied potential that drives redox reactions. (Bard and Faulkner, 2001). The current measured indicates the electron transfer within the analyte and electrode surface. In voltammetry, the benefits of GNRs are fast electron transport and large surface area. Besides, GNR could also decrease the overpotential in voltammetry usually observed with standard electrodes. Further, GNR composites formed with metal oxide nanoparticles would provide favorable electrochemical properties for voltammetric biosensing (Apath et al., 2020). GNR-based biosensors can provide extraordinarily high oxidation peak currents. Meanwhile, rGNR has enhanced conductivity for voltammetric applications due to a large number of sp^2 carbons (Martín et al., 2014). Cyclic voltammetry (CV) is one of the common linear sweep voltammetric methods, in which electrical potential is swept in both forward and backward directions in full, partial, or series of cycles. In cyclic voltammetry-based biosensors, GNR or its derivatives can improve the electron-transfer reaction of the electroactive species such as ferricyanide by increasing the conductivity of the electrode. Also, GNR favors a fast electron transfer rate (Pajooheshpour et al., 2018). Besides CV, other voltammetric methods have been introduced to enhance the detection limit in quantitative measurements. These methods are based on pulse technologies, in which a potential pulse is applied before the measurement of current. Normal pulse voltammetry (NPV), Differential pulse voltammetry, square-wave voltammetry are often applied depending on the excitation waveform (Ambrosi et al., 2014; Bard and Faulkner, 2001; Cesewski and Johnson, 2020). Amperometric methods, together with these methods, are commonly used in GNR-based biosensing for environmental and clinical applications.

Electrochemical impedance spectroscopy (EIS) is another sensitive transducing technique and can be valuably utilized for the biosensing protocols of graphene-based platforms. Impedimetric biosensors allow the direct recognition of biomolecules without any enzyme labels and are usually measured by applying an AC potential to an electrochemical cell, followed by the measurement of current through the cell. It is a non-destructive technique, can be operated with or without the presence of a redox couple (Anusha et al., 2019; Bahadir and Sezgintürk, 2016). This method has been adopted with graphene-based materials for the detection of protein, DNA, and cell. In biosensors of EIS type, the use of GNRs ensures high current intensities and low potential values leading to superior electrochemical output. These benefits emerge from enhanced charge electron transfer and the effective surface area by GNRs (Sainz et al., 2020). Potentiometric biosensors detect the charge potential of an electrochemical reaction at the working electrode compared to the reference electrode. Polymeric membrane-based ion--selective electrode (ISE) is an established and commonly used technology in potentiometric sensing; it consists of an ion-selective membrane that prevents interferences by allowing the exchange of only one target ion between sample solution and inner solution. High electrocatalytic activity and electrical conductivity are possible advantages of GNRs in

their use in ISEs (Yan et al., 2016). A new generation ISE was developed to overcome the disadvantages of conventional ISE, based on a solid-contact that integrates solid transducers between the selective membrane and conductive electrode surface. Highly conductive graphene and other carbon nanostructures show excellent performances as solid transducers, which helps achieve flexibility and miniaturization in sensing (Ambrosi et al., 2014; Xu et al., 2020a). Therefore, GNR has a potential future in ISE based potentiometric sensing.

6.1.1. Electrochemical biosensors for the detection of biomarkers

6.1.1.1. Biosensing of glucose. Diabetes mellitus (DM) is a condition characterized by an increased level of glucose. Determination of glucose level is important to manage the complications related to DM. Glucose sensors are not only used in the management of DM but also used in food industries and bioprocessing. Glucose biosensors are mainly categorized into enzymatic and non-enzymatic. Enzymatic biosensors are most studied due to their high selectivity towards glucose. Unfortunately, difficulty in immobilization, poor reproducibility, poor stability, and critical operating situations are their disadvantages. These problems lead to the advancement of non-enzymatic biosensors. Tremendous efforts in fabricating non-enzymatic sensors utilized metal and transition metal oxide nanoparticles for the electrochemical identification of glucose (Lavanya et al., 2017; Palanisamy et al., 2012). Similarly, GNR-based glucose biosensors are also studied, and their features are provided in Table 2.

6.1.1.1.1. Enzymatic glucose biosensors. Enzymatic glucose biosensors utilize some glucose oxidizing enzymes as receptors for glucose detection. Glucose oxidase (GOx) catalyzes the conversion of glucose to D-glucono-1,5 lactone and hydrogen peroxide (H_2O_2) via oxidation (Krishnan et al., 2019).

A third-generation reagentless electrochemical glucose biosensor was designed by connecting GOxon GNRs. GNRs produced from oxidative unzipping of MWCNTs were immobilized by adsorption. Flavine adenine nucleotide (FAD) was covalently connected to GONR adsorbed on a screen-printed carbon electrode (SPCE), and the apoenzyme separated from its co-enzyme was attached to FAD bound to holoenzyme. It creates a direct transfer of electrons from cofactor FAD to an electrode, and the whole biolayer was stabilized with a Nafion membrane (Mehmeti et al., 2017) (Fig. 7a). A disposable enzymatic sensor was fabricated in another study with MnO_2 nanoparticles decorated on GNRs. GOx attached MnO_2/GNR nanocomposite confined on an SPCE showed excellent stability, reproducibility, and satisfactory accuracy and precision (Vukojević et al., 2018b).

6.1.1.1.2. Non-enzymatic glucose biosensors. A non-enzymatic electrochemical hybrid glucose sensor fabricated provides extreme sensitivity and selectivity towards glucose. The unique electrochemical properties of GNRs are conducive to fabricate sensitive non-enzymatic glucose biosensors. Additionally, the conjugation of supporting inorganic nanoparticles can enhance the electrocatalytic performance of the GNRs. Thus, noble metal nanoparticles modified GNRs improve the catalytic performance towards the sensitive detection of glucose molecules.

GONRs can be used as a substrate electrode for making a sensitive platform for glucose and hydrogen peroxide. Here, GONRs allows the formation of a stable film of MnO_2 nanoparticles because of its high surface area. These GONRs functionalized with MnO_2 nanoparticles can be supported on a glassy carbon electrode (GCE). Interestingly, on comparing with the MnO_2-SWCNTs-GCE design, MnO_2-GONR-GCE provided greater linear range and sensitivity in the detection of hydrogen peroxide. Glucose detection with this hybrid material is indirect by measuring the H_2O_2formed during the addition of analyte (glucose) to glucose oxidase solution (Zakaria and Leszczynska, 2019). In another system, graphene sheet/graphene nanoribbon/nickel nanoparticles (GS/GNR/Ni) were attached to a GCE to detect the level of

Table 2
Features of GNR based glucose sensors.

Biosensor	Electrode	Method	Applied potential	Linear range	LOD	Sensitivity	Supporting electrolyte	Real sample analysis and recovery rate	References
Enzymatic	GONR/FAD/apo-GOx/Nf/SPCE	CV	+0.475 V	50 to 2000 mg/L	20 mg/L	–	Oxygen free PBS, pH7.5	Serum 102–104%	Mehmeti et al. (2017)
Enzymatic	GOx/Naf/MnO_2-GNR/SPCE	CV and HChA	+0.5 V	0.1–1.4 mM	0.050 mM	56.32 μA/mM/cm^2	0.1 M phosphate buffer, pH 7.4	Honey	Vukojević et al. (2018b)
Non enzymatic	MnO_2/GONR/GCE	AmperometryCV	0.85 V	0.01–1.2 mM	1.2 μM	–	0.1 M phosphate buffer, pH 7.4	–	Zakaria and Leszczynska (2019)
Non-enzymatic	GS/GNR/Ni	Amperometry	+0.5 V	5 nM-5 mM	2.5 nM	2.32 mA/mM/cm^2	0.1 M NaOH	serum	Lavanya et al. (2017)
Non-enzymatic	AuNP/GONR/CS	ChA LSV	+0.20 −0.4 to +0.8 V	0.005–4.92 mM 4.92–10 mM	5 μM 0.5 μM	59.1 μA/mM/cm^2 31.4 μA/mM/cm^2	0.1 M PBS	–	Ismail et al. (2014)

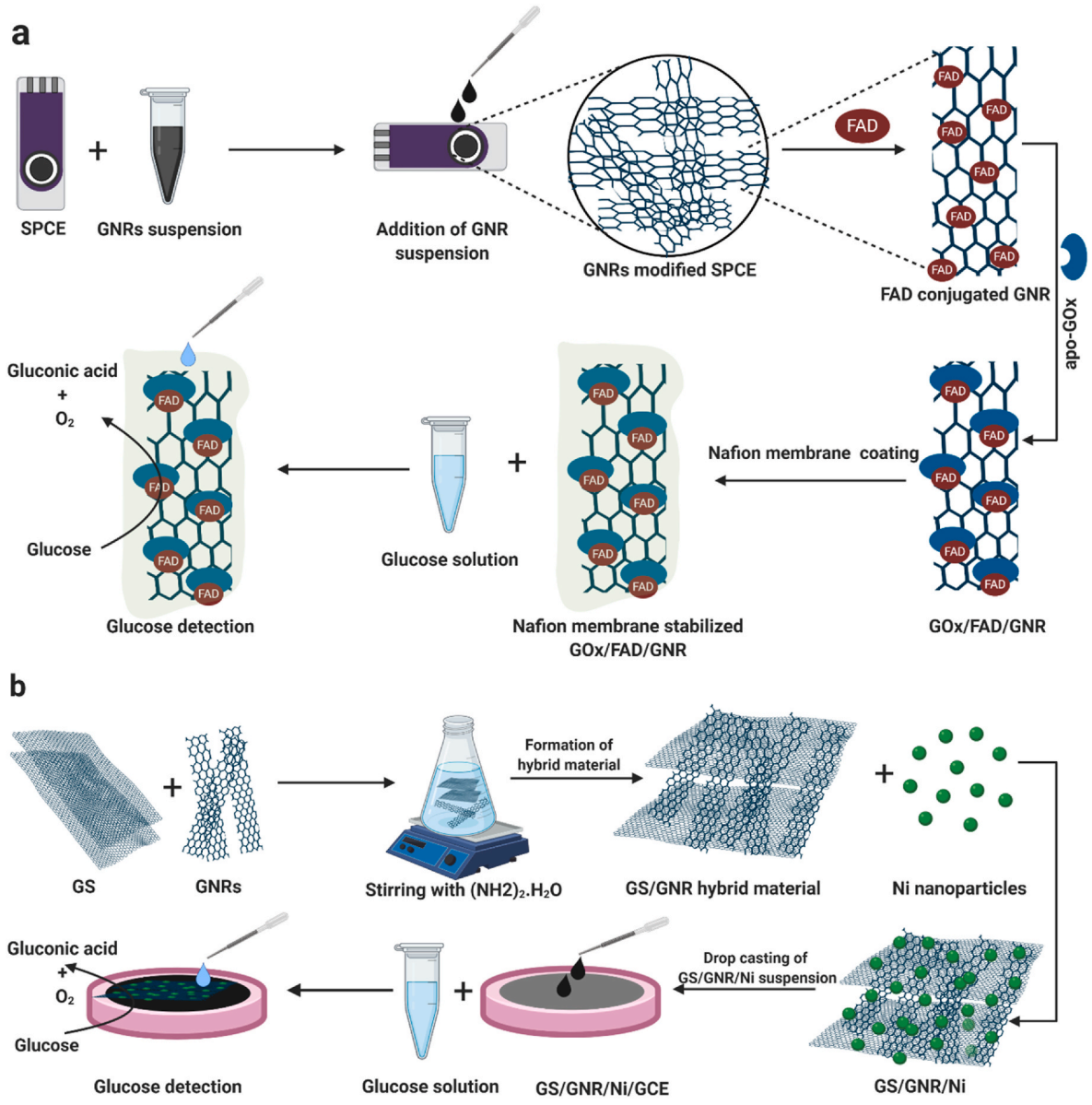

Fig. 7. Fabrication of glucose biosensors. **a**) Fabrication of enzymatic apo-GOx/FAD/GNR/Nf/SPCE sensor and glucose detection. **b**) Fabrication of non-enzymatic GS/GNR/Ni/GCE sensor and glucose detection.

glucose. The GS/GNR hybrid material reduced the aggregation and stacking of graphene and offered four times higher surface area than rGO. The Ni nanoparticles on hybrid nanomaterial increased the electrocatalytic property. High electrochemical activity exhibited a wide linear amperometric response, low limit of detection, and enhanced sensitivity towards glucose. In real sample analysis, common interfering molecules like dopamine, uric acid, sucrose, and chlorine were insensitive to this modified sensor. Further, the results were consistent with a glucose meter, and the recovery rate was found to be $\geq$ 95% (Lavanya et al., 2017) (Fig. 7b).

In another study of glucose detection, a non-enzymatic electrochemical sensor was created with the deposition of AuNPs/GONR nanocomposite on a carbon sheet followed by thermal activation. Thermal treatment not only increases the activity of AuNPs but also improves the active surface area. GONR acts as a three-dimensional backbone, and it noncovalently binds with the AuNPs. To improve the selectivity, the sensor was protected with a membrane made up of Nafion and polypyrrole. The study results also showed that the protection with the membrane is crucial for recovering the catalytic activity of AuNPs from the poisoning with electroactive species (Ismail et al., 2014).

6.1.1.2. Biosensing of DNA. GNR-nanocomposites, wherein GNR surface or edges are decorated with nanoparticles, not only give the individual characteristics of the nanoparticles, but also enhance the effect of GNR by the combined actions. The inherent characteristics of GNRs like ultra-high surface area, electron transfer, optical properties, etc., are enhanced by the conjugated nanoparticles. In the construction of electrochemical biosensors, nanoparticles can improve the catalytic property of the sensing system (Feng et al., 2018; Krishnan et al., 2019).

A target driven stochastic DNA walking electrochemical biosensor was recently developed for the ultrasensitive sensing of target DNA. Here, the gold nanocages attached to the GNRs benefitted from the combined effect of their high surface area and good conductivity. The designed sensing platform not only improved the electron transfer kinetics but also improved the loading capacity of stem-loop structural DNA. The stochastic DNA walker can transport DNA from one location to another location on the surface of the electrode, which will give

detectable signal amplification. Further, a combination of gold nanocages with porous structure and large surface area of GNRs offers improved electron communication capacity and additional active sites for immobilizing DNA strands. The stochastic DNA walker system showed good performance for the recognition of DNA from complex mediums such as serum (Feng et al., 2018).

Recently, a study explored the potential of boron, sulfur, and nitrogen-doped GNRs in the sensing of DNA nucleobases. The doping enhanced the properties of transmission curves as well as the electron transport properties. Doping of 8-AGNR with boron and nitrogen leads to the formation of p and n-type semiconductors based on the dopant position. The numerical study reports showed that the position of dopant could strongly affect the density of states and modify the GNR sensitivity to DNA bases (Rastgoo and Fathipour, 2019).

6.1.1.3. Biosensing of amino acids (AA) and proteins. By exploiting the electroactivity of clinically relevant AA, such as methionine and tyrosine, disposable GONR screen printed electrodes are fabricated for the in-situ measurement of L- and D-AA. Tyrosine and methionine are the relevant biomarkers in *Bacillus subtilis* and *Vibrio cholerae* infections, respectively. The scheme of sensing includes simultaneous enantiomeric resolution and detection of L- and D-AA. Detection is based on the simultaneous biosensing of D-AA using a class enzyme (D-amino acid oxidase) that reacts selectively with D-enantiomer to form H_2O_2 and direct electrochemical sensing of the L-enantiomer by GONR transducers. The biosensor exhibited fast, selective, and reproducible sensing from the urine sample (Martín et al., 2015a). In a study, a combination of GONR and metallic nanoparticle was used in the detection of histamine. This combination is drop-casted on the surface of the edge plane pyrolytic graphite (EPPG). GONR-AgNPs-EPPG showed greater catalytic activity to the oxidation of histamine and higher selectivity, even in the presence of interfering agents in blood plasma(Kumar and Goyal, 2018). Cysteine (CySH), another AA, can be detected by the GONR, and Nafion-modified GCE (GONR-Nafion/GCE). The unusual level of CySH in the body can be correlated to many diseases such as liver disease, weakness, and growth retardation. The presence of oxygen-containing functionalities, especially the unsaturated aldehyde group on the oxygenated GNR with Nafion, is used for the sensitive and electrochemical detection of CySH. Interaction of CySH on electrode develops a cyclic addition between aldehyde on GONRs and the N-terminal group of CySH. This leads to the formation of the thiazolidine transition, followed by deprotonation and electrooxidation of CySH. This sensor is also applicable for homocysteine and glutathione (Wu et al., 2012).

Recently, an electrochemical immunosensor was designed for the ultrasensitive detection of matrix metallopeptidase-9 (MMP-9) and interleukin-6 (IL-6). MMP levels in serum samples are used to assess the ischemic stroke index. IL plays a significant role in biological processes such as immune responses, hematopoietic regulation, and acute phase reactions. The sensor used polystyrene (PS)@polydopamine (PDA) metal composite material and rGONR-modified heated SPCE (HSPCE). The rGONR was used for antibody (Ab) immobilization and signal amplification. A sandwich-type design was developed with rGONR/HSPCE, Ab, and PS@PDA-metal composite. The PS@PDA-metal composite was used to label the Ab and to create a strong electrochemical signal (Fig. 8a)(Shi et al., 2014). Another sandwich-type

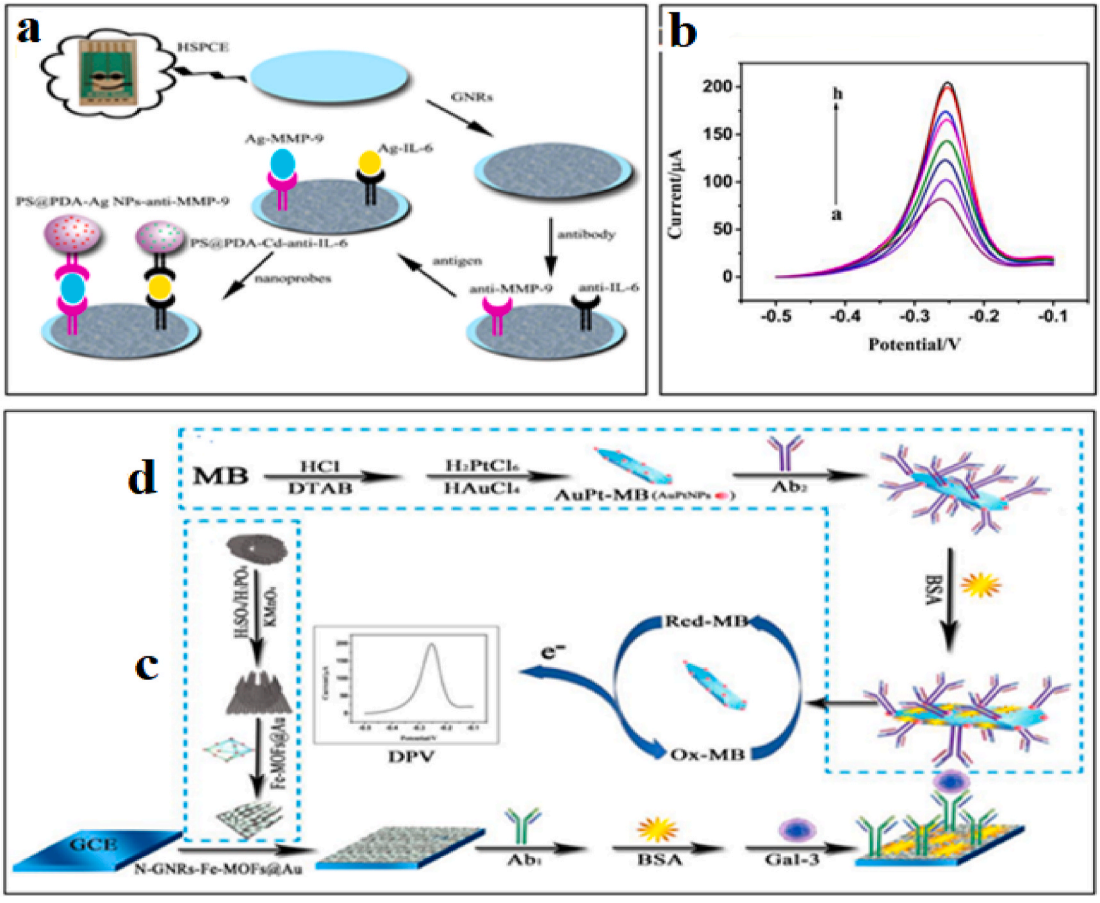

Fig. 8. **(a)** Mechanism of electrochemical immunosensor for the detection of MMP-9 and IL-6. Reprinted with permission from (Shi et al., 2014) Copyright (2014) Elsevier, **(b)** DPV responses of the different concentrations (a–h) (0.0001–50 ng/mL) of galectin-3 in 0.1 M PBS, Schematic representation of the fabrication of electrochemical immunosensor Ab-AuNP- Fe-MOF- N-GNRs/GCE **(c)** for detection of galectin-3, and **(d)** AuPt-MB-Ab2. Reprinted with permission from (Tang et al., 2017) Copyright (2017) Elsevier.

electrochemical immunosensor was fabricated for the identification of Galectin-3 (Gal-3) (a biomarker of heart failure). Ab against Gal-3 immobilized AuNPs deposited Fe-based-metal organic framework (Fe-MOF) was attached to an N-doped GNRs (N-GNRs), and it was used to modify the GCE. A novel redox-active species AuPt-methylene blue (AuPt-MB) was used as a label for the amplification of the analytical signal. MB acted as an electron transfer mediator in an amperometric sensor for the enhancement of signals. Rod-like AuPt-MB, showed good electrochemical activity and combined with Ab-AuNP- Fe-MOF-N-GNRs/GCE to form sandwich-type electrochemical immunosensor (Fig. 8b and c, and d) (Tang et al., 2017). A dual-type responsive electrochemical immunosensor was fabricated in a study for the sensitive detection of proprotein convertase subtilisin/kexin type 9 (PCSK9), a significant biomarker for cardiovascular diseases. The sensing matrix was fabricated by palladium platinum alloy (PdPt) reduced on to an amino-functionalized fullerene (n-C60), followed by deposition on N-doped-GNR attached on GCE (n-C60-PdPt-N-GNR/GCE). This matrix can generate electrochemical signals through H_2O_2 reduction, and it also acts as a carrier for protein immobilization. Then the matrix was functionalized with *Staphylococcus* protein-A (SPA) with Ab orientation function to enhance the immunoreaction for label-free immunosensor. Pt-poly (methylene blue) nanocomposite was used as a label to enhance the sensitivity for sandwich-type immunosensor. The resultant sensor showed a wide range of detection, low LOD, and satisfactory stability for PCSK9 detection (Yan Li et al., 2017).

Cancer is one of the prominent reasons for mortality worldwide. Primary detection of this condition is most important for effective monitoring, therapy, and ultimately for the survival of the patient (Krishnan et al., 2019). Accurate estimation of cancer biomarkers provides authentic information for the early finding of cancer. Recently, a label-free electrochemical immunosensor was fabricated for the sensing of alpha-fetoprotein (AFP), a significant clinical biomarker for the detection of hepatocellular carcinoma. Here, the hybrid nanomaterial consisting of porous GNR (PGNR), and AuNPs immobilized with anti-AFP deposited on GCE (anti-AFP-AuNPs-PGNR-GCE) exhibited high electrocatalytic activity towards the AFP molecule. Porous GNR provides a large surface area and enhanced electron transfer between the electrode and redox probe while AuNPs attached to porous GNR helps to immobilize anti-AFP protein, and it also facilitates the electron transfer. Differential pulse voltammetric (DPV) studies of anti-AFP-AuNPs-PGNR-GCE exhibited a wide linear range and low LOD in physiological pH (Jothi et al., 2020). In another study, a sandwich-type electrochemical immunosensor was fabricated for the sensing of AFP. The sensing matrix was fabricated by the immobilization of functionalized anti-AFP on β-cyclodextrin conjugated graphene sheets (β-CD-GS), and it could enhance the electron transfer. Whereas palladium-nickel alloy nanoparticles conjugated N-doped GNRs (Pd/Ni/N-GNRs) were used as the secondary anti-AFP labels. Pd/Ni nanoparticles demonstrated a great catalytic performance towards the reduction of H_2O_2. Under optimum conditions, the proposed sensor exhibited high stability, good reproducibility, high specificity, a wide linear range, and a low LOD (Li et al., 2015). The features of GNR-based sensors for the detection of amino acids and protein are provided in Table 3.

6.1.1.4. Biosensing of dopamine, ascorbic acid, and uric acid. Many studies are reported to separate the signal potential of dopamine (DA), ascorbic acid (AsA), and uric acid (UA) with significant sensitivity and selectivity; because these three analytes exhibited electrooxidation peaks almost at similar potentials (Krishnan et al., 2019; Zhang et al., 2001). Imbalance of dopamine neurotransmitters leads to various disorders such as Parkinson's disease (PD), attention deficit hyperactivity disorder, restless leg syndrome, etc. (Jothi et al., 2018). AsA is avital vitamin that plays a major role in developing immunity, prevention of

Table 3
Features of GNR based sensors for the detection of amino acid and protein biomarkers.

Electrode	Method	Analyte	Linear range	LOD	Sensitivity	Stability (days) and percentage reduction of activity	Real sample Analysis and recovery rate (%)	Supporting electrolyte	Reference
GONR-AgNPs-EPPG	SWV	Histamine	1–50 μM 60–500 μM	0.049 μM	0.158 μA/μM 0.083 μA/μM	24, 5.8%	Plasma >99%	PBS pH 7.2	Kumar and Goyal (2018)
GONR/SPCE	DPV	D-tyrosine L-tyrosine	–	60 μM 100 μM	–	–	urine	10 mM Phosphate buffer pH 7	Martín et al. (2015a)
GONR-Nafion/GCE	DPV	Cysteine Glutathione Homocysteine	25 nM −500 μM 300 μM–1.0 mM 300 μM–2.0 mM	100 μM 100 μM 100 μM	–	–	Serum 93.3–117%	0.1 M PBS pH 7	Wu et al. (2012)
Ab- rGONR/HSPCE	SWV	IL-6 MMP-9	10^{-5} to 103 ng/mL 10^{-5} to 103 ng/mL	0.1 pg/mL 5 fg/mL	–	14, No significant change	serum	HAc/NaAc buffer, pH 4.6	Shi et al. (2014)
Ab-AuNP- Fe-MOF- N-GNRs/GCE	DPV	Galectin-3	100 fg/mL - 50 ng/mL	33.33 fg/mL	–	21, 4.83 %	Serum 98–104%	0.1 M PBS pH 7	Tang et al. (2017)
n-C60- PdPt- N-GNR/GCE sandwich type label free type	DPV	PCSK9	0.0001–100 ng/mL 0.01–100 ng/mL	0.033 ng/mL 3.33 ng/mL	–	28, 11.4% 28, 11.8%	Serum 96.2–103.37% 97.89 %–104.24 %	0.1 M PBS pH 7.4	Yan Li et al. (2017)
GNR-ISFET	FET	PSA	–	0.4 pg/mL	–	–	–	–	Zhang and Cui (2013)
anti-AFP-AuNPs-PGNR-GCE	DPV	AFP	5–60 ng/mL	1 ng/mL	–	30, 9.4%	Serum 99.9%-102 %	pH 7.4	Jothi et al. (2020)
β-CD-GS and Pd/Ni/N-GNRs	Amperometry	AFP	0.0001–16 ng/mL	0.03 pg/mL	–	20, 10%	Serum 99.6 to 103%	pH 7	Li et al. (2015)

cancers, and repair of the body. AsA deficiency leads to a condition called scurvy (Arrigoni and De Tullio, 2002). The metabolism of purine nucleotide releases uric acid as its end product; abnormal concentration can cause gout, renal failure, etc. (Liu et al., 2014).

GONRs are excellent nanomaterials for the detection of AsA, UA, and DA due to their high anodic oxidation currents towards these biomolecules on cyclic voltammetry measurements. Short GONRs were used for the modification of GCE for the electrochemical sensing in a study for the improved detection of these biomarkers in PD.The short GONRs were prepared by microwave-assisted synthesis from MWCNTs showed low LOD for the sensing AsA, UA, and DA (Sun et al., 2015). Similarly, for the real-time and reagentless detection of AsA, DA, and UA, a hybrid material of GS/GONR functionalized with nitrogen/argon radiofrequency plasma (N_2/Ar/RF/GS/GONR) supported on a GCE was used. The combination of GS and GNR enhances the electrical conductivity and surface area of the sensing system. Various nitrogen groups on the hybrid nanomaterial act as an electroactive center for the electrooxidation of the three analytes (Jothi et al., 2018). Biosensing potential of the oxidized and reduced GONRs were investigated for the fabrication of SPCE based disposable electrochemical sensors of GNRs. Compared to other related carbon nanomaterials, rGONRs exhibited high sensing potential. AsA, UA, and levodopa can be detected accurately and selectively within 100 s with this sensor (Martín et al., 2015b).

Through the simultaneous chemical reduction of GS and GONRs, a hybrid electrode material (GS/GONR) was developed and attached to a GCE for the detection of AsA. GNRs improve the surface area and dispersion of the hybrid material by acting as a carbon spacer between GS. The EIS studies reveal that the charge transfer resistance of GS/GONR/GCE was less than that of chemically reduced graphene oxide sheets (rGOS) modified GCE (rGOS/GCE) and bare GCE. The proposed electrochemical sensor showed a significant electrocatalytic activity towards the AsA with increased peak current and less over potential in comparison to rGOS/GCE, GS/CNT/GCE, and bare electrode. GS/GNR exhibited high sensitivity and low LOD towards the analyte, even with interfering substances like DA, UA, and citric acid(Lavanya and Gomathi, 2015). A study described the interaction of fully characterized GNR with a set of relevant target molecules (DA,AsA,UA,L-tyrosine, benzene diols, hydroquinone, catechol, and resorcinol). GNRs showed excellent electrochemical responses compared to MWCNTs and bare GCE. The chemistry of the few layers of graphene exhibited a great influence on their electrochemical properties. It was found that oxidized form of GNRs are excellent material for the sensing of molecules having high oxidation potential, whereas reduced GNRs showed high sensitivity to aromatic molecules dominating π-π interactions or conjugated 1,2 diols (Martín et al., 2014).

6.1.1.5. Biosensing of other biomarkers. In a study, GNRs were used for the detection of oxidative or reductive analytes in combination with PtNPs. This nanocomposite exhibited abundant functional groups and effectually reduced charge transfer resistance of the electrode. This nanocomposite offered a significant catalytic activity towards H_2O_2 and β-nicotinamide adenine dinucleotide (NADH). Amperometric study results of PtNPs/GONRs showed good selectivity (in the presence of interfering molecules), towards H_2O_2 and NADH (Lee et al., 2018a). GNR and ruthenium dioxide (RuO_2) deposited SPCE was designed for the electrocatalytic detection of NADH. RuO_2/GNR/SPCE with immobilized alcohol dehydrogenase also showed a good response towards ethanol (Vukojević et al., 2018a).

6.1.2. Electrochemical biosensors for the detection of plant-derived molecules

The antioxidant property of the quercetin flavonoid is good for health. But it is necessary to detect excess quercetin because it leads to serious complications like kidney cancer. An electrochemical sensor for quercetin was constructed by modification of GCE with molybdenum disulfide (MoS_2-CNT@GONRs) and thiol-β-cyclodextrin (HS-CD)/aminated GQDs (N-GQDs). This nanocomposite showed outstanding performance towards the detection of quercetin due to the synergistic effects of strong catalytic activity of MoS_2, good electrochemical activity of CNT@GONRs, improved performance of HS-CD, and high stability and biocompatibility of N-GQDs (Zhao et al., 2019). An enzymatic electrochemical sensor for the quantitative detection of tea catechin was designed in a study with immobilized polyphenol oxidase (PPO) enzyme to a graphite electrode modified with GONRs combined with AgNPs (PPO-Gr/GONR-AgNPs). The GONR-AgNPs combination made the matrix more biocompatible and provided more area for electrochemical activity. Analysis of catechol levels in different green tea samples with the PPO-Gr/GONR-AgNPs sensor and HPLC showed 99% agreement in the results (Sandeep et al., 2018). The features of GNR-based sensors for the detection of UA, AsA, DA, plant-based molecules, and other biomarkers are shown in Table 4.

6.1.3. Electrochemical biosensors for the detection of drugs

Determination of drug content in the human body is important when administering drugs like potent drugs, drugs causing serious side effects, and toxicity. This is extremely important in therapeutic drug monitoring of narrow therapeutic index drugs. The drug content can be detected from blood, plasma, serum, and urine using appropriate biosensors (Garzón et al., 2019). A GONR-modified GCE electrode was studied for the detection of norepinephrine tartrate (NT), which is used in the treatment of various disorders. GONRs on GCE enhanced the electrochemical redox of NT by significantly increase the rate of electron transfer. The peak current obtained for NT with GONRs/GCE was higher than MWCNTs/GCE due to the improved electron transfer owing to the presence of functional groups and electrochemical intermediates (Fig. 9a) (Song et al., 2016).

Nimesulide is an NSAID having analgesic and antipyretic properties. However, the over usage of this NSAID causes acute side effects related to gastric, CNS, and genitourinary systems. Hence, the detection of nimesulide content will help to avoid these side effects. Electrochemically reduced GONRs-modified SPCE based electrochemical sensor was fabricated for the determination of nimesulide from biological samples. rGONRs is a potential material for sensing application since it possesses edge defects, functional groups, chemically active sites, high surface area compared to MWCNTs (Fig. 9b)(Govindasamy et al., 2017b). A new sensing platform was designed with a narrow rGONRs composite film polymerized with aniline. The proposed rGONRs/polyaniline (rGONRs/PANI) composite film modified GCE sensing platform showed a remarkable performance in the electrochemical sensing of dobutamine. In comparison to bare GCE, rGONRs/PANI/GCE showed 10 times higher peak current; due to the high specific surface area of GNRs and the electrocatalytic effect of polyaniline towards the oxidation of dobutamine. Serum sample analysis also showed reasonable results (Fig. 9c) (Asadian et al., 2014).

Nifedipine, a calcium channel blocker widely used in cardiovascular therapy, require an accurate and sensitive method for its determination since it overdose causes various side effects. A hybrid material consists of ionic liquid (IL) functionalized GNRs and hollow PdAg NPs (hPdAg NPs) showed excellent electrochemical response towards nifedipine. AgNPs can reduce the nifedipine; however, the combination of Pd and Ag metals exhibited better electrochemical behavior than Ag alone. The use of hollow metals is also advantageous over their solid parts. The sensor showed a 97.6 % to 101 % recovery rate when applied to the detection of nifedipine from the real sample (Fig. 9d)(Shang et al., 2015). Recently an electrochemical sensor was fabricated for the detection of anticancer drug imatinib by the in situ growth of metal-organic framework (MOF) HKUST-1 on GONRs modified GCE (HKUST-1/GONRs/GCE). MOF exhibited a large surface area. But the MOF does not have good conductivity. The conductivity of the MOF enhances in combination with GONRs. The cyclic voltammetric response towards imatinib was higher due to the synergistic activity of GONRs

Table 4
Features of GNR-based sensors for the detection of UA, AsA, DA, plant-based molecules, and other biomarkers.

Electrode	Method	Analyte	Linear range	LOD	Sensitivity	Response time	Stability and percentage reduction of activity	Real sample Analysis and recovery rate	Supporting electrolyte	Reference
N_2/Ar/RF/GS/ GONR	CV DPV	AsA UA DA	0.1–1400 μM 0.02–350 μM 0.01–400 μM	5.3 nM 2.5 nM 5.7 nM	501 μA/ μM/cm^2 576 μA/ μM/cm^2 652 μA/ μM/cm^2	5s	30 days 2.7%, 2.8%. 3.6%	Human serum 94–104%	0.1M PBS, pH 7.4	Jothi et al. (2018)
GONR/GCE	Amperometry DPV	AsA UA DA	0.1–8.5 μM 0.1–8.5 μM 0.1–8.5 μM	26 nM 98 nM 24 nM	– 24.2 μA/μM/ cm^2 40.9 μA/ μM/cm^2	–	–	–	0.1 M PBS, pH 7	Sun et al. (2015)
rGONR/SPCE	DPV	AA LD UA	1–5 mM 10–50 μM 10–50 μM	4 mM 0.05 mM 0.05 mM	2.2 μA/mM 145.6 μA/ mM 256.9 μA/ mM	100 s	15 days 7 ± 3%	Urine 97–101%	0.10 M PBS pH 7.4	Martín et al. (2015b)
GS/GONR/GCE	CV amperometry	AA	10–360 μM	230 nM	22 nA/μM/ cm^2	–	50 min	Vit C tablets	PBS pH 7	Lavanya and Gomathi (2015)
GONR/AgNPs	colorimetry	DA GSH	0.25–10 μM 1–75 μM	0.04 μM 0.23 μM	–	15 min 20 min	7 days	Human serum 92–107.5% 92–102.5%	pH 5	Rostami et al. (2020)
ChOx -CdTeQDs-MWCNTs-rGONRs	ECL	cholesterol	1 μM - 1 mM	0.33 μM	–	–	7 days 8.4 %	Human serum Milk 93.4–104.9%	0.10 M PBS pH 9.0	Huan et al. (2015)
rGONRs-FET	FET	ATP	5–150 μM	5 mM	–	–	–	–	PBS, pH 7.2	Dong et al. (2011)
PtNPs/GONRs	CV	H_2O_2 NADH	250–2500 μM 25–325 μM	37.78 μM 0.22 μM	378.5 μA/ mM/cm-^{2} 724.3 μA/ mM/cm-^{2}	–	21 days 10 %	–	PBS, pH 7	(M. Lee et al., 2018a)
RuO_2/GNR/SPCE	CV EIS	NADH Ethanol	1–1300 μM	1.9 μM	4.5 μA/ mM.cm^2	–	–	–	PBS pH 7.5	Vukojević et al. (2018a)
MoS_2-CNT@GONRs/ HS-CD/N-GQDs/GCE	DPV	quercetin	2.0×10^{-9} - 1.6×10^{-6} M	8.2×10^{-10} M	89 μA/μM	–	5 weeks 12.9%	Orange juice 99.8–103.2% Lemon jouice 95.8–98.8% Grape juice 99.1–106.3% Pomegranite juice 98.2 95.4% Honey 104.2–101.5	0.1 M PBS pH 6.5	Zhao et al. (2019)
PPO-Gr/GONR-AgNPs	CV EIS	Catechol	2–2300 μM	0.03 μM	6.28 μA/mM/ cm^2	–	15 days 6.7 %	Green tea samples 99.5–10.6%	PBS pH 7	Sandeep et al. (2018)

and HKUST-1(Rezvani Jalal et al., 2020). The features of some GNR-based electrochemical sensors for drug detection are provided in Table 5.

6.1.4. Electrochemical biosensors for the detection of chemicals

Bisphenol-A (BPA) is a widely used chemical in the polymer industry, dental fillings, and food cans fabrication. But BPA is considered an endocrine disruptor that causes reproductive problems and cancer. An electrochemical BPA sensor based on MWCNT/GONR hybrid material exhibited electron transfer ability, electrocatalytic property, and high adsorption capacity in the BPA sensing. Meanwhile, chitosan (CS) modification improved electrochemical behavior by forming a film over MWCNTs/GONR (Xin et al., 2015). 4-Nonyl-phenol (4-NP) is another endocrine disruptor, having the activity of 17-estradiol. An electrochemical sensor was fabricated with molecularly imprinted polymer (MIP), nitrogen-doped GNRs (N-GNR), and ionic liquid (MIP/N-GNR/IL) drop casted on a GCE. The MIP/N-GNR/IL/GCE showed a good response towards NP with a linear concentration range of 0.04 to 6 mM(Pan et al., 2015). 2- aminophenol (2-AP) and 4-aminophenol (4-AP) are important industrial chemicals but can seriously affect animals and plants because of their penetration through skin and cell membranes. The simultaneous determination of these two chemicals is a great challenge owing to their structural similarity. β-cyclodextrin (β-CD) and L-arginine (L-Arg) electropolymerized on the surface of CNTs@GNRs hybrid material-modified electrode exhibited a sensitive and simultaneous detection of 2 and 4-AP. Synergistic effects of host-guest interaction of β-CD, electrocatalytic ability of L-Arg, electrochemical properties and high surface area of CNTs@GNRs facilitated excellent responses towards 2, and 4-AP (Yi et al., 2016).

2, 4 dichlorophenol (2,4-DCP) and methylene blue (MB) are other two chemicals for which GNR-based sensors are developed. Effective detection of 2,4-DCP is important due to health concerns as it is a drinking water pollutant. An electrochemical sensor was designed with nitrogen-doped vacancy ZGNRs (NV-ZGNRs) for the 2,4-DCP detection. Compared to pristine ZGNRs, NV-ZGNRs showed enhanced sensitivity to 2,4 DCP, because of the adsorption to the nitrogen-vacancy in ZGNRs.

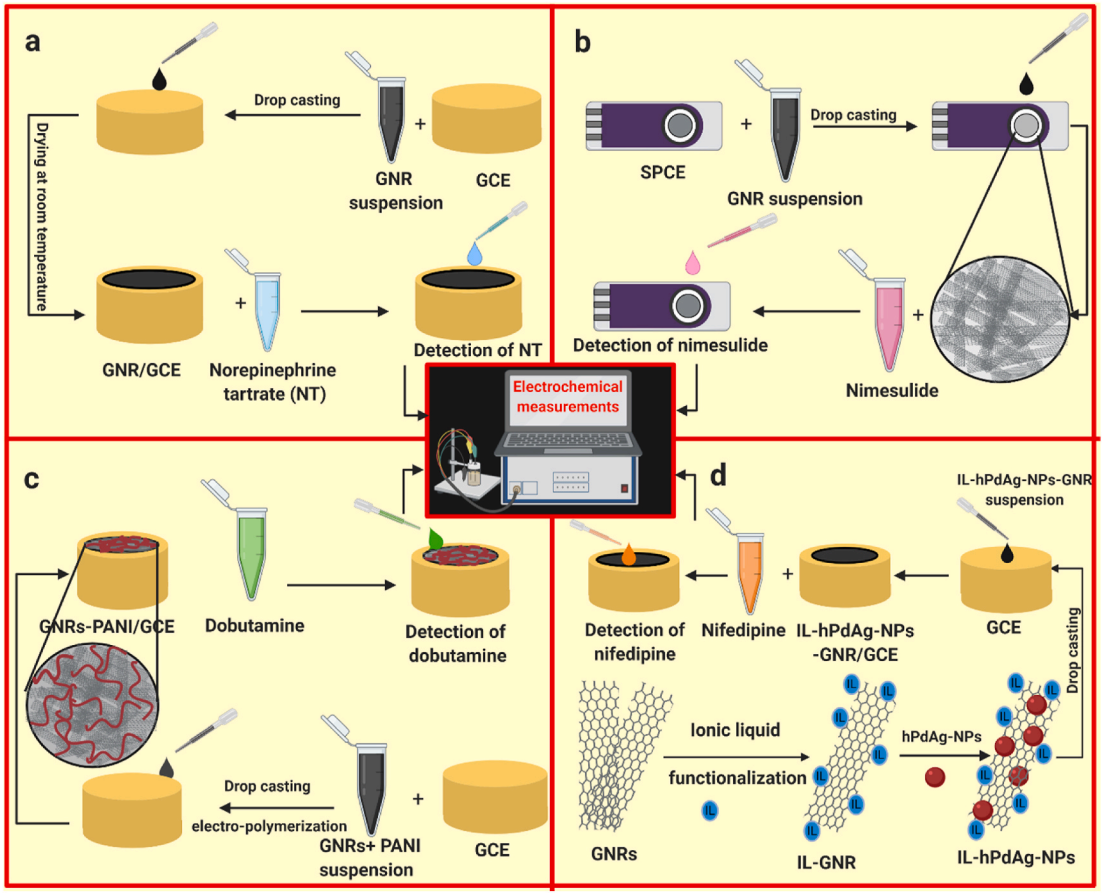

Fig. 9. Fabrication and detection of drug sensors. **a**) detection of norepinephrine tartarate, **b**) detection of nimesulide, **c**) detection of dobutamine, and **d**) detection of nifedipine.

Table 5
Features of some GNR based electrochemical sensors for drug detection.

Electrode	Method	Analyte	Linear range	LOD	Sensitivity	Stability and percentage of reduction of activity	Real sample analysis and recovery rate	Supporting electrolyte and recovery rate	References
GONRs/ GCE	CV	Norepinephrine tartrate	6.0×10^{-6} -1.5×10^{-4} M	2.1×10^{-8} M	24.751 μA/ mM	–	–	0.1 M PBS pH 7.3	Song et al. (2016)
rGONRs/ SPCE	Amperometry	Nimesulide	1.0×10^{-8} to 1.50×10^{-3}	3.50 nM	1.20 μA/μM/ cm^2	14 days, 7.9 %	Urine 98.6% Tablets 96.8%	PBS pH 7	Govindasamy et al. (2017b)
rGONRs/ PANI/ GCE	CV	Dobutamine	1.0×10^{-7} to 1.50×10^{-5}	–	–	–	Serum	PBS pH 7	Asadian et al. (2014)
IL-GNR/ hPdAg NPs	DPV	Nifedipine	10 to 4000 nM	4 nM	–	21 days, 6.7 %	Tablets 97.6–101%	0.1 M PBS pH 7	Shang et al. (2015)
HKUST-1/ GONRs/ GCE	CV	Imatinib	0.04–1.0 μM/Land 1.0–80 μM/L	0.006 μM/L	45.33 μAL μM^{-1}	9 days, 5%	Urine Serum 96.5–102.7%	BRB solution pH 7	Rezvani Jalal et al. (2020)

The enhanced sensitivity induced by nitrogen-vacancy opens wide possibilities in health and environmental monitoring (Li et al., 2016a).

6.1.5. Electrochemical biosensors for the detection of insecticides, pesticides, and toxins

Pesticides and insecticides, even at trace concentrations, can generate long-term toxicity to human health and affect the environment (Liu et al., 2015). Hence the determination of their level in food, water, and air has gained more consideration in recent years. Fenubocarb is a carbamate-family pesticide producing serious health complications and environmental problems. rGONR-ionic liquid-cobalt phthalocyanine modified SPCE (rGONR-IL-CoPc/SPCE) was fabricated for the sensitive determination of fenubocarb. Amperometric current response towards the oxidation of alkaline hydrolysis product of fenubocarb (2-sec-butyl-phenol) was obtained. This sensor showed a good response to the detection of fenubocarb in vegetable samples(Kalcher and Samphao, 2019). A sensitive electrochemical biosensor was designed by immobilizing acetylcholinesterase (AChE) on MWCNTs/GONRs hybrid material

for the sensing of carbaryl pesticide. The resulting biosensor showed superior sensitivity based on the change in electrochemical response of enzymatic activity induced by carbaryl pesticide. The sensor exhibited significant reproducibility, acceptable stability, and sensitivity (Liu et al., 2015). An electrochemical sensor was fabricated in a study with silver nanoparticles (AgNPs) decorated rGONRs on SPCE for the detection of organophosphorus pesticide methyl parathion. The resulted sensor showed excellent electrochemical activity towards the reduction of methyl parathion. The synergistic effects of AgNPs and rGONRs provide enhanced sensitivity to methyl parathion. Methyl parathion detection in vegetables and fruits achieved low LOD, good reproducibility, and stability (Govindasamy et al., 2017a). Acetamiprid is a neonicotinoid insecticide, causing acute mammalian toxicity. A label-free impedimetric aptasensor was fabricated by decorating AuNPs on MWCNT/rGONR hybrid material for the sensitive detection of acetamiprid. The Au-MWCNT/rGONR composite is used as a support for the immobilization of aptamer. The resultant sensor (Aptamer-Au-MWCNT/rGONR) showed high sensitivity in comparison to pure AuNPs and MWCNT/rGONR hybrid materials. The detection mechanism is based on the change in electron transfer resistance due to the acetamiprid-aptamer binding (Fei et al., 2015).

Brevetoxin-B (BTX-2) is a marine neurotoxin created by algae *Ptychodiscus brevis Davis* or *Gymnodinium breve Davis*. Consumption of BTX-2-contained shellfish can cause serious intoxication and even death. Therefore, to detect the presence of BTX-2 in seafood, researchers developed a magneto controlled electrochemical immunosensor consist of guanine functionalized GNRs (GGNRs) conjugated with bovine serum albumin-BTX-2 conjugates (BSA-BTX-2) as molecular tags and anti-BTX-2 antibody-conjugated magnetic beads as immunosensing probes on a magnetic carbon paste electrode (MCPE). Based on competitive immunoassay the BTX-2 competes with the BSA-BTX-2 for the anti-BTX-2 antibody on the magnetic beads. The guanine coupling to GNRs amplifies the signals of electrochemical immunoassay. The experimental results reported that GNRs lowered the overpotential of guanines and improved sensitivity. Linear range and LOD have enhanced greatly with the GNR molecular tags in comparison to the pure guanine labeled molecular tags (Tang et al., 2012).

The features of GNR-based biosensors for the detection of chemicals, insecticides, and pesticides are provided in Table 6.

6.2. GNR-based optical biosensors

An optical biosensor is a device consisting of a biorecognition element incorporated with an optical transducer. They offer many advantages over conventional sensing techniques. Optical sensors allow the real-time identification of various substances with high sensitivity and specificity(Yet al., 2016). An optical sensor can create signals that are proportionate to the analyte concentration. Optical biosensors monitor the analyte binding induced alterations in the inherent optical properties of a surface like absorbance, fluorescence quenching, chemiluminescence, Fluorescence resonance energy transfer (FRET), reflectance, light scattering, or any differences in refractive index (Chauhan et al., 2017). Fluorescent and chemiluminescent biosensors are the most developed biosensors in the field of optical sensors. Fluorescence is an attractive method for biosensing due to its incredible advantages like high sensitivity, selectivity, fast response time, portability, and low LOD. Optical biosensors require a very short time for the detection of analytes compared to electrochemical detectors. GNR based transducers were employed in different optical sensors due to their unique optical and other physicochemical characteristics. It can absorb photons from terahertz to visible and IR (Goenka et al., 2014). Integration of QDs and graphene nanomaterial is an efficient approach to enhance the electrochemiluminescence intensity and reduction of overpotential of ECL systems (Huan et al., 2015).In optical biosensors, colorimetric sensors are cost-effective, fast, and accurate. These are straightforward sensors that generate signals that are visible to the naked eye. Colorimetric sensors usually utilize catalysts (enzyme or enzyme-like substances) for getting colored chemical reactions(Hu et al., 2013; Vermisoglou et al., 2020).

6.2.1. Luminescent biosensors

Considering the emerging concern towards the potential environmental and health risk, it is important to detect the transgenic soybean with a reliable method. In a study, the fluorescence resonance energy transfer (FRET) method is used for the sensing of transgenic soybean through effective self-assembly between quantum dots (QDs) and MWCNTs/GONRs. The MWCNTs/GONRs with FRET technology provides fluorescent “on-off-on” switching for the determination of dual-target DNAs of promoter cauliflower mosaic virus 35s (P35s) and terminator nopaline synthase (TNOS) from transgenic soybean. To

Table 6
Features of GNR-based biosensors for the detection of chemicals, insecticides, and pesticides.

Electrode	Method	Analyte	Linear range	Analyte	Sensitivity	Stability and percentage reduction of activity	Real sample analysis and recovery rate	Supporting electrolyte	references
CS/MWCNT/GONR/GCE	Amperometry	Bisphenol-A	0.005–150 μg/L	1 ng/L	–	21, 8 %	River water 93.3–16.7%	PBS pH 7.4	Xin et al. (2015)
MIP/N-GNR/IL/GCE	LSV	4-Nonyl-phenol	0.04 to 6 mM	8 nM	3.4 μA/μM	14 days, 4.7 %	Lake, river, and tap water	PBS pH 7	Pan et al. (2015)
β-CD/L-Arg/CNTs@GNRs/GCE	CV DPV	2-aminophenol 4-aminophenol	25–1300 nM 25–1300 nM	6.5 nM 3.5 nM	6.2 μA/μM 8.5 μA/μM	30 days, 6.7%	River water 97.6–107.2%	PBS pH 7	Yi et al. (2016)
rGONR-FET	FET	Methylene blue		4.7 nM	12.5 μA/mM	–	–	Deionized water	Lin et al. (2016)
rGONR-IL-CoPc/SPCE	Amperometry	Fenubocarb	0.025–110 μM	0.0089 μM	0.0884 M/A.cm^2	7 days, 20 %	Chinese cabbage and cucumber	PBS pH 8	Kalcher and Samphao (2019)
AChE/MWCNTs/GONRs	Amperometry	carbaryl pesticide	5 nM to 5000 nM	1.7 nM	–	30 days, 14%	Cabbage 95.5–96.8%	PBS pH 7	Liu et al. (2015)
AgNPs-rGONRs/SPCE	Amperometry	Methyl parathion	0.005–2780 nM	0.5 nM	0.5940 μA/μM/cm^2	14 days, 7.97%	Cabbage Green beans Strawberry Nectarine fruit	PBS pH 7	Govindasamy et al. (2017a)
Aptamer- Au-MWCNT/rGONR	Impedimetry	Acetamiprid	5×10^{-14}M to 1×10^{-5}M	1.7×10^{-14}M	–	12 days, No significant change	Water 96–106.6%	PBS pH 7	Fei et al. (2015)

obtain the fluorescence signals, the capture DNAs were confined to QDs. Due to the FRET method, π–π interaction of ssDNA probes with MWCNTs/GONRs lead to slight background fluorescence (turning off). The P35s and TNOS targets were detected by dual fluorescent probes to form dsDNA from the specific hybridization of target DNAs and ssDNA probes. Dual fluorescent probes create strong fluorescent signals when the dsDNA is released from the MWCNTs/GONRs (turning on). High efficiency of hybridization, great quenching capacity of MWCNTs/GONRs, and high quantum yield of QDs combine to provide significant benefits than conventional detection methods (Fig. 10a) (Yaqi Li et al., 2017).

Cholesterol is a relevant biomarker of many diseases. An amplified electrochemiluminescent solid-state biosensor was constructed for the sensing of cholesterol in near IR range based on the CdTe quantum dots (CdTeQDs) arranged on MWCNTs at reduced GONRs (CdTeQDs-MWCNTs-rGONRs). This design provides amplified electrochemiluminescence intensity by nearly 4.5 fold. Cholesterol oxidase (ChOx) was confined to the CdTeQDs-MWCNTs-rGONRs for the sensing of cholesterol from biological fluids and food samples. ChOx oxidized the cholesterol molecules and generated H_2O_2. As formed, H_2O_2 acts as a co-reactant in the electrochemiluminescence system of CdTeQDs-MWCNTs-rGONRs. This biosensor showed good reproducibility, selectivity, acceptable linear range (1 μM to 1 mM), and relatively low LOD of 0.33 μM (Huan et al., 2015).

6.2.2. Colorimetric biosensors

Integration of metal nanoparticles with graphene derivatives is one of the best approaches to improve surface plasmon of noble metal nanoparticles. Graphene-metal hybrid improves the plasmonic tunability from visible to IR range. Graphene plasmon can be tuned by altering the structural properties and lowering the dimension. Hence GNRs exhibited excellent plasmonic features with additional advantages. On the external electromagnetic field, the excited free electrons oscillate and create surface plasmon inside the ribbon. Therefore, the GNR-metal hybrid can generate synergistic surface plasmon effects and are more sensitive to environmental changes (Rostami et al., 2020). By changing the position and localized surface plasmon resonance (LSPR), absorption intensity, colorimetric sensors were designed.

Recently researchers developed a colorimetric detection of DA and glutathione (GSH) from serum by exploiting the benefit of plasmon hybridization in GONR/AgNPs hybrid. GSH plays a vital role in biological processes and cellular functions. Imbalance of GSH level causes cell damage, liver damage, heart diseases, loss of leukocytes, and cancer. DA detection is based on the etching of label-free AgNPs with GONRs, which leads to the morphological transformation and a blue shift in the plasmonic band with green to red color change. Consecutively, GSH induced aggregation of nanoparticles decreases the absorption intensity of nanoparticles' plasmonic band, and red to gray color change occurs. The study was conducted on graphene oxide (GO) and MWCNTs too instead of GONRs. The results revealed the importance of GNRs in improving performance and sensitivity (Rostami et al., 2020).

6.3. GNR-based FET biosensors

FETs are a type of electrical biosensors, have a great interest in the research field due to their compatibility with the point of care applications with fast detection ability(Zhou et al., 2017).GNRsare attractive materials for FETs due to their unique characteristics such as high on/off

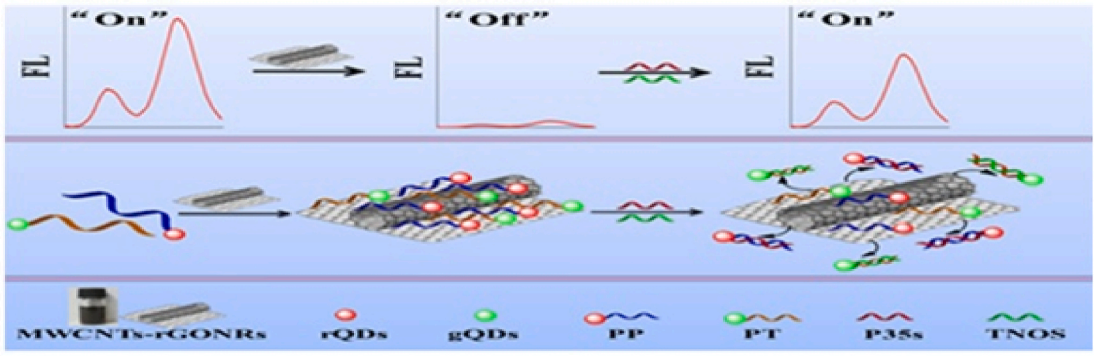

a

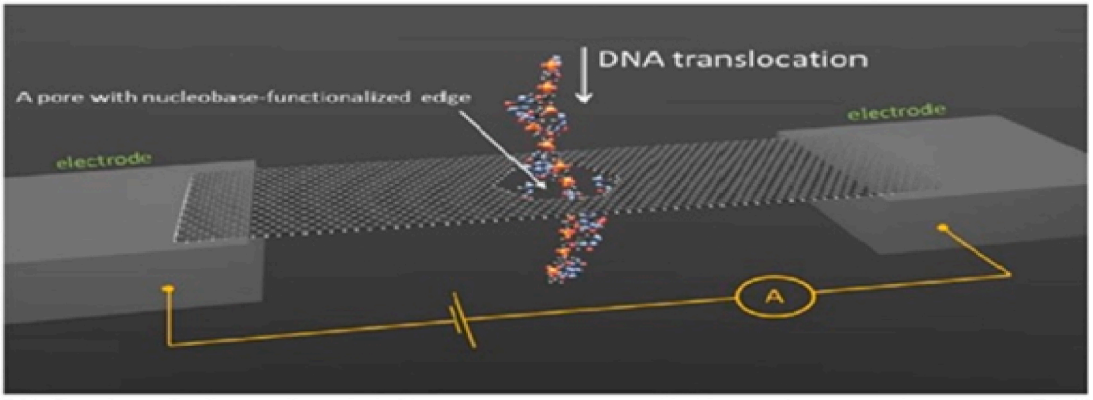

b

Fig. 10. a) Detection of target DNA with Fluorescent "on-off-on" switching sensor based on QDs coupled with MWCNTs@GNRs. Reprinted with permission from (Yaqi Li et al., 2017) Copyright (2017) Elsevier. **b)**DNA translocation through nucleobase functionalized nanopore. Reprinted with permission from (Paulechka et al., 2016) Copyright (2017) Royal Society of Chemistry.

ratio, tunable field-effect characteristics, tunable conductivity, good oxidation level, and comparatively low 1/f noise (Lin et al., 2016; Zhang and Cui, 2013).The FET biosensor is usually made up of a channel, drain, substrates, and a source. In GNR-FET biosensors, a GNR-based transducer functionalized with a biorecognition element acts as the channel. The bioreceptor and analyte recognition reaction makes a variation in the electrical conductivity of the GNR based transducer. Biosensing happens when the electrical conductance variation is high enough for measurement (Sang et al., 2016; Xu et al., 2018). In GNR based FET, GNR based channel is placed on a dielectric substrate usually made up of a silicon substrate with an oxide. The GNR is placed between drain and source electrodes and is biased, usually by the back gate or top gate. The electrical field created by the bias controls the current between the source and drain electrodes.

In a study, a double gate GNR based FET for the recognition of DNA was designed and developed. The designed sensor was simulated by using the Schrodinger equation. For the electrical detection of DNA, the dielectric function modulation technique was used. The whole GNR with a cavity is embedded between two SiO_2 dielectric layers. The sensitivity of the detection was analyzed as a function of physical and dimensional parameters. By increasing the thickness of the cavity and decreasing the length of the channel, the sensitivity of the neutral DNA was amplified. Enhanced sensitivity and electrical performance were shown by this sensor in comparison with other FET based sensors (Tamersit and Djeffal, 2016). An rGONR-based field-effect transistor (rGONRs-FET) exhibited a high on/off ratios on electrical measurements of Adenosine triphosphate (ATP) molecules under a liquid gate configuration. It was higher in comparison to rGOs, single layer pristine graphene, and graphene produced by the CVD process. The limit of detection achieved with this sensor was 5 mM, which is remarkably lower than that of the SWCNTs sensor (500 mM) (Dong et al., 2011). MB is an essential chemical having a wide range of applications as a color indicator. Quantitative analysis of MB gives valuable information regarding pH, redox level, bacterial growth rate, etc. A solution-processed rGONR based FET biosensor was constructed for the detection of MB. The immersion of rGONR in MB causes the enhanced conduction of rGONR and improved sensitivity (Lin et al., 2016)

An ion-sensitive field-effect transistor (ISFET) based on the suspended GNR produced by shrink lithography was used for the sensing of pH/cancer biomarkers. GNR patterns are achieved by the hot embossing process of shrink thermoplastic film. For the biomarker sensing, the GNR surface is functionalized by the immobilization of anti-prostate specific antigen-antibody (anti-PSA-Ab). The detection limit for PSA molecules is down to 0.4 pg mL^{-1}.The pH sensing studies showed that with increasing pH from 5 to 9, GNR-ISFET shows a positive shift of the Dirac point. This positive shift is mainly due to the electrostatic gating effect of charged ions. The decrease in pH value leads to the negative shift of the Dirac point. The surface of GNRs has positively charged, so it needed a negative gate voltage to attain a balanced condition. GNR can act as a p-type material with applied negative potential, which will increase the Id of the ISFET with rising pH. Similarly, p-type material is converted to n-type with applied positive potential with a decrease in Id with increasing pH (Zhang and Cui, 2013). A study has investigated the edge effects of electrolyte gated graphene FETs on pH response enhancement. It was found that GNRs are an effective pH sensing material in comparison to pristine graphene. Pristine graphene and defect-free CNT-FETs will not respond to pH changes due to the absence of a free bond on the saturated graphene surface. The pH response has been increased from 4.2 to 24.6 mV/pH after downscaling of the pristine graphene to GNRs by oxygen plasma etching and electron beam lithography. More number of hydroxyl groups attached to edge defects is attributed to the improved pH response (Tan et al., 2013).

A GNR-FET, along with a nanogap inserted on a top gate oxide biosensor system, has been investigated for the sensing of the streptavidin-biotin binding system. An increase in drain current due to the introduction of a biomolecule into the nanogap is considered as the response of the biosensor (Anvarifard et al., 2020). Identification of the conformation changes of protein or peptide is important in diagnosing diseases and determining dynamic function. Different protein conformation was distinguished with several layers of GNR-nanopore sensors. The conformations of octapeptideangiotensin II was detected by estimating the protein-induced electrostatic potential while passing through the nanopore. Each conformation induced a unique electrostatic potential (Qiu and Skafidas, 2014).

6.3.1. FET biosensors for DNA sequencing

Mapping of the entire human genome provides a powerful approach to identify the traits influenced by inheritance, predisposition of diseases, and to get personalized medicines. But the total cost for genome mapping is not affordable, and it is very time consuming (Altshuler et al., 2008). To promote genome sequencing, it is critical to develop sophisticated low-cost techniques. Biological and solid-state nanopore sequencing methods are attractive in this field. David Dreamer proposed the concept of third-generation sequencing devices, measuring the differences in the conductivity of a DNA molecule in ionic liquid while passing via a nanopore (Rastgoo and Fathipour, 2019). A solid-state nanopore is more stable and reliable, but the thickness of the pore is higher than the distance between two nucleotides. So, new material like GNRs having a low thickness was tried. The monolayer of graphene having about 0.3 nm thickness is exactly equal to the distance between DNA nucleobases. Hence, GNR nanopore sequencing method offers tremendous advantages in this field (Wasfi et al., 2019). When DNA bases passing through the nanopore on the GNR surface, the electronic current changes specifically with each DNA bases.

A study on the supramolecular assembly of DNA on GNRs revealed the high affinity of single-stranded DNA (ssDNA) to GNRs. An important change in the electronic characteristics of GNRs happens with the electron-donating ssDNA. The donor-acceptor interactions of DNA and GNRs and van der Waals force enables the self-assembly of DNA on GNRs. Also, an anisotropic nanopatterning is observed with ssDNA and pComb-5 dsDNA on GNRs (Reuven et al., 2013).

A two-terminal device for DNA sequencing was developed by exploiting the electronic transport and local current density confined around the zig-zag edges. The device consists of a nanopore on zig-zag edged GNRs. When different DNA nucleobases are translocated through the hydrogen passivated nanopore, device conductance changed according to the nucleobases. Further, the drilling of nanopore does not reduce the conductance of GNRs. Insertion of nucleobase into the nanopore leads to the modulation of edge conduction current and change in charge density(Saha et al., 2012). Most of the typical membrane insulated solid-state nanopores are nearly 15 bases thick, which complicated the sensing of individual bases. The similarity in the thickness of GNRs to space between two nucleotide bases offers the simultaneous detection of DNA bases. Changes in local voltage and reduction in ionic current in the transistor in response to the passage of DNA through nanopore can be used to detect the molecules. Nanopore drilled on GNR and thin SiNx membrane was used for the identification of DNA molecules (Traversi et al., 2013).

The device current changes significantly with the interaction of nucleobases with nanopore because of the different chemical composition and coupling strength of nucleobases. The distinguished ability of the sensor depends on the nanopore position. For different bias voltage, edge nanopore GNR shows current downward order for different nucleobases is I(C)>I(T)>I(A)>I(G). Hence, the device can distinguish the nucleobases through the simultaneous detection of device current (Ouyang et al., 2011). A hybrid Z-shaped GNR biosensor was fabricated with a two metallic electrode (ZGNRs) connected with a central semiconducting electrode (AGNR). A nanopore was drilled on the center of the central AGNR, and the pore was passivated with hydrogen. The passage of different nucleotides through the hydrogen passivated nanopore leads to the unique change in the current, conductance, and transmission spectrum of the sensor. This is due to the significant change

in electric current passing through and the charge density of the surrounding nanopore. The change is unique for each nucleotide; hence, it is possible to sequence the DNA in a fast and reliable manner (Wasfi et al., 2019).

A high-speed sensor for DNA sequencing can be constructed with a cytosine incorporated nanopore. The mechanism of detection combines the Watson and Crick complementary base pairing with the GNR capability for altering the anisotropic lattice strain to electric current change at the nanoscale. During the translocation of different nucleobases through the nanopore, the complementary base pair of cytosine makes a hydrogen bond with the cytosine. The translocation pulls upon the bond and alters the direction of GNR to out of the plane. At last, it makes a slip when it gets sufficient strength to rupture the hydrogen bond. The difference in strain generates a provisional change in electric current, and it serves as the response for DNA sequencing. Similarly, the functionalization of nanopore with different DNA bases is selective to its complementary base pairs. Nanopore functionalized with A/T/C/G helps in the detection of T/A/G/C, respectively (Fig. 10b) (Paulechka et al., 2016).

7. GNRs versus graphene: Which should I use?

Pristine graphene is the pure and unoxidized form of a two-dimensional single-layer graphite sheet without any structural defects. Defect-free and inert chemical surfaces of pristine graphene show poor electrochemical activity (Martín et al., 2015b). Oxidation and exfoliation of graphite lead to the formation of GO with reduced aromaticity and heterogeneous electron transfer than pristine graphene. The reduction of GO to rGO recovers the aromaticity and heterogeneous electron transfer, but it is not exactly equivalent to the pristine graphene due to the presence of defects and new heteroatoms (Martín et al., 2015b). Polycrystalline graphene is a form of graphene comprising of single-crystalline domains of graphitic carbon with varying lattice orientations and connected by grain boundaries. Large area graphene produced by epitaxial growth is expected to be polycrystalline due to the substrate imperfections and kinetic bottlenecks of the growth process. This orientational disorder is characterized by the presence of topological defects such as disclinations, dislocations, and grain boundaries, which clearly distinguishes the polycrystalline graphene from graphene/pristine graphene. These defects strongly affect the electrical, thermal, thermoelectric, mechanical, and chemical properties of polycrystalline graphene. Tailoring these defects by introducing and manipulating topological disorders could promise interesting functionalities useful for thermoelectric devices. However, the atomically precise engineering of individual topological defects is a major challenge that limits the application of polycrystalline graphene in new nanoscale devices (Paul et al., 2011; Wang et al., 2014; Yazyev and Chen, 2014; Yazyev and Louie, 2010). To date, only a few studies have been reported on polycrystalline graphene nanoribbons.

GNR is a miniaturized one-dimensional version of pristine graphene with a very high aspect ratio (length to width). These quasi-one-dimensional strips of graphene possess a width of less than 50 nm, combines the properties of the two-dimensional structure of graphene and the one-dimensional structure of CNTs. GNRs possess a larger surface area and more active sites than pure graphene, and it could enhance the adsorption and electrocatalysis of some molecules (Li et al., 2015; Vukojević et al., 2018b; Zhao et al., 2019). The major disadvantage of graphene is its zero bandgap; greatly prevents the application in electronic and optoelectronic devices. However, the cutting of two-dimensional graphene into one-dimensional GNR opens up the bandgap by lateral quantum confinement and edge effects (Hao et al., 2020; Sun et al., 2015). Owing to their open bandgap, GNRs show interesting optical characteristics. GNRs show a broad photoluminescence activity around 533 nm in the visible range (Hu et al., 2018; Senkovskiy et al., 2017). The open bandgap of GNRs can be controlled by tuning of atomic-scale structures. Chemical reactivity, charge transfer, electrocatalytic ability, and optical properties can be enhanced by controlling the bandgap (Lee et al., 2018a). Unlike graphene, the bandgap opening imparts a semiconducting behavior to GNRs. Therefore, in comparison to graphene, GNRs can control the electricity with on-off switching ability (graphene is always on) (Lavanya and Gomathi, 2015; Rauti et al., 2019). Compared to all other carbon-based nanomaterials, GNRs possess the highest edge density and edge defects. In comparison to graphene, GNRs exhibit higher area normalized edge plane structures and chemically active sites. Therefore, GNR is considered a superior electrode material for electroanalytical chemistry (Govindasamy et al., 2017b). GNRs possess abundant sp^2 domains and rich edge chemistry; hence, the immobilization of biomolecules is easy with GNRs (Rajaji et al., 2018). Compared with graphene, GNRs have straight and atomically smooth edges and a high length to width ratio (Feng et al., 2018; Kausar, 2019).

GNRs show the densest and abundant edge defects with greater chemical reactivity within the single channel units. Owing to the nonbonding of the localized states and the nearness of the flat band to Fermi level, edge sites of GNR should be like a radical; hence, GNRs show more sensitivity to analyte binding than pristine graphene (Cho et al., 2018). Graphene is a chemically inert material and makes interactions via physical adsorption. But the different chemical groups on the edges of GNRs render them more chemically reactive. Additionally, depending on the edge pattern, reactivity could change. The sensing abilities of GNRs are superior to graphene due to the highest number of reactive edges (Terrones et al., 2010). GNRs possess a more open-ended structure than graphene. It provides a high density of reaction edges and a large active surface area, which helps attach enzymes or other biomolecules via π-π and electrostatic interaction (Sandeep et al., 2018). The functionalization of GNRs is comparatively easier than graphene due to the higher edge reactivity of GNRs (Tan et al., 2013). GNRs possess good surface integration with very few defects and or holes on the basal plane of nanoribbons. Hence it is the best platform for signal transduction with integrated materials. GNRs are more favorable for the gathering of significant aromatic molecules by π-π interactions. The abundant edge density improves the electrocatalytic performances (Pan et al., 2015).

GO is an oxidized form of graphene composed of an unoxidized hydrophobic graphitic basal plane and oxidized domain-containing functionalities such as carboxyl, hydroxyl, carbonyl, and epoxide groups (Dideikin and Vul', 2019; Krishnan et al., 2012). GONR is an oxidized form of GNR that resembles the miniaturized but laterally extended version of GO. In GONRs and GO, the presence of high oxygen moieties provides sites for covalent functionalization, and the aromatic regions offer sites for the non-covalent binding of molecules through π-π stacking interactions. The carboxyl functionalities of GONRs and GO permits easier cross-linking with the amine groups of proteins via carbodiimide crosslinker chemistry. Oxygenation reduces the sp^2 character and introduces sp^3 domains. Therefore, the electron transfer between the analyte and GONRs/GO occurs via sp^2 domains. But it is facilitated by oxygen functionalities in sp^3 domains (Jin et al., 2020; Rajaji et al., 2018). GO shows a broad photoluminescence peak around 710 nm in the visible range, chemiluminescence, and fluorescence properties owing to its wider bandgap. GONR shows photoluminescence activity similar to GNRs but with a prominent blue shift(Mei et al., 2019). Compared to GO, GONR has more edges, an open-ended structure, and high oxygen functionalities making it more reactive than GO. Also, GONR exhibits enhanced sensor response due to its narrow width, high surface to volume ratio, high specific surface area, enriched edge defects, edge density, fast electron transfer, and rich oxygen functional groups. (Martín et al., 2014). From this perspective, GONR can serve as a better host compared to GO for the immobilization of sensing agents such as enzymes, redox proteins, antibodies, antigens RNA, drugs, DNA, and viruses (Chowdhury et al., 2015; Rajaji et al., 2018; Rostami et al., 2020; Valentini et al., 2013). In addition, GONRs show high chemical stability, biocompatibility, ability to increase enzyme activity, good dispersibility, and enhanced sensitivity, which qualify them as desired material in

biosensing applications (Rajaji et al., 2018).

rGO is an analog of GO obtained by removing oxidized functional groups in GO. It shows better conductivity and has more resemblance to graphene than to GO. The residual oxygen functionalities and defects make it a potential material for sensing applications (Chiang et al., 2016). rGONR is a miniaturized form rGO with a long length derived from GONR via different reduction reactions (Chowdhury et al., 2015; Rajaji et al., 2018) It has more resemblance to the unoxidized GNR than GONR, but it contains high sp^2 carbon content with a few remaining oxygen functionalities (Martín et al., 2015b). rGONR exhibits a higher on/off ratio than rGO (Dong et al., 2011). It is more conductive and possesses better sensing characteristics than GONR. Its open-ended structure, coupled with a fine-tunable bandgap, makes it suitable for optoelectronic applications (Mogha et al., 2018). Photoluminescence activity of rGONRs is similar to GNR in the visible range. rGO exhibits photoluminescence near in UV-visible range of 300 to 800 nm range (Krishnamoorthy et al., 2012). In rGONRs the charge transport is dominated by localized states and their edges since it is highly sensitive to local molecular targeting (Dong et al., 2011). The open-ended reactive structure, high specific surface area, high edge defects, edge density, and oxygen content increase the sensing application of rGONRs than rGO.

Transfer of charge variation in narrow width GNR is faster than the GO and rGO with a relatively large width. Hence, GNR-based sensors exhibited a faster response than GO and rGO (Cho et al., 2018). High sp^2 carbon content and low oxygen content increases the conductivity of rGONRs than GONRs. Both GONR and rGONRs exhibit electrochemical performance, but rGONR is an exceptional material due to the restored sp2 structure and remaining oxygen (Martín et al., 2014; Sharma et al., 2015). The GNR derivatives GONR and rGONR are expected to show good optical characteristics suitable for optical sensing applications because of the nature of their bandgap. However, these properties are not much studied to date, and this is an interesting area of research to explore. The advantage behind the use of GNR as a potential material for sensing is its high accessibility to functionalization and doping owing to its narrow width, open edge, and highly dense edge defect sites (Cho et al., 2018). A summary of the differential characteristics of GNR, pristine graphene, and their derivatives are provided in Fig. 11.

8. Prospects of GNR in biosensing and bioelectronics

Healthcare is an important aspect, and the detection of biomarkers and the factors that affect health and well-being are essential in health care. Thus we need sensors that are ideal and practically applicable in diverse fields and conditions. In the future, we need biosensors of high sensitivity, selectivity, and stability as well as less bulky and low-cost devices that can ensure point-of-care detection.

A recent study reported the synthesis of highly conductive narrow GNR from the wrinkles and edges of graphene flakes(Park et al., 2016). This method opens the possibilities for highly conductive electrochemical biosensing. This review is discussed the *in vitro* GNR-based biosensing technologies alone; the *in vivo* biosensing technology is not yet experimented with GNRs.The biocompatibility, biodegradability, and toxicity studies are not well established so far. So, in the future, GONRs can be utilized for biosensing with the appropriate biocompatibility, biodegradability, and toxicity data. The sensitive and selective detection of pathogenic microorganisms remains a big challenge and practical problem for disease diagnosis. GS, graphene, GO, and rGO were used in the detection of viruses, bacteria, and bacterial toxins; still, there are no such studies reported with GNRs. In this era of COVID-19 pandemic, fast and reliable sensing of the presence of a virus is the needy thing for early detection and treatment. Thus, this fascinating material can be explored for the detection of pathogenic organisms with specific Ab attachments in the future.

GNRs also exhibit significant optical properties. It is possible to develop more sensitive devices based on fluorescence, photoluminescence, and surface plasmon resonance techniques in the future. FRET technology is a highly sensitive method for the detection of biomolecules. But not many studies have carried on this contest yet. Further studies regarding fluorescence quenching of GNR is required to explore this area like the other derivatives. Surface-enhanced Raman scattering (SERS) effects are not yet well explored for GNR. Graphene enhanced

rGONR	GONR	GNR	Characteristics	Pristine graphene	GO	rGO
1D	1D	1D	Dimensionality	2D	2D	2D
Ribbon like	Ribbon like	Ribbon like	Shape	Sheet like	Sheet like	Sheet like
Open band gap	Open band gap	Open band gap	Band gap	Zero band gap	Open/large band gap	Zero/low band gap
Semiconductor	Semiconductor	Semiconductor /metallic	Conductivity	Conductor	Semiconductor /insulator	Conductor
On-off switching ability	On-off switching ability	On-off switching ability	Current flow	Always ‘on’	On-off switching ability	Resistive on-off switching ability
Chemically active	Chemically active	Chemically active	Chemical activity	Chemically inert	Chemically active	Chemically active
More	More	More	Active sites	Less	More	Less
Moderate	High	Moderate	Surface area	Less	High	Less
High	High	High	Length to width ratio	Less	Less	Less
High edge density, edge defect, and reactive edge	High edge density, edge defect, and reactive edge	High edge density, edge defect, reactive edge	Edge	Comparatively low edge density, edge defect, and edge reactivity	Comparatively low edge density, edge defect, and edge reactivity	Comparatively low edge density, edge defect, and edge reactivity
A few	High	Nil	Oxygen functionalities	Nil	High	A few

Fig. 11. Differential characteristics of GNR, pristine graphene, and their derivatives.

Raman scattering (GERS) can improve the SERS effect by combining its spectral fingerprinting of molecules, graphene's simple processing, single-molecule sensitivity,and superior uniformity. This enables the enhanced signaling and sensitivity of biomolecules. Wearable biosensors are a promising field in live and continuous health care and fitness monitoring. Graphene-based wearable wireless sensors are reported; they can send data to mobile phones or computers via Bluetooth. In the future, GNR-based wearable sensors can be fabricated because GNR offers favorable characteristics for making better sensors than any other graphene–family nanomaterials. For future wearable sensor designs, biofouling, stability, and degradation should be addressed.

3-D printing technology is an emerging field but not yet utilized for GNR-based sensing. The devices developed by 3-D printing technology can respond to electronic, optical, thermal, and electrochemical stimuli (Muñoz and Pumera, 2020). In the future, this technology would facilitate developing customized, atomically precise, and properties-controlled GNRs from GNR sheets, specifically for biosensing applications. 3-D printing of GNR allows the translation of desired properties to well defined, ordered GNR structures suitable for practical applications. A study reported '3-D solution printing' of GONR without using any supporting surfactants or polymers (Wang et al., 2016). Various ink-based 3-D printing technologies are available for graphene-based materials. These can have application the fabrication of GNR-based electrodes for biosensing. The 3-D printing of a GNR sensing platform can avoid the obstacles of conventional fabrication of sensors like tedious fabrication procedure, high cost, etc. But it is then necessary to develop new ideas for functionalization, doping, fabrication of nanocomposites, and immobilization strategies for 3-D printed GNR biosensors. The use of advanced functional materials for 3-D printing will open up new opportunities in the next-generation biosensors.

The increasing need for point-of-care detection enhances the availability of miniaturized devices in the sensing field. Hence to meet future needs, it is crucial to design new methods for miniaturization. The emergence of micro and nanomotors in biosensing shows successful dimensions like true miniaturization, low cost, and simplification. In the future, the fabrication of GNR-based micro and nanomotors by template-directed electrodeposition protocol or by GNR rolled up method can be expected for highly sensitive and portable biosensors (Baptista-pires et al., 2017; Jurado-Sánchez, 2018).

A combination of the CRISPR/Cas system with a GNR-based platform can be utilized for the production of next-generation biosensors. As in the case of GO, covalent functionalization of the CRISPR/Cas complex with oxidized carbonyl groups of GONR can be done easily with carbodiimide cross-linking chemistry (Zihni et al., 2020). Combined advantages of GNR sensing platform and CRISPR/Cas system will be a hopeful platform for the detection of mutated tumor cells, genotyping, pathogenic microorganisms, etc. In the future, it is possible to develop electrochemical or optical GNR-based G-quadruplex biosensors, since it is applicable for the detection of pathogens (including SARS-CoV-2), metal ions, biomarkers, etc.

Even though many procedures are available to synthesize GNRs, the synthesis of atomically precise GNR is the primary prerequisite for the fabrication of GNR based biosensors. But atomically defined, high yield, and reproducible synthesis of GNRs pose a challenge. Also, fabrication of the GNR-based electrode is usually expensive, time-consuming, and involves multistep procedures. Hence an affordable, simple, and easy fabrication method for the GNR-based biosensors is highly desirable. 3-D printing of GNRs is a hopeful method to overcome these issues. Meanwhile, biocompatibility and toxicity are serious issues when biosensors are intended for *in vivo* applications. Unfortunately, GNR and its derivatives can be more toxic than pristine graphene and its derivatives (Khim Chng et al., 2014). It is also noted that structural disruption of GNR enhances its toxicity. Such issues are hurdles in the success of GNR-based biosensors for clinical applications. Luckily, chemical surface modifications such as PEGylation are promising in the reduction of toxicity of GNRs (Akhavan et al., 2012). But the effect of chemical surface modifications of GNR (and its derivatives) on biosensor characteristics needs serious consideration.

9. Conclusion

The application of GNR in the biosensing field is not well explored. But in comparison with all other biomedical applications, biosensing is the most studied application of GNR. There is still an imperative necessity existing for new ideas for developing real biosensors of high sensitivity and selectivity at an affordable cost. Compared to conventional biosensing techniques, GNR-based biosensing has benefits like high sensitivity, selectivity, fast response, a large surface area for adsorption, easy fabrication, synergistic effects with combined materials, etc. To improve their biosensing characteristics and to reduce the device-to-device variations, interdisciplinary approaches are needed. It could be a perfect aspirant for next-generation biosensors. However, scientific breakthrough efforts need to commercialize the GNR based biosensors.

Funding

This work was funded by the Indian Council of Medical Research, New Delhi, India (RFC Number: NCD/Adhoc/58/2019-20 Dt 23/8/2019).

Declaration of competing interest

The authors declare that they have no known competing financial interests or personal relationships that could have appeared to influence the work reported in this paper.

Acknowledegements

HVG acknowledges the Indian Council of Medical Research, New Delhi, India for providing funding for the project (RFC Number: NCD/Adhoc/58/2019-20 Dt 23/8/2019). APJ acknowledges the Indian Council of Medical Research, New Delhi, India for providing the fellowship (JRF/SRF, Ref No. NCD/Adhoc/58/2019-20 Dt 23/8/2019). APJ also thanks Dr. M.P. Venkatesh, Assistant Professor, Department of Pharmaceutics, and Dr. Saravana Babu, Associate Professor, Department of Pharmacology, JSS College of Pharmacy, JSS Academy of Higher Education and Research, Mysuru, India, for their help and support in the project.The authors also thank Mr. Shahid M, Ph.D. Scholar, IISER, Tirupati, India, for his help in the preparation of some chemical structures.

References

Abbas, A.N., Liu, G., Liu, B., Zhang, L., Liu, H., Ohlberg, D., Wu, W., Zhou, C., 2014. Patterning, characterization, and chemical sensing applications of graphene nanoribbon arrays down to 5 nm using helium ion beam lithography. ACS Nano 8, 1538–1546. https://doi.org/10.1021/nn405759v.

Abramova, V., Slesarev, A.S., Tour, J.M., 2013. Meniscus-mask lithography for narrow graphene nanoribbons. ACS Nano 7, 6894–6898. https://doi.org/10.1021/nn403057t.

Akhavan, O., Ghaderi, E., Emamy, H., 2012. Nontoxic concentrations of PEGylated graphene nanoribbons for selective cancer cell imaging and photothermal therapy. J. Mater. Chem. 22, 20626–20633. https://doi.org/10.1039/C2JM34330D.

Altshuler, D., Daly, M.J., Lander, E.S., 2008. Genetic mapping in human disease. Science (80-.) 322, 881–888. https://doi.org/10.1126/science.1156409.

Ambrosi, A., Chua, C.K., Bonanni, A., Pumera, M., 2014. Electrochemistry of graphene and related materials. Chem. Rev. 114, 7150–7188. https://doi.org/10.1021/cr500023c.

Anusha, J.R., Kim, B.C., Yu, K.H., Raj, C.J., 2019. Electrochemical biosensing of mosquito-borne viral disease, dengue: a review. Biosens. Bioelectron. 142, 111511. https://doi.org/10.1016/j.bios.2019.111511.

Anvarifard, M.K., Ramezani, Z., Amiri, I.S., 2020. Proposal of an embedded nanogap biosensor by a graphene nanoribbon field-effect transistor for biological samples detection. Phys. Status Solidi Appl. Mater. Sci. 217, 1–7. https://doi.org/10.1002/pssa.201900879.

Apath, D., Moyo, M., Shumba, M., 2020. TiO_2 nanoparticles decorated graphene nanoribbons for voltammetric determination of an anti-HIV drug nevirapine. J. Chem. 2020, 3932715. https://doi.org/10.1155/2020/3932715.

Arrigoni, O., De Tullio, M.C., 2002. Ascorbic acid: much more than just an antioxidant. Biochim. Biophys. Acta Gen. Subj. https://doi.org/10.1016/S0304-4165(01)00235-5.

Arsenin, A.V., Stebunov, Y.V., Volkov, V.S., 2018. Graphene oxide linking layers for highly sensitive SPR biosensing of small molecules. In: Materials Today: Proceedings. Elsevier Ltd, pp. 17437–17441. https://doi.org/10.1016/j.matpr.2018.06.046.

Asadian, E., Shahrokhian, S., Zad, A.I., Jokar, E., 2014. In-situ electro-polymerization of graphene nanoribbon/polyaniline composite film: application to sensitive electrochemical detection of dobutamine. Sensor. Actuator. B Chem. 196, 582–588. https://doi.org/10.1016/j.snb.2014.02.049.

Azeredo, N.F.B., Gonçalves, J.M., Rossini, P.O., Araki, K., Wang, J., Angnes, L., 2020. Uric acid electrochemical sensing in biofluids based on Ni/Zn hydroxide nanocatalyst. Microchim. Acta 187, 1–11. https://doi.org/10.1007/s00604-020-04351-2.

Bahadir, E.B., Sezgintürk, M.K., 2016. A review on impedimetric biosensors. Artif. Cells, Nanom. Biotechnol. https://doi.org/10.3109/21691401.2014.942456.

Balarastaghi, M., Ahmadi, V., Darvish, G., 2016. Electro-optical properties of new structure photodetectors based on graphene nanoribbons: an ab initio study. J. Opt. Soc. Am. B 33, 2368. https://doi.org/10.1039/C5CP06533J.

Baptista-pires, L., Orozco, J., Guardia, P., Merkoçi, A., 2017. Architecting graphene oxide rolled-up Micromotors :A simple paper-based manufacturing technology. https://doi.org/10.1002/smll.201702746, 1702746, 1-8.

Bard, A.J., Faulkner, L.R., 2001. Electrochemical methods: fundamentals and applications. Russ. J. Electrochem. 38 (2001), 1364–1365. https://doi.org/10.1023/A:1021637209564.

Barzegar, H.R., Pham, T., Talyzin, A.V., Zettl, A., 2016. Synthesis of graphene nanoribbons inside boron nitride nanotubes. Phys. Status Solidi B 3, 1–3. https://doi.org/10.1002/pssb.201600294.

Benelmekki, M., Erbe, A., 2019. Chapter 1 - nanostructured thin films–background, preparation and relation to the technological revolution of the 21st century. In: Benelmekki, M., Erbe, A.B.T.-F., N (Eds.), Nanostructured Thin Films. Elsevier, pp. 1–34. https://doi.org/10.1016/B978-0-08-102572-7.00001-5.

Bhushan, R., Kumar, P., Thakur, A.K., 2020. Catalyst-free solvothermal synthesis of ultrapure elemental N- and B-doped graphene for energy storage application. Solid State Ionics 353, 115371. https://doi.org/10.1016/j.ssi.2020.115371.

Bianco, A., Cheng, H.M., Enoki, T., Gogotsi, Y., Hurt, R.H., Koratkar, N., Kyotani, T., Monthioux, M., Park, C.R., Tascon, J.M.D., Zhang, J., 2013. All in the graphene family - a recommended nomenclature for two-dimensional carbon materials. Carbon N. Y. https://doi.org/10.1016/j.carbon.2013.08.038.

Biercuk, M.J., Llaguno, M.C., Radosavljevic, M., Hyun, J.K., Johnson, A.T., Fischer, J.E., 2002. Carbon nanotube composites for thermal management. Appl. Phys. Lett. 80, 2767–2769. https://doi.org/10.1063/1.1469696.

Bu, H., Chen, Y., Zou, M., Yi, H., Bi, K., Ni, Z., 2009. Atomistic simulations of mechanical properties of graphene nanoribbons. Phys. Lett. A 373, 3359–3362. https://doi.org/10.1016/j.physleta.2009.07.048.

Campos, L.C., Manfrinato, V.R., Sanchez-Yamagishi, J.D., Kong, J., Jarillo-Herrero, P., 2009. Anisotropic etching and nanoribbon formation in single-layer graphene. Nano Lett. 9, 2600–2604. https://doi.org/10.1021/nl900811r.

Campos-Delgado, J., Romo-Herrera, J.M., Jia, X., Cullen, D.A., Muramatsu, H., Kim, Y.A., Hayashi, T., Ren, Z., Smith, D.J., Okuno, Y., Ohba, T., Kanoh, H., Kaneko, K., Endo, M., Terrones, H., Dresselhaus, M.S., Terrones, M., 2008. Bulk production of a new form of sp 2 carbon: crystalline graphene nanoribbons. Nano Lett. 8, 2773–2778. https://doi.org/10.1021/nl801316d.

Celis, A., Nair, M.N., Conrad, E.H., Berger, C., 2016. Graphene nanoribbons : fabrication , properties and devices. J. Phys. D Appl. Phys. 143001, 143001. https://doi.org/10.1088/0022-3727/49/14/143001.

Cervantes-Sodi, F., Csányi, G., Piscanec, S., Ferrari, A.C., 2008. Edge-functionalized and substitutionally doped graphene nanoribbons: electronic and spin properties. Phys. Rev. B 77, 165427. https://doi.org/10.1103/PhysRevB.77.165427.

Cesewski, E., Johnson, B.N., 2020. Electrochemical biosensors for pathogen detection. Biosens. Bioelectron. 159, 112214. https://doi.org/10.1016/j.bios.2020.112214.

Chang, Shen-Lin, Wu, Bi-Ru, Po-Hua Yang, M.-F.L., 2016. Geometric , magnetic and electronic properties of folded graphene nanoribbons. RSC Adv. 6, 64852–64860. https://doi.org/10.1039/C6RA08372B.

Chauhan, N., Maekawa, T., Kumar, D.N.S., 2017. Graphene based biosensors - accelerating medical diagnostics to new-dimensions. J. Mater. Res. 32, 2860–2882. https://doi.org/10.1557/jmr.2017.91.

Chen, Z., Zhang, W., Palma, C., Rizzini, A.L., Liu, B., Abbas, N., Richter, N., Martini, L., Wang, X., Cavani, N., Lu, H., Coletti, C., Berger, R., Klappenberger, F., Kläui, M., Affronte, M., Zhou, C., Renzi, V. De, Pennino, U., Barth, J.V., Räder, H.J., Narita, A., Feng, X., Müllen, K., 2016. Synthesis of graphene nanoribbons by ambient-pressure chemical vapor deposition and device integration. J. Am. Chem. Soc. https://doi.org/10.1021/jacs.6b10374.

Chiang, W.H., Lin, T.C., Li, Y.S., Yang, Y.J., Pei, Z., 2016. Toward bandgap tunable graphene oxide nanoribbons by plasma-assisted reduction and defect restoration at low temperature. RSC Adv. 6, 2270–2278. https://doi.org/10.1039/c5ra21537d.

Cho, K.M., Cho, S.Y., Chong, S., Koh, H.J., Kim, D.W., Kim, J., Jung, H.T., 2018. Edge-functionalized graphene nanoribbon chemical sensor: comparison with carbon nanotube and graphene. ACS Appl. Mater. Interfaces 10, 42905–42914. https://doi.org/10.1021/acsami.8b16688.

Chowdhury, R., Scarpa, F., Adhikari, S., Chowdhury, R., Scarpa, F., Adhikari, S., 2012. Molecular-scale bio-sensing using armchair graphene. J. Appl. Phys. 112, 014905 https://doi.org/10.1063/1.4733689.

Chowdhury, S.M., Surhland, C., Sanchez, Z., Chaudhary, P., Suresh Kumar, M.A., Lee, S., Peña, L.A., Waring, M., Sitharaman, B., Naidu, M., 2015. Graphene nanoribbons as a drug delivery agent for lucanthone mediated therapy of glioblastoma multiforme. Nanomedicine Nanotechnology, Biol. Med. 11, 109–118. https://doi.org/10.1016/j.nano.2014.08.001.

Chung, H.C., Chang, C.P., Lin, C.Y., Lin, M.F., 2016. Electronic and optical properties of graphene nanoribbons in external fields. Phys. Chem. Chem. Phys. 18, 7573–7616. https://doi.org/10.1039/c5cp06533j.

Corso, M., Carbonell-Sanromà, E., de Oteyza, D.G., 2018. Bottom-up fabrication of atomically precise graphene nanoribbons. In: On-Surface Synthesis II. Springer, Cham, pp. 113–152. https://doi.org/10.1007/978-3-319-75810-7_6.

Curri, M.L., Comparelli, R., Striccoli, M., Agostiano, A., 2010. Emerging methods for fabricating functional structures by patterning and assembling engineered nanocrystals. Phys. Chem. Chem. Phys. 12, 11197–11207. https://doi.org/10.1039/B926146J.

de Sousa Araújo Cassiano, T., Monteiro, F.F., Evaristo de Sousa, L., Magela e Silva, G., de Oliveira Neto, P.H., 2020. Smooth gap tuning strategy for cove-type graphene nanoribbons. RSC Adv. 10, 26937–26943. https://doi.org/10.1039/D0RA02997A.

Demers, L.M., Ginger, D.S., Park, S.-J., Li, Z., Chung, S.-W., Mirkin, C.A., 2002. Direct patterning of modified oligonucleotides on metals and insulators by dip-pen nanolithography. Science (80- 296, 1836–1838. https://doi.org/10.1126/science.1071480.

Dideikin, A.T., Vul', A.Y., 2019. Graphene oxide and derivatives: the place in graphene family. Front. Physiol. https://doi.org/10.3389/fphy.2018.00149.

Dimiev, A.M., Khannanov, A., Vakhitov, I., Kiiamov, A., Shukhina, K., Tour, J.M., 2018. Revisiting the mechanism of oxidative unzipping of multiwall carbon nanotubes to graphene nanoribbons. ACS Nano 12, 3985–3993. https://doi.org/10.1021/acsnano.8b01617.

Dong, X., Long, Q., Wang, J., Chan-Park, M.B., Huang, Y., Huang, W., Chen, P., 2011. A graphene nanoribbon network and its biosensing application. Nanoscale 3, 5156–5160. https://doi.org/10.1039/c1nr11006c.

Dutta, S., Pati, S.K., 2010. Novel properties of graphene nanoribbons: a review. J. Mater. Chem. 20, 8207–8223. https://doi.org/10.1039/c0jm00261e.

Dutta, S., Manna, A.K., Pati, S.K., 2009. Intrinsic half-metallicity in modified graphene nanoribbons. Phys. Rev. Lett. 102, 96601. https://doi.org/10.1103/PhysRevLett.102.096601.

Elias, A.L., Botello-Méndez, A.R., Meneses-Rodríguez, D., González, V.J., Ramírez-González, D., Ci, L., Muñoz-Sandoval, E., Ajayan, P.M., Terrones, H., Terrones, M., 2010. Longitudinal cutting of pure and doped carbon nanotubes to form graphitic nanoribbons using metal clusters as nanoscalpels. Nano Lett. 10, 366–372. https://doi.org/10.1021/nl901631z.

Elmarakbi, A., Ciardiello, R., Tridello, A., Innocente, F., Martorana, B., Bertocchi, F., Cristiano, F., Elmarakbi, M., Belingardi, G., 2020. Effect of graphene nanoplatelets on the impact response of a carbon fibre reinforced composite. Mater. Today Commun. 101530 https://doi.org/10.1016/j.mtcomm.2020.101530.

Fan, Y., Li, J., Liu, X., Wang, L., Sun, S., Kawasaki, A., Jiang, W., Chen, X., 2010. A microexplosion method for the synthesis of graphene nanoribbons. Carbon N. Y. 49, 1439–1445. https://doi.org/10.1016/j.carbon.2010.12.013.

Fei, A., Liu, Q., Huan, J., Qian, J., Dong, X., Qiu, B., Mao, H., Wang, K., 2015. Label-free impedimetric aptasensor for detection of femtomole level acetamiprid using gold nanoparticles decorated multiwalled carbon nanotube-reduced graphene oxide nanoribbon composites. Biosens. Bioelectron. 70, 122–129. https://doi.org/10.1016/j.bios.2015.03.028.

Feng, Q., Zhao, X., Guo, Y., Liu, M., Wang, P., 2018. Stochastic DNA walker for electrochemical biosensing sensitized with gold nanocages@graphene nanoribbons. Biosens. Bioelectron. 108, 97–102. https://doi.org/10.1016/j.bios.2018.02.050.

Fujihara, M., Miyata, Y., Kitaura, R., Nishimura, Y., Camacho, C., Irle, S., Iizumi, Y., Okazaki, T., Shinohara, H., 2012. Dimerization-initiated preferential formation of coronene-based graphene nanoribbons in carbon nanotubes. J. Phys. Chem. C 116, 15141–15145. https://doi.org/10.1021/jp3037268.

Garzón, V., Pinacho, D.G., Bustos, R.H., Garzón, G., Bustamante, S., 2019. Optical biosensors for therapeutic drug monitoring. Biosensors. https://doi.org/10.3390/bios9040132.

Geim, A.K., Novoselov, K.S., 2007. The rise of graphene. Nat. Mater. 6, 183–191. https://doi.org/10.1038/nmat1849.

Genorio, B., Znidarsic, A., 2014. Functionalization of graphene nanoribbons. J. Phys. D Appl. Phys. 47, 094012 https://doi.org/10.1088/0022-3727/47/9/094012.

Ghosh, S., Calizo, I., Teweldebrhan, D., Pokatilov, E.P., Nika, D.L., Balandin, A.A., Bao, W., Miao, F., Lau, C.N., 2008. Extremely high thermal conductivity of graphene: prospects for thermal management applications in nanoelectronic circuits. Appl. Phys. Lett. 92, 151911. https://doi.org/10.1063/1.2907977.

Goenka, S., Sant, V., Sant, S., 2014. Graphene-based nanomaterials for drug delivery and tissue engineering. J. Contr. Release 173, 75–88. https://doi.org/10.1016/j.jconrel.2013.10.017.

Gong, X., Zhang, L., Huang, Y., Wang, S., Pan, G., Li, L., 2020. Directly writing fl exible temperature sensor with graphene nanoribbons for disposable healthcare devices. RSC Adv. 10, 22222–22229. https://doi.org/10.1039/D0RA02815K.

Gorjizadeh, N., Kawazoe, Y., 2010. Chemical functionalization of graphene nanoribbons. J. Nanomater. 2010. https://doi.org/10.1155/2010/513501.

Govindasamy, M., Mani, V., Chen, S.M., Chen, T.W., Sundramoorthy, A.K., 2017a. Methyl parathion detection in vegetables and fruits using silver@graphene nanoribbons nanocomposite modified screen printed electrode. Sci. Rep. 7, 1–11. https://doi.org/10.1038/srep46471.

Govindasamy, M., Mani, V., Chen, S.M., Maiyalagan, T., Selvaraj, S., Chen, T.W., Lee, S. Y., Chang, W.H., 2017b. Highly sensitive determination of non-steroidal anti-

inflammatory drug nimesulide using electrochemically reduced graphene oxide nanoribbons. RSC Adv. 7, 33043–33051. https://doi.org/10.1039/c7ra02844j.
Guo, Z.-X., Zhang, D., Gong, X.-G., 2009. Thermal conductivity of graphene nanoribbons. Appl. Phys. Lett. 95, 163103. https://doi.org/10.1063/1.3246155.
Han, M.Y., Özyilmaz, B., Zhang, Y., Kim, P., 2007. Energy band-gap engineering of graphene nanoribbons. Phys. Rev. Lett. 98, 206805. https://doi.org/10.1103/PhysRevLett.98.206805.
Hao, Z., Zhang, H., Ruan, Z., Yan, C., Lu, J., Cai, J., 2020. Tuning electronic properties of atomically precise graphene nanoribbons by bottom-up fabrications. chemnano mat 6, 493–515. https://doi.org/10.1002/cnma.201900706.
Haridas, V., Sukhananazerin, A., Mary Sneha, J., Pullithadathil, B., Narayanan, B., 2020. α-Fe2O3 loaded less-defective graphene sheets as chemiresistive gas sensor for selective sensing of NH3. Appl. Surf. Sci. 517, 146158. https://doi.org/10.1016/j.apsusc.2020.146158.
He, M., Dong, J., Wang, H., Xue, H., Wu, Q., Xin, B., 2019. Advance in close-edged graphene Nanoribbon : property investigation and structure fabrication. Small 1804473, 1–19. https://doi.org/10.1002/smll.201804473.
He, M., Wang, Y., Wang, S., Luo, S., 2020. Laser-induced graphene enabled 1D fiber electronics. Carbon N. Y. 168, 308–318. https://doi.org/10.1016/j.carbon.2020.06.084.
Hernandez, Y., Pang, S., Feng, X., Müllen, K., Planck, M., 2012. Graphene and its Synthesis, Polymer Science:A Comprehensive Reference. Elsevier B.V. https://doi.org/10.1016/B978-0-444-53349-4.00216-8.
Hod, O., Scuseria, G.E., 2006. Electronic structure and stability of semiconducting graphene nanoribbons. Nano Lett. 6, 2748–2754. https://doi.org/10.1021/nl0617033.
Holmes, J.D., Johnston, K.P., Doty, R.C., Korgel, B.A., 2000. Control of thickness and orientation of solution-grown silicon nanowires. Science (80- 287, 1471–1473. https://doi.org/10.1126/science.287.5457.1471.
Hossain, M.F., Park, J.Y., 2017. Fabrication of sensitive enzymatic biosensor based on multi-layered reduced graphene oxide added PtAu nanoparticles-modified hybrid electrode. PLoS One 12, 1–16. https://doi.org/10.1371/journal.pone.0173553.
Hou, Z., Yee, M., 2007. Electronic and transport properties of graphene nanoribbons. Proc. 7th IEEE Int. Conf. Nanotechnol. 554–557.
Hou, I.C.-Y., Hu, Y., Narita, A., Müllen, K., 2018. Diels–Alder polymerization: a versatile synthetic method toward functional polyphenylenes, ladder polymers and graphene nanoribbons. Polym. J. 50, 3–20. https://doi.org/10.1038/pj.2017.69.
Hsu, H., Reichl, L.E., 2007. Selection rule for the optical absorption of graphene nanoribbons. Phys. Rev. B 1–5. https://doi.org/10.1103/PhysRevB.76.045418.
Hu, L., Zhang, Y., Nie, L., Xie, C., Yan, Z., 2013. Colorimetric detection of trace Hg2+ with near-infrared absorbing squaraine functionalized by dibenzo-18-crown-6 and its mechanism. Spectrochim. Acta Part A Mol. Biomol. Spectrosc. 104, 87–91. https://doi.org/10.1016/j.saa.2012.11.026.
Hu, Y., Xie, P., De Corato, M., Ruini, A., Zhao, S., Meggendorfer, F., Straasø, L.A., Rondin, L., Simon, P., Li, J., Finley, J.J., Hansen, M.R., Lauret, J.-S., Molinari, E., Feng, X., Barth, J.V., Palma, C.-A., Prezzi, D., Müllen, K., Narita, A., 2018. Bandgap engineering of graphene nanoribbons by control over structural distortion. J. Am. Chem. Soc. 140, 7803–7809. https://doi.org/10.1021/jacs.8b02209.
Huan, J., Liu, Q., Fei, A., Qian, J., Dong, X., Qiu, B., Mao, H., Wang, K., 2015. Amplified solid-state electrochemiluminescence detection of cholesterol in near-infrared range based on CdTe quantum dots decorated multiwalled carbon nanotubes@reduced graphene oxide nanoribbons. Biosens. Bioelectron. 73, 221–227. https://doi.org/10.1016/j.bios.2015.06.004.
Ismail, N.S., Le, Q.H., Yoshikawa, H., Saito, M., Tamiya, E., 2014. Development of non-enzymatic electrochemical glucose sensor based on graphene oxide nanoribbon - gold nanoparticle hybrid. Electrochim. Acta 146, 98–105. https://doi.org/10.1016/j.electacta.2014.08.123.
Jiao, L., Zhang, L., Wang, X., Diankov, G., Dai, H., 2009. Narrow graphene nanoribbons from carbon nanotubes. Nature 458, 877–880. https://doi.org/10.1038/nature07919.
Jiao, L., Zhang, L., Ding, L., Liu, J., Dai, H., 2010. Aligned graphene nanoribbons and crossbars from unzipped carbon nanotubes. Nano Res. 3, 387–394. https://doi.org/10.1007/s12274-010-1043-z.
Jin, S., Mavoori, H., 1998. Processing and properties of CVD diamond for thermal management. J. Electron. Mater. 27, 1148–1153. https://doi.org/10.1007/s11664-998-0063-x.
Jin, Y., Zheng, Y., Podkolzin, S.G., Lee, W., 2020. Band gap of reduced graphene oxide tuned by controlling functional groups. J. Mater. Chem. C 8, 4885–4894. https://doi.org/10.1039/c9tc07063j.
Johnson, A.P., Gangadharappa, H.V., Pramod, K., 2020. Graphene nanoribbons: a promising nanomaterial for biomedical applications. J. Contr. Release 325, 141–162. https://doi.org/10.1016/j.jconrel.2020.06.034.
Jothi, L., Neogi, S., Jaganathan, S. kumar, Nageswaran, G., 2018. Simultaneous determination of ascorbic acid, dopamine and uric acid by a novel electrochemical sensor based on N2/Ar RF plasma assisted graphene nanosheets/graphene nanoribbons. Biosens. Bioelectron. 105, 236–242. https://doi.org/10.1016/j.bios.2018.01.040.
Jothi, L., Jaganathan, S.K., Nageswaran, G., 2020. An electrodeposited Au nanoparticle/porous graphene nanoribbon composite for electrochemical detection of alpha-fetoprotein. Mater. Chem. Phys. 242, 122514. https://doi.org/10.1016/j.matchemphys.2019.122514.
Jurado-Sánchez, B., 2018. Nanoscale biosensors based on self-propelled objects. Biosensors 8, 1–15. https://doi.org/10.3390/bios8030059.
Kalcher, K., Samphao, A., 2019. A highly sensitive fenobucarb electrochemical sensor based on graphene nanoribbons-ionic liquid-cobalt phthalocyanine composites modified on screen-printed carbon electrode coupled with a flow injection analysis. J. Electroanal. Chem. 855, 113630. https://doi.org/10.1016/j.jelechem.2019.113630.
Kan, E.J., Li, Z., Yang, J., Hou, J.G., 2008. Half-metallicity in edge-modified zigzag graphene nanoribbons. J. Am. Chem. Soc. 130, 4224–4225. https://doi.org/10.1021/ja710407t.
Kausar, A., 2019. Graphene nanoribbon : fundamental aspects in polymeric nanocomposite. Polym. Technol. Mater. 1–18. https://doi.org/10.1080/25740881.2018.1563108, 00.
Khim Chng, E.L., Chua, C.K., Pumera, M., 2014. Graphene oxide nanoribbons exhibit significantly greater toxicity than graphene oxide nanoplatelets. Nanoscale 6, 10792–10797. https://doi.org/10.1039/C4NR03608E.
Kim, K., Sussman, A., Zettl, A., 2010. Graphene nanoribbons obtained by electrically unwrapping carbon nanotubes. ACS Nano 4, 1362–1366. https://doi.org/10.1021/nn901782g.
Kosynkin, D.V., Lu, W., Sinitskii, A., Pera, G., Sun, Z., Tour, J.M., 2011. Highly conductive graphene nanoribbons by longitudinal splitting of carbon nanotubes using potassium vapor. ACS Nano 5, 968–974. https://doi.org/10.1021/nn102326c.
Krishnamoorthy, K., Veerapandian, M., Mohan, R., Kim, S., 2012. Investigation of Raman and photoluminescence studies of reduced graphene oxide sheets. Appl. Phys. A 106, 501–506. https://doi.org/10.1007/s00339-011-6720-6.
Krishnan, D., Kim, F., Luo, J., Cruz-silva, R., Cote, L.J., Jang, H.D., Huang, J., 2012. Energetic graphene oxide : challenges and opportunities. Nano Today 7, 137–152. https://doi.org/10.1016/j.nantod.2012.02.003.
Krishnan, S.K., Singh, E., Singh, P., Meyyappan, M., Nalwa, H.S., 2019. A review on graphene-based nanocomposites for electrochemical and fluorescent biosensors. RSC Adv. 9, 8778–8781. https://doi.org/10.1039/c8ra09577a.
Kudr, J., Zhao, L., Nguyen, E.P., Arola, H., Nevanen, T.K., Adam, V., Zitka, O., Merkoçi, A., 2020. Inkjet-printed electrochemically reduced graphene oxide microelectrode as a platform for HT-2 mycotoxin immunoenzymatic biosensing. Biosens. Bioelectron. 156, 112109. https://doi.org/10.1016/j.bios.2020.112109.
Kumar, N., Goyal, R.N., 2018. Chemical Silver nanoparticles decorated graphene nanoribbon modified pyrolytic graphite sensor for determination of histamine. Sensor. Actuator. B Chem. 268, 383–391. https://doi.org/10.1016/j.snb.2018.04.136.
Kumar, P., Panchakarla, L.S., Rao, C.N.R., 2011. Laser-induced unzipping of carbon nanotubes to yield graphene nanoribbons. Nanoscale 3, 2127–2129. https://doi.org/10.1039/c1nr10137d.
Lacatus, E., 2020. Graphene-based metasurface: 4D shape-shift biosensing interface. Mater. Today Proc. https://doi.org/10.1016/j.matpr.2019.12.346.
Lavanya, J., Gomathi, N., 2015. High-sensitivity ascorbic acid sensor using graphene sheet/graphene nanoribbon Hybrid material as an enhanced electrochemical sensing platform. Talanta 144, 655–661. https://doi.org/10.1016/j.talanta.2015.07.018.
Lavanya, J., Nithyaa, J., Saravanakumar, J., Gomathi, N., 2017. Ultrasensitive and selective non-enzymatic electrochemical glucose sensor based on hybrid material of graphene sheet/graphene nanoribbon/nickel nanoparticle. Mater. Res. Bull. https://doi.org/10.1016/j.materresbull.2017.10.020.
Lee, Y.-L., Kim, S., Park, C., Ihm, J., Son, Y.-W., 2010. Controlling half-metallicity of graphene nanoribbons by using a ferroelectric polymer. ACS Nano 4, 1345–1350. https://doi.org/10.1021/nn9019064.
Lee, M., Wang, S., Chiang, W., Feng, H., Huang, T., 2018a. Platinum nanoparticles decorated graphene nanoribbon with eco-friendly unzipping process for electrochemical sensors. J. Taiwan Inst. Chem. Eng. 96, 566–574. https://doi.org/10.1016/j.jtice.2018.11.012.
Lee, Y.-L., Zhao, F., Cao, T., Ihm, J., Louie, S.G., 2018b. Topological phases in cove-edged and chevron graphene nanoribbons: geometric structures, Z2 invariants, and junction states. Nano Lett. 18, 7247–7253. https://doi.org/10.1021/acs.nanolett.8b03416.
Lherbier, A., Blase, X., Niquet, Y.-M., Triozon, F., Roche, S., 2008. Charge transport in chemically doped 2D graphene. Phys. Rev. Lett. 101, 36808. https://doi.org/10.1103/PhysRevLett.101.036808.
Li, N., Ma, H., Cao, W., Wu, D., Yan, T., Du, B., Wei, Q., 2015. Highly sensitive electrochemical immunosensor for the detection of alpha fetoprotein based on PdNi nanoparticles and N-doped graphene nanoribbons. Biosens. Bioelectron. 74, 786–791. https://doi.org/10.1016/j.bios.2015.07.049.
Li, K., Chen, L., Qi, J., 2016a. Improved sensor based on nitrogen-doped vacancy graphene nanoribbons for detecting 2, 4- dichlorophenol: atomistic simulations. Mater. Lett. 188, 5–7. https://doi.org/10.1016/j.matlet.2016.09.073.
Li, Y., Liao, J., Wang, S., Chiang, W., 2016b. Intercalation-assisted longitudinal unzipping of carbon nanotubes for green and scalable synthesis of graphene nanoribbons. Sci. Rep. 6, 22755. https://doi.org/10.1038/srep22755.
Li, Yan, He, J., Chen, J., Niu, Y., Zhao, Y., Zhang, Y., Yu, C., 2017. A dual-type responsive electrochemical immunosensor for quantitative detection of PCSK9 based on n-C60-PdPt/N-GNRs and Pt-poly (methylene blue) nanocomposites. Biosens. Bioelectron. 101, 7–13. https://doi.org/10.1016/j.bios.2017.09.043.
Li, Yaqi, Sun, L., Qian, J., Long, L., Li, H., Liu, Q., Cai, J., Wang, K., 2017. Fluorescent "on-off-on" switching sensor based on CdTe quantum dots coupled with multiwalled carbon nanotubes@graphene oxide nanoribbons for simultaneous monitoring of dual foreign DNAs in transgenic soybean. Biosens. Bioelectron. 92, 26–32. https://doi.org/10.1016/j.bios.2017.01.057.
Li, Z., Zhang, W., Xing, F., 2019. Graphene optical biosensors. Int. J. Mol. Sci. 20, 2461. https://doi.org/10.3390/ijms20102461.
Liao, C., Li, Y., Tjong, S.C., 2018. Graphene nanomaterials: synthesis, biocompatibility, and cytotoxicity. Int. J. Mol. Sci. 19 https://doi.org/10.3390/ijms19113564.
Lin, T., Li, Y., Chiang, W., Pei, Z., 2016. A high sensitivity fi eld effect transistor biosensor for methylene blue detection utilize graphene oxide nanoribbon. Biosens. Bioelectron. 89, 511–517. https://doi.org/10.1016/j.bios.2016.03.046.

Liu, Speranza, 2019. Functionalization of carbon nanomaterials for biomedical applications. C — J. Carbon Res. 5, 72. https://doi.org/10.3390/c5040072.
Liu, G., Wu, Y., Lin, Y.-M., Farmer, D.B., Ott, J.A., Bruley, J., Grill, A., Avouris, P., Pfeiffer, D., Balandin, A.A., Dimitrakopoulos, C., 2012. Epitaxial graphene nanoribbon array fabrication using BCP-assisted nanolithography. ACS Nano 6, 6786–6792. https://doi.org/10.1021/nn301515a.
Liu, G., Ma, W., Luo, Y., Sun, D., Shao, S., 2014. Simultaneous determination of uric acid and xanthine using a poly(methylene blue) and electrochemically reduced graphene oxide composite film modified electrode. J. Anal. Methods Chem. 2014. https://doi.org/10.1155/2014/984314.
Liu, Q., Fei, A., Huan, J., Mao, H., Wang, K., 2015. Effective amperometric biosensor for carbaryl detection based on covalent immobilization acetylcholinesterase on multiwall carbon nanotubes/graphene oxide nanoribbons nanostructure. J. Electroanal. Chem. 740, 8–13. https://doi.org/10.1016/j.jelechem.2014.12.037.
Liu, L., Shen, Z., Zhang, X., Ma, H., 2020. Highly conductive graphene/carbon black screen printing inks for flexible electronics. J. Colloid Interface Sci. https://doi.org/10.1016/j.jcis.2020.07.106.
Lyu, L., Jaswal, P., Xu, G., 2018. Effect of channel-width and chirality on graphene field-effect transistor based real- time biomolecule sensing. AIP Adv. 8, 035322 https://doi.org/10.1063/1.5021959.
Ma, L., Wang, J., Yip, J., Ding, F., 2014. Mechanism of transition-metal nanoparticle catalytic graphene cutting. J. Phys. Chem. Lett. 5, 1192–1197. https://doi.org/10.1021/jz500254u.
Mao, S., Chen, J., 2017. Graphene-based electronic biosensors. J. Mater. Res. 32, 2954–2965. https://doi.org/10.1557/jmr.2017.129.
Marmolejo-Tejada, J.M., Velasco-Medina, J., 2016. Review on graphene nanoribbon devices for logic applications. Microelectron. J. 48, 18–38. https://doi.org/10.1016/j.mejo.2015.11.006.
Martín, A., Hernández-Ferrer, J., Vázquez, L., Martínez, M.T., Escarpa, A., 2014. Controlled chemistry of tailored graphene nanoribbons for electrochemistry: a rational approach to optimizing molecule detection. RSC Adv. 4, 132–139. https://doi.org/10.1039/c3ra44235g.
Martín, A., Batalla, P., Hernández-ferrer, J., Teresa, M., Escarpa, A., 2015a. Graphene oxide nanoribbon-based sensors for the simultaneous bio- electrochemical enantiomeric resolution and analysis of amino acid biomarkers. Biosens. Bioelectron. 68, 163–167. https://doi.org/10.1016/j.bios.2014.12.030.
Martín, A., Hernández-Ferrer, J., Martínez, M.T., Escarpa, A., 2015b. Graphene nanoribbon-based electrochemical sensors on screen-printed platforms. Electrochim. Acta 172, 2–6. https://doi.org/10.1016/j.electacta.2014.11.090.
Mazilova, T.I., Sadanov, E.V., Mikhailovskij, I.M., 2019. Tensile strength of graphene nanoribbons: an experimental approach. Mater. Lett. 242, 17–19. https://doi.org/10.1016/j.matlet.2019.01.051.
Mehdi Pour, M., Lashkov, A., Radocea, A., Liu, X., Sun, T., Lipatov, A., Korlacki, R.A., Shekhirev, M., Aluru, N.R., Lyding, J.W., Sysoev, V., Sinitskii, A., 2017. Laterally extended atomically precise graphene nanoribbons with improved electrical conductivity for efficient gas sensing. Nat. Commun. 8, 820. https://doi.org/10.1038/s41467-017-00692-4.
Mehmeti, E., Stanković, D.M., Chaiyo, S., Zavasnik, J., Žagar, K., Kalcher, K., 2017. Wiring of glucose oxidase with graphene nanoribbons: an electrochemical third generation glucose biosensor. Microchim. Acta 184, 1127–1134. https://doi.org/10.1007/s00604-017-2115-5.
Mei, Q., Liu, B., Han, G., Liu, R., Han, M., 2019. Graphene Oxide : from tunable structures to diverse luminescence behaviors. Adv. Sci. 1900855. https://doi.org/10.1002/advs.201900855.
Menazea, A.A., Ahmed, M.K., 2020. Synthesis and antibacterial activity of graphene oxide decorated by silver and copper oxide nanoparticles. J. Mol. Struct. 1218, 128536. https://doi.org/10.1016/j.molstruc.2020.128536.
Meyer, J.C., Geim, A.K., Katsnelson, M.I., Novoselov, K.S., Booth, T.J., Roth, S., 2007. The structure of suspended graphene sheets. Nature 446, 60–63. https://doi.org/10.1038/nature05545.
Min, S.-Y., Kim, T.-S., Kim, B.J., Cho, H., Noh, Y.-Y., Yang, H., Cho, J.H., Lee, T.-W., 2013. Large-scale organic nanowire lithography and electronics. Nat. Commun. 4, 1773. https://doi.org/10.1038/ncomms2785.
Mogha, N.K., Sahu, V., Sharma, R.K., Masram, D.T., 2018. Reduced graphene oxide nanoribbon immobilized gold nanoparticle based electrochemical DNA biosensor for the detection of: Mycobacterium tuberculosis. J. Mater. Chem. B 6, 5181–5187. https://doi.org/10.1039/c8tb01604f.
Mousavi, S.M., Soroshnia, S., Hashemi, S.A., Babapoor, A., Ghasemi, Y., Savardashtaki, A., Amani, A.M., 2019. Graphene nano-ribbon based high potential and efficiency for DNA, cancer therapy and drug delivery applications. Drug Metab. Rev. 51, 91–104. https://doi.org/10.1080/03602532.2019.1582661.
Muñoz, J., Pumera, M., 2020. 3D-printed biosensors for electrochemical and optical applications. TrAC Trends Anal. Chem. (Reference Ed.) 128. https://doi.org/10.1016/j.trac.2020.115933.
Nakada, K., Fujita, M., Dresselhaus, G., Dresselhaus, M.S., 1996. Edge state in graphene ribbons : nanometer size effect and edge shape dependence. Phys. Rev. B 54, 954–961.
Narita, A., Feng, X., Hernandez, Y., Jensen, S.A., Bonn, M., Yang, H., Verzhbitskiy, I.A., Casiraghi, C., Hansen, M.R., Koch, A.H.R., Fytas, G., Ivasenko, O., Li, B., Mali, K.S., Balandina, T., Mahesh, S., De Feyter, S., Müllen, K., 2014. Synthesis of structurally well-defined and liquid-phase-processable graphene nanoribbons. Nat. Chem. 6, 126–132. https://doi.org/10.1038/nchem.1819.
Narita, A., Chen, Z., Chen, Q., Müllen, K., 2019. Solution and on-surface synthesis of structurally defined graphene nanoribbons as a new family of semiconductors. Chem. Sci. 10, 964–975. https://doi.org/10.1039/C8SC03780A.
Niu, W., Liu, J., Mai, Y., Müllen, K., Feng, X., 2019. Synthetic engineering of graphene nanoribbons with excellent liquid-phase processability. Trends Chem. 1, 549–558. https://doi.org/10.1016/j.trechm.2019.06.008.
Orlov, A.V., Ovid'ko, I.A., 2015. Mechanical properties of graphene nanoribbons : a selective review. Rev. Adv. Mater. Sci. 40, 249–256.
Ouyang, F.P., Peng, S.L., Zhang, H., Weng, L.B., Xu, H., 2011. A biosensor based on graphene nanoribbon with nanopores: a first-principles devices-design. Chin. Phys. B 20, 1–5. https://doi.org/10.1088/1674-1056/20/5/058504.
Pajooheshpour, N., Rezaei, M., Hajian, A., Afkhami, A., Sillanpää, M., Arduini, F., Bagheri, H., 2018. Protein templated Au-Pt nanoclusters-graphene nanoribbons as a high performance sensing layer for the electrochemical determination of diazinon. Sensor. Actuator. B Chem. 275, 180–189. https://doi.org/10.1016/j.snb.2018.08.014.
Palanisamy, S., Chen, S.M., Sarawathi, R., 2012. A novel nonenzymatic hydrogen peroxide sensor based on reduced graphene oxide/ZnO composite modified electrode. Sensor. Actuator. B Chem. 166–167, 372–377. https://doi.org/10.1016/j.snb.2012.02.075.
Pan, Y., Shang, L., Zhao, F., Zeng, B., 2015. A novel electrochemical 4-nonyl-phenol sensor based on molecularly imprinted poly (o-phenylenediamine-co-o-toluidine)-nitrogen- doped graphene nanoribbons-ionic liquid composite film. Electrochim. Acta 151, 423–428. https://doi.org/10.1016/j.electacta.2014.11.044.
Park, J., Akbari-sharbaf, A., Ezugwu, S., Bauld, R., Fanchini, G., 2016. Direct synthesis of highly conducting graphene nanoribbon thin films from graphene ridges and wrinkles. Acta Mater. 107, 96–101. https://doi.org/10.1016/j.actamat.2016.01.029.
Park, J., Sempionatto, J.R., Kim, J., Jeong, Y., Gu, J., Wang, J., Park, I., 2020. Microscale biosensor array based on flexible polymeric platform toward lab-on-a-needle: real-time multiparameter biomedical assays on curved needle surfaces. ACS Sens. 5, 1363–1373. https://doi.org/10.1021/acssensors.0c00078.
Parkash, O., Shueb, R., 2015. Diagnosis of dengue infection using conventional and biosensor based techniques. Viruses 7, 5410–5427. https://doi.org/10.3390/v7102877.
Pathmanapan, S., Periyathambi, P., Anandasadagopan, S.K., 2020. Fibrin hydrogel incorporated with graphene oxide functionalized nanocomposite scaffolds for bone repair — in vitro and in vivo study. Nanomedicine Nanotechnology, Biol. Med. 29, 102251. https://doi.org/10.1016/j.nano.2020.102251.
Paul, R.K., Badhulika, S., Niyogi, S., Haddon, R.C., Boddu, V.M., Costales-nieves, C., Bozhilov, K.N., Mulchandani, A., 2011. The production of oxygenated polycrystalline graphene by one-step ethanol-chemical vapor deposition. Carbon N. Y. 49, 3789–3795. https://doi.org/10.1016/j.carbon.2011.04.070.
Paulechka, E., Wassenaar, T.A., Kroenlein, K., Kazakov, A., Smolyanitsky, A., 2016. Nucleobase-functionalized graphene nanoribbons for accurate high-speed DNA sequencing. Nanoscale 8, 1861–1867. https://doi.org/10.1039/c5nr07061a.
Pefkianakis, E.K., Sakellariou, G., Vougioukalakis, G.C., 2015. Chemical synthesis of graphene nanoribbons. Arkivoc 2015, 167–192. https://doi.org/10.3998/ark.5550190.p008.995.
Pham, T., Ramnani, P., Villarreal, C.C., Lopez, J., Das, P., Lee, I., Neupane, M.R., Rheem, Y., Mulchandani, A., 2019. MoS2-graphene heterostructures as efficient organic compounds sensing 2D materials. Carbon N. Y. 142, 504–512. https://doi.org/10.1016/j.carbon.2018.10.079.
Prezzi, D., Varsano, D., Ruini, A., Marini, A., Molinari, E., 2008. Optical properties of graphene nanoribbons: the role of many-body effects. Phys. Rev. B Condens. Matter 77, 1–4. https://doi.org/10.1103/PhysRevB.77.041404.
Pumera, M., 2011. Graphene in biosensing. Mater. Today 14, 308–315. https://doi.org/10.1016/S1369-7021(11)70160-2.
Qiu, W., Skafidas, E., 2014. Detection of protein conformational changes with multilayer graphene nanopore sensors. ACS Appl. Mater. Interfaces 6, 16777–16781. https://doi.org/10.1021/am5040279.
Rajaji, U., Arumugam, R., Chen, S.-M., Chen, T.-W., Tseng, T.-W., Chinnapaiyan, S., 2018. Graphene nanoribbons in electrochemical sensors and biosensors: a review. Int. J. Electrochem. Sci. https://doi.org/10.20964/2018.07.51.
Rashid, M.H., Koel, A., Rang, T., 2020. Simulations of graphene nanoribbon field effect transistor for the detection of propane and butane gases: a first principles study. Nanomaterials 10. https://doi.org/10.3390/nano10010098.
Rastgoo, M., Fathipour, M., 2019. Interaction of DNA nucleobases with boron, nitrogen, and sulfur doped graphene nano-ribbon for sequencing: an Ab initio study. Appl. Surf. Sci. 492, 634–643. https://doi.org/10.1016/j.apsusc.2019.06.208.
Rauti, R., Musto, M., Bosi, S., Prato, M., Ballerini, L., 2019. Properties and behavior of carbon nanomaterials when interfacing neuronal cells: how far have we come? Carbon N. Y. https://doi.org/10.1016/j.carbon.2018.11.026.
Reina, G., González-Domínguez, J.M., Criado, A., Vázquez, E., Bianco, A., Prato, M., 2017. Promises, facts and challenges for graphene in biomedical applications. Chem. Soc. Rev. 46, 4400–4416. https://doi.org/10.1039/c7cs00363c.
Reuven, D.G., Mihiri Shashikala, H.B., Mandal, S., Williams, M.N.V., Chaudhary, J., Wang, X.Q., 2013. Supramolecular assembly of DNA on graphene nanoribbons. J. Mater. Chem. B 1, 3926–3931. https://doi.org/10.1039/c3tb20397b.
Rezvani Jalal, N., Madrakian, T., Afkhami, A., Ghoorchian, A., 2020. In situ growth of metal-organic framework HKUST-1 on graphene oxide nanoribbons with high electrochemical sensing performance in imatinib determination. ACS Appl. Mater. Interfaces 12, 4859–4869. https://doi.org/10.1021/acsami.9b18097.
Rostami, S., Mehdinia, A., Niroumand, R., Jabbari, A., 2020. Enhanced LSPR performance of graphene nanoribbons-silver nanoparticles hybrid as a colorimetric sensor for sequential detection of dopamine and glutathione. Anal. Chim. Acta. https://doi.org/10.1016/j.aca.2020.04.060.
Saha, K.K., Drndić, M., Nikolić, B.K., 2012. DNA base-specific modulation of microampere transverse edge currents through a metallic graphene nanoribbon with a nanopore. Nano Lett. 12, 50–55. https://doi.org/10.1021/nl202870y.

Sainz, R., del Pozo, M., Vilas-Varela, M., Castro-Esteban, J., Pérez Corral, M., Vázquez, L., Blanco, E., Peña, D., Martín-Gago, J.A., Ellis, G.J., Petit-Domínguez, M.D., Quintana, C., Casero, E., 2020. Chemically synthesized chevron-like graphene nanoribbons for electrochemical sensors development: determination of epinephrine. Sci. Rep. 10, 14614. https://doi.org/10.1038/s41598-020-71554-1.

Sandeep, S., Santhosh, A.S., Swamy, N.K., Suresh, G.S., Melo, J.S., Chamaraja, N.A., 2018. A biosensor based on a graphene nanoribbon/silver nanoparticle/polyphenol oxidase composite matrix on a graphite electrode: application in the analysis of catechol in green tea samples. New J. Chem. 42, 16620–16629. https://doi.org/10.1039/C8NJ02325E.

Sang, S., Wang, Y., Feng, Q., Wei, Y., Ji, J., Zhang, W., 2016. Progress of new label-free techniques for biosensors: a review. Crit. Rev. Biotechnol. https://doi.org/10.3109/07388551.2014.991270.

Schwab, M.G., Narita, A., Osella, S., Hu, Y., Maghsoumi, A., Mavrinsky, A., Pisula, W., Castiglioni, C., Tommasini, M., Beljonne, D., Feng, X., Müllen, K., 2015. Bottom-up synthesis of necklace-like graphene nanoribbons. Chem. Asian J. 10, 2134–2138. https://doi.org/10.1002/asia.201500450.

Seekaew, Y., Arayawut, O., Timsorn, K., Wongchoosuk, C., 2018. Synthesis, characterization, and applications of graphene and derivatives. In: Carbon-Based Nanofillers and Their Rubber Nanocomposites: Carbon Nano-Objects. Elsevier, pp. 259–283. https://doi.org/10.1016/B978-0-12-813248-7.00009-2.

Semenov, O., Vassighi, A., Sachdev, M., 2006. Impact of self-heating effect on long-term reliability and performance degradation in CMOS circuits. IEEE Trans. Device Mater. Reliab. 6, 17–27. https://doi.org/10.1109/TDMR.2006.870340.

Senkovskiy, B.V., Pfeiffer, M., Alavi, S.K., Bliesener, A., Zhu, J., Fedorov, A.V., German, R., Hertel, D., Haberer, D., Petaccia, L., Fischer, R., Meerholz, K., Van Loosdrecht, P.H.M., Lindfors, K., Grueneis, A., 2017. Making graphene nanoribbons photoluminescent. https://doi.org/10.1021/acs.nanolett.7b00147.

Shahabi, M., Raissi, H., 2020. Payload delivery of anticancer drug Tegafur with the assistance of graphene oxide nanosheet during biomembrane penetration: molecular dynamics simulation survey. Appl. Surf. Sci. 517, 146186. https://doi.org/10.1016/j.apsusc.2020.146186.

Shang, L., Zhao, F., Zeng, B., 2015. Highly dispersive hollow PdAg alloy nanoparticles modified ionic liquid functionalized graphene nanoribbons for electrochemical sensing of nifedipine. Electrochim. Acta 168, 330–336. https://doi.org/10.1016/j.electacta.2015.04.024.

Sharafat Hossain, M., Al-Dirini, F., Hossain, F.M., Skafidas, E., 2015. High performance graphene nano-ribbon thermoelectric devices by incorporation and dimensional tuning of nanopores. Sci. Rep. 5, 11297. https://doi.org/10.1038/srep11297.

Sharma, D., Kanchi, S., Sabela, M.I., Bisetty, K., 2015. Insight into the biosensing of graphene oxide : present and future prospects. Arab. J. Chem. https://doi.org/10.1016/j.arabjc.2015.07.015.

Shi, J., He, T., Jiang, F., Abdel-halim, E.S., Zhu, J., 2014. Ultrasensitive multi-analyte electrochemical immunoassay based on GNR-modi fi ed heated screen-printed carbon electrodes and PS @ PDA-metal labels for rapid detection of MMP-9 and IL-6. Biosens. Bioelectron. 55, 51–56. https://doi.org/10.1016/j.bios.2013.11.056.

Shi, L., Niu, X., Liu, T., Zhao, H., Lan, M., 2015. Electrocatalytic sensing of hydrogen peroxide using a screen printed carbon electrode modified with nitrogen-doped graphene nanoribbons. Microchim. Acta 182, 2485–2493. https://doi.org/10.1007/s00604-015-1605-6.

Shinde, D.B., Majumder, M., Pillai, V.K., 2014. Counter-ion dependent, longitudinal unzipping of multi-walled carbon nanotubes to highly conductive and transparent graphene nanoribbons. Sci. Rep. 4, 4363. https://doi.org/10.1038/srep04363.

Si, S., Wang, J., Li, J., Li, W., Cong, H., Liu, J., Tang, J., Jiang, C., Xia, R., Xiao, X., 2020. Enhancing resistance to radiation hardening and radiation thermal conductivity degradation by tungsten/graphene interface engineering. J. Nucl. Mater. 539, 152348. https://doi.org/10.1016/j.jnucmat.2020.152348.

Son, J.G., Son, M., Moon, K.-J., Lee, B.H., Myoung, J.-M., Strano, M.S., Ham, M.-H., Ross, C.A., 2013. Sub-10 nm graphene nanoribbon array field-effect transistors fabricated by block copolymer lithography. Adv. Mater. 25, 4723–4728. https://doi.org/10.1002/adma.201300813.

Song, Y.Z., Yang, M.J., Yuan, J., Han, X.L., 2016. Determination of norepinephrine tartrate at oxidized graphene nanoribbon modified glassy carbon electrode. Int. J. Electrochem. Sci. 11, 9030–9040. https://doi.org/10.20964/2016.11.20.

Su, J., Zhang, X., Tong, X., Wang, X., Yang, P., Yao, F., Guo, R., Yuan, C., 2020. Preparation of graphene quantum dots with high quantum yield by a facile one-step method and applications for cell imaging. Mater. Lett. 271, 127806. https://doi.org/10.1016/j.matlet.2020.127806.

Sun, C.L., Su, C.H., Wu, J.J., 2015. Synthesis of short graphene oxide nanoribbons for improved biomarker detection of Parkinson's disease. Biosens. Bioelectron. 67, 334–341. https://doi.org/10.1016/j.bios.2014.08.046.

Tabarraei, A., Shadalou, S., Song, J.H., 2015. Mechanical properties of graphene nanoribbons with disordered edges. Comput. Mater. Sci. 96, 10–19. https://doi.org/10.1016/j.commatsci.2014.08.001.

Talirz, L., Ruffi, P., Fasel, R., 2016. On-surface synthesis of atomically precise graphene nanoribbons. Adv. Mater. 1–10 https://doi.org/10.1002/adma.201505738.

Talyzin, A.V., Anoshkin, I.V., Krasheninnikov, A.V., Nieminen, R.M., Nasibulin, A.G., Jiang, H., Kauppinen, E.I., 2011. Synthesis of graphene nanoribbons encapsulated in single-walled carbon nanotubes. Nano Lett. 11, 4352–4356.

Tamersit, K., Djeffal, F., 2016. Double-gate graphene nanoribbon field-effect transistor for DNA and gas sensing applications: simulation study and sensitivity analysis. IEEE Sensor. J. 16, 4180–4191. https://doi.org/10.1109/JSEN.2016.2550492.

Tan, X., Chuang, H.J., Lin, M.W., Zhou, Z., Cheng, M.M.C., 2013. Edge effects on the ph response of graphene nanoribbon field effect transistors. J. Phys. Chem. C 117, 27155–27160. https://doi.org/10.1021/jp409116r.

Tang, J., Hou, L., Tang, D., Zhou, J., Wang, Z., Li, J., Chen, G., 2012. Magneto-controlled electrochemical immunoassay of brevetoxin B in seafood based on guanine-functionalized graphene nanoribbons. Biosens. Bioelectron. 38, 86–93. https://doi.org/10.1016/j.bios.2012.05.006.

Tang, Z., He, J., Chen, J., Niu, Y., Zhao, Y., Zhang, Y., Yu, C., 2017. A sensitive sandwich-type immunosensor for the detection of galectin-3 based on N-GNRs-Fe- MOFs@ AuNPs nanocomposites and a novel AuPt- Methylene blue nanorod. Biosens. Bioelectron. 101, 253–259. https://doi.org/10.1016/j.bios.2017.10.026.

Tapasztó, L., Dobrik, G., Lambin, P., Biró, L.P., 2008. Tailoring the atomic structure of graphene nanoribbons by scanning tunnelling microscope lithography. Nat. Nanotechnol. 3, 397–401. https://doi.org/10.1038/nnano.2008.149.

Terrones, M., Botello-méndez, A.R., Campos-delgado, J., López-urías, F., Vega-cantú, Y. I., Rodríguez-macías, F.J., Laura, A., Mu, E., Cano-márquez, A.G., Charlier, J., Terrones, H., 2010. Graphene and graphite nanoribbons : morphology , properties , synthesis , defects and applications. https://doi.org/10.1016/j.nantod.2010.06.010.

Terse-Thakoor, T., Ramnani, P., Villarreal, C., Yan, D., Tran, T.T., Pham, T., Mulchandani, A., 2019. Graphene nanogap electrodes in electrical biosensing. Biosens. Bioelectron. 126, 838–844. https://doi.org/10.1016/j.bios.2018.11.049.

Thiruppathi, A.R., Sidhureddy, B., Salverda, M., Wood, P.C., Chen, A., 2020. Novel three-dimensional N-doped interconnected reduced graphene oxide with superb capacitance for energy storage. J. Electroanal. Chem. 113911 https://doi.org/10.1016/j.jelechem.2020.113911.

Traversi, F., Raillon, C., Benameur, S.M., Liu, K., Khlybov, S., Tosun, M., Krasnozhon, D., Kis, A., Radenovic, A., 2013. Detecting the translocation of DNA through a nanopore using graphene nanoribbons. Nat. Nanotechnol. 8, 939–945. https://doi.org/10.1038/nnano.2013.240.

Valentini, F., Carbone, M., Palleschi, G., 2013. Graphene oxide nanoribbons (GNO), reduced graphene nanoribbons (GNR), and multi-layers of oxidized graphene functionalized with ionic liquids (GO-IL) for assembly of miniaturized electrochemical devices. Anal. Bioanal. Chem. 405, 3449–3474. https://doi.org/10.1007/s00216-012-6615-1.

Vermisoglou, E., Panáček, D., Jayaramulu, K., Pykal, M., Frébort, I., Kolář, M., Hajdúch, M., Zbořil, R., Otyepka, M., 2020. Human virus detection with graphene-based materials. Biosens. Bioelectron. 166 https://doi.org/10.1016/j.bios.2020.112436.

Viculis, L.M., Mack, J.J., Mayer, O.M., Hahn, H.T., Kaner, R.B., 2005. Intercalation and exfoliation routes to graphite nanoplatelets. J. Mater. Chem. 15, 974–978. https://doi.org/10.1039/B413029D.

Vukojević, V., Djurdjić, S., Antić, B., Kalcher, K., Stanković, D.M., 2018a. RuO2/graphene nanoribbon composite supported on screen printed electrode with enhanced electrocatalytic performances toward ethanol and NADH biosensing. Biosens. Bioelectron. 117, 392–397. https://doi.org/10.1016/j.bios.2018.06.038.

Vukojević, V., Djurdjić, S., Ognjanović, M., Fabián, M., Samphao, A., Kalcher, K., Stanković, D.M., 2018b. Enzymatic glucose biosensor based on manganese dioxide nanoparticles decorated on graphene nanoribbons. J. Electroanal. Chem. 823, 610–616. https://doi.org/10.1016/j.jelechem.2018.07.013.

Wang, Y., Song, Z., Xu, Z., 2014. Characterizing phonon thermal conduction in polycrystalline graphene. J. Mater. Res. 29, 362–372. https://doi.org/10.1557/jmr.2013.380.

Wang, M., Zhang, S., Song, Y., Dong, J., 2016. Fabrication of light, flexible and multifunctional graphene nanoribbon fibers via a 3D solution printing method. Nanotechnology 27, 1–7. https://doi.org/10.1088/0957-4484/27/46/465702.

Wang, Y., Yang, S., Chang, H., Li, W., Chen, X., Hou, R., Yan, J., Yi, X., Wang, J., Wei, T., 2020. Flexible graphene-assisted van der Waals epitaxy growth of crack-free AlN epilayer on SiC by lattice engineering. Appl. Surf. Sci. 520, 146358. https://doi.org/10.1016/j.apsusc.2020.146358.

Wasfi, A., Awwad, F., Ayesh, A.I., 2019. Electronic signature of DNA bases via Z-shaped graphene nanoribbon with a nanopore. Biosens. Bioelectron. X 1, 100011. https://doi.org/10.1016/j.biosx.2019.100011.

Wu, J., Gherghel, L., Watson, M.D., Li, J., Wang, Z., Simpson, C.D., Kolb, U., Müllen, K., 2003. From branched polyphenylenes to graphite ribbons. Macromolecules 36, 7082–7089. https://doi.org/10.1021/ma0257752.

Wu, Z., Ren, W., Gao, L., Liu, B., Jiang, C., Cheng, H., 2008. Synthesis of high-quality graphene with a pre-determined number of layers. Carbon N. Y. 47, 493–499. https://doi.org/10.1016/j.carbon.2008.10.031.

Wu, M., Wu, X., Zeng, X.C., 2010a. Exploration of half metallicity in edge-modified graphene nanoribbons. J. Phys. Chem. C 114, 3937–3944. https://doi.org/10.1021/jp100027w.

Wu, Z.-S., Ren, W., Gao, L., Liu, B., Zhao, J., Cheng, H.-M., 2010b. Efficient synthesis of graphene nanoribbons sonochemically cut from graphene sheets. Nano Res. 3, 16–22. https://doi.org/10.1007/s12274-010-1003-7.

Wu, S., Lan, X., Huang, F., Luo, Z., Ju, H., Meng, C., Duan, C., 2012. Selective electrochemical detection of cysteine in complex serum by graphene nanoribbon. Biosens. Bioelectron. 32, 293–296. https://doi.org/10.1016/j.bios.2011.12.006.

Xie, G., Shi, Z., Yang, R., Liu, D., Yang, W., Cheng, M., Wang, D., Shi, D., Zhang, G., 2012. Graphene edge lithography. Nano Lett. 12, 4642–4646. https://doi.org/10.1021/nl301936r.

Xin, X., Sun, S., Li, H., Wang, M., Jia, R., 2015. Electrochemical bisphenol A sensor based on core – shell multiwalled carbon nanotubes/graphene oxide nanoribbons. Sensor. Actuator. B Chem. 209, 275–280. https://doi.org/10.1016/j.snb.2014.11.128.

Xu, H., Suslick, K.S., 2011. Sonochemical preparation of functionalized graphenes. J. Am. Chem. Soc. 133, 9148–9151. https://doi.org/10.1021/ja200883z.

Xu, M., Tabarraei, A., Paci, J.T., Oswald, J., Belytschko, T., 2012. A coupled quantum/continuum mechanics study of graphene fracture. Int. J. Fract. 173, 163–173. https://doi.org/10.1007/s10704-011-9675-x.

Xu, W., Lee, T., Lee, T., 2016. Recent progress in fabrication techniques of graphene nanoribbons. Mater. Horiz. 3, 186–207. https://doi.org/10.1039/c5mh00288e.
Xu, S., Jiang, S., Zhang, C., Yue, W., Zou, Y., Wang, G., Liu, H., Zhang, X., Li, M., Zhu, Z., Wang, J., 2018. Ultrasensitive label-free detection of DNA hybridization by sapphire-based graphene field-effect transistor biosensor. Appl. Surf. Sci. 427, 1114–1119. https://doi.org/10.1016/j.apsusc.2017.09.113.
Xu, J., Zhang, Z., Gan, S., Gao, H., Kong, H., Song, Z., Ge, X., Bao, Y., Niu, L., 2020a. Highly stretchable fiber-based potentiometric ion sensors for multichannel real-time analysis of human sweat. ACS Sens. 5, 2834–2842. https://doi.org/10.1021/acssensors.0c00960.
Xu, L., Shoaie, N., Jahanpeyma, F., Zhao, J., Azimzadeh, M., Al−Jamal, K.T., 2020b. Optical, electrochemical and electrical (nano)biosensors for detection of exosomes: a comprehensive overview. Biosens. Bioelectron. 161, 112222. https://doi.org/10.1016/j.bios.2020.112222.
Y, P.D., Svitel, J., Katrl, J., 2016. Optical biosensors. Essays Biochem. 91–100. https://doi.org/10.1042/EBC20150010.
Yan, R., Qiu, S., Tong, L., Qian, Y., 2016. Review of progresses on clinical applications of ion selective electrodes for electrolytic ion tests: from conventional ISEs to graphene-based ISEs. Chem. Speciat. Bioavailab. 28, 72–77. https://doi.org/10.1080/09542299.2016.1169560.
Yang, X., Dou, X., Rouhanipour, A., Zhi, L., Ra, H.J., Mu, K., 2008. Two-Dimensional Graphene Nanoribbons 5, 4216–4217.
Yang, X., Yu, X., Liu, X., 2018. Obtaining a sustainable competitive advantage from patent information: a patent analysis of the graphene industry. Sustain. Times 10. https://doi.org/10.3390/su10124800.
Yazyev, O.V., Chen, Y.P., 2014. Polycrystalline graphene and other two-dimensional materials. Nat. Nanotechnol. 9, 755–767. https://doi.org/10.1038/nnano.2014.166.
Yazyev, O.V., Louie, S.G., 2010. Topological defects in graphene: dislocations and grain boundaries. Phys. Rev. B Condens. Matter 81, 195420. https://doi.org/10.1103/PhysRevB.81.195420.
Ye, Z.-Q., Cao, B.-Y., Yao, W.-J., Feng, T., Ruan, X., 2015. Spectral phonon thermal properties in graphene nanoribbons. Carbon N. Y. 93, 915–923. https://doi.org/10.1016/j.carbon.2015.06.008.
Yi, Y., Zhu, G., Wu, X., Wang, K., 2016. Highly sensitive and simultaneous electrochemical determination of 2-aminophenol and 4-aminophenol based on poly (l-arginine)-β-cyclodextrin/carbon nanotubes@graphene nanoribbons modified electrode. Biosens. Bioelectron. 77, 353–358. https://doi.org/10.1016/j.bios.2015.09.052.
Yu, S.S., Zheng, W.T., Wen, Q.B., Jiang, Q., 2008. First principle calculations of the electronic properties of nitrogen-doped carbon nanoribbons with zigzag edges. Carbon N. Y. 46, 537–543. https://doi.org/10.1016/j.carbon.2008.01.006.
Zakaria, A.B.M., Leszczynska, D., 2019. Electrochemically prepared unzipped single walled carbon nanotubes-MnO2 nanostructure composites for hydrogen peroxide and glucose sensing. Chemosensors 7. https://doi.org/10.3390/CHEMOSENSORS7010001.
Zhang, B., Cui, T., 2013. Suspended graphene nanoribbon ion-sensitive field-effect transistors formed by shrink lithography for pH/cancer biomarker sensing. J. Microelectromechan. Syst. 22, 1140–1146. https://doi.org/10.1109/JMEMS.2013.2254701.
Zhang, L., Sun, Y., Lin, X., 2001. Separation of anodic peaks of ascorbic acid and dopamine at an α-alanine covalently modified glassy carbon electrode. Analyst 126, 1760–1763. https://doi.org/10.1039/b104886b.
Zhao, P., Ni, M., Xu, Y., Wang, C., Chen, C., Zhang, X., Li, C., Xie, Y., Fei, J., 2019. A novel ultrasensitive electrochemical quercetin sensor based on MoS2 - carbon nanotube @ graphene oxide nanoribbons/HS-cyclodextrin/graphene quantum dots composite film. Sensor. Actuator. B Chem. 299, 126997. https://doi.org/10.1016/j.snb.2019.126997.
Zheng, X.H., Wang, X.L., Abtew, T.A., Zeng, Z., 2010. Building half-metallicity in graphene nanoribbons by direct control over edge states occupation. J. Phys. Chem. C 114, 4190–4193. https://doi.org/10.1021/jp911203n.
Zhou, L., Mao, H., Wu, C., Tang, L., Wu, Z., Sun, H., Zhang, H., Zhou, H., Jia, C., Jin, Q., Chen, X., Zhao, J., 2017. Label-free graphene biosensor targeting cancer molecules based on non-covalent modification. Biosens. Bioelectron. 87, 701–707. https://doi.org/10.1016/j.bios.2016.09.025.
Zhu, Y., Higginbotham, A.L., Tour, J.M., 2009. Covalent functionalization of surfactant-wrapped graphene nanoribbons. Chem. Mater. 21, 5284–5291. https://doi.org/10.1021/cm902939n.
Zihni, D., Uygun, O., Yen, L., Chimica, A., Received, A., Date, R., Date, A., Uygun, O., All, E.B.V., 2020. CRISPR-dCas9 powered impedimetric biosensor for label-free detection of circulating tumor DNAs. Anal. Chim. Acta 1121, 35–41. https://doi.org/10.1016/j.aca.2020.04.009.